Vol. 23, no. 4, 2023

eISSN 2687-1653

PEER-REVIEWED SCIENTIFIC AND PRACTICAL JOURNAL

Advanced Engineering Research (Rostov-on-Don)

Mechanics

Machine Building and Machine Science

Information Technology, Computer Science and Management

www.vestnik-donstu.ru

DOI 10.23947/2687-1653

Advanced Engineering Research (Rostov-on-Don)

Peer-reviewed scientific and practical journal (published since 2000)

eISSN 2687–1653
DOI: 10.23947/2687–1653

Vol. 23, no. 4, 2023

The journal is aimed at informing the readership about the latest achievements and prospects in the field of mechanics, mechanical engineering, computer science and computer technology. The publication is a forum for cooperation between Russian and foreign scientists, it contributes to the convergence of the Russian and world scientific and information space.

The journal is included in the List of the leading peer-reviewed scientific publications (Higher Attestation Commission under the Ministry of Science and Higher Education of the Russian Federation), where basic scientific results of dissertations for the degrees of Doctor and Candidate of Science in scientific specialties and their respective branches of science should be published.

The journal publishes articles in the following fields of science:

– Theoretical Mechanics, Dynamics of Machines (Engineering Sciences)
– Deformable Solid Mechanics (Engineering, Physical and Mathematical Sciences)
– Mechanics of Liquid, Gas and Plasma (Engineering Sciences)
– Mathematical Simulation, Numerical Methods and Program Systems (Engineering Sciences)
– System Analysis, Information Management and Processing, Statistics (Engineering Sciences)
– Automation and Control of Technological Processes and Productions (Engineering Sciences)
– Software and Mathematical Support of Machines, Complexes and Computer Networks (Engineering Sciences)
– Computer Modeling and Design Automation (Engineering, Physical and Mathematical Sciences)
– Computer Science and Information Processes (Engineering Sciences)
– Machine Science (Engineering Sciences)
– Machine Friction and Wear (Engineering Sciences)
– Technology and Equipment of Mechanical and Physicotechnical Processing (Engineering Sciences)
– Engineering Technology (Engineering Sciences)
– Welding, Allied Processes and Technologies (Engineering Sciences)
– Methods and Devices for Monitoring and Diagnostics of Materials, Products, Substances and the Natural Environment (Engineering Sciences)
– Hydraulic Machines, Vacuum, Compressor Equipment, Hydraulic and Pneumatic Systems (Engineering Sciences)

Indexing and archiving	RSCI, CyberLeninka, EBSCO, Dimensions, DOAJ, Index Copernicus, Internet Archive, Google Scholar
Name of the body that registered the publication	Extract from the Register of Registered Mass Media ЭЛ № ФС 77 – 78854 dated August 07, 2020, issued by the Federal Service for Supervision of Communications, Information Technology and Mass Media
Founder and publisher	Federal State Budgetary Educational Institution of Higher Education Don State Technical University (DSTU)
Periodicity	4 issues per year
Address of the founder and publisher	1, Gagarin sq., Rostov-on-Don, 344003, Russian Federation
E-mail	vestnik@donstu.ru
Telephone	+7 (863) 2–738–372
Website	http://vestnik-donstu.ru/
Date of publication	30.12.2023

Advanced Engineering Research (Rostov-on-Don)

Рецензируемый научно-практический журнал (издается с 2000 года)

eISSN 2687–1653
DOI: 10.23947/2687–1653

Том 23, № 4, 2023

Создан в целях информирования читательской аудитории о новейших достижениях и перспективах в области механики, машиностроения, информатики и вычислительной техники. Издание является форумом для сотрудничества российских и иностранных ученых, способствует сближению российского и мирового научно-информационного пространства.

Журнал включен в перечень рецензируемых научных изданий, в котором должны быть опубликованы основные научные результаты диссертаций на соискание ученой степени кандидата наук, на соискание ученой степени доктора наук (Перечень ВАК) по следующим научным специальностям:

1.1.7 – Теоретическая механика, динамика машин (технические науки)
1.1.8 – Механика деформируемого твердого тела (технические, физико-математические науки)
1.1.9 – Механика жидкости, газа и плазмы (технические науки)
1.2.2 – Математическое моделирование, численные методы и комплексы программ (технические науки)
2.3.1 – Системный анализ, управление и обработка информации, статистика (технические науки)
2.3.3 – Автоматизация и управление технологическими процессами и производствами (технические науки)
2.3.5 – Математическое и программное обеспечение вычислительных систем, комплексов и компьютерных сетей (технические науки)
2.3.7 – Компьютерное моделирование и автоматизация проектирования (технические, физико-математические науки)
2.3.8 – Информатика и информационные процессы (технические науки)
2.5.2 – Машиноведение (технические науки)
2.5.3 – Трение и износ в машинах (технические науки)
2.5.5 – Технология и оборудование механической и физико-технической обработки (технические науки)
2.5.6 – Технология машиностроения (технические науки)
2.5.8 – Сварка, родственные процессы и технологии (технические науки)
2.5.9 – Методы и приборы контроля и диагностики материалов, изделий, веществ и природной среды (технические науки)
2.5.10 – Гидравлические машины, вакуумная, компрессорная техника, гидро- и пневмосистемы (технические науки)

Индексация и архивация:	РИНЦ, CyberLeninka, CrossRef, Dimensions, DOAJ, EBSCO, Index Copernicus, Internet Archive, Google Scholar
Наименование органа, зарегистрировавшего издание	Выписка из реестра зарегистрированных средств массовой информации ЭЛ № ФС 77 – 78854 от 07 августа 2020 г., выдано Федеральной службой по надзору в сфере связи, информационных технологий и массовых коммуникаций
Учредитель и издатель	Федеральное государственное бюджетное образовательное учреждение высшего образования «Донской государственный технический университет» (ДГТУ)
Периодичность	4 выпуска в год
Адрес учредителя и издателя	344003, Российская Федерация, г. Ростов-на-Дону, пл. Гагарина, 1
E-mail	vestnik@donstu.ru
Телефон	+7 (863) 2–738–372
Сайт	http://vestnik-donstu.ru/
Дата выхода в свет	30.12.2023

Contents

Содержание

MECHANICS

UDC 531.36 Original article
https://doi.org/10.23947/2687-1653-2023-23-4-346-355

Software Control of the Movement of a Differential Drive Robot for Different I

EDN: INDAIS

Maksim S. Salimov ✉, **Igor V. Merkuryev**
National Research University "Moscow Power Engineering Institute", Moscow, Russian Federation
✉ SalimovMS@mpei.ru

Abstract
Introduction. Designing motion control systems for mobile robots requires the construction of mathematical models. Researchers have repeatedly addressed this topic. In particular, works have been published on the calculations of multiphysical processes, modeling the movement of various types of wheels under certain conditions. In addition, the dynamics of deformable contacting bodies during sliding, rolling and rotation, issues of autonomy and controllability of mobile robots were considered. Note, however, that the dynamics and positioning accuracy of wheeled robots is largely determined by friction. The literature does not present studies on the dynamics of a robot with a differential drive taking into account the interrelationships of sliding, spinning and rolling friction effects based on the theory of multicomponent friction. Research in this area can reveal new dynamic effects. Based on the data obtained in this way, it is possible to improve the accuracy of positioning in building mathematical control models. The presented work aims at investigating the movement of an automatic device with a differential drive taking into account three contact models: nonholonomic, Coulomb friction, and multicomponent models.
Materials and Methods. The scheme of a two-wheeled robot with differential drive and continuous movement on the support surface was adopted as the basic one. The movement of the device was provided through software control. The dynamics was described in the form of Appel equations. Mathematical models were used for calculations, taking into account friction in different ways. Coordination of the actions of the mechanism was formed at a dynamic level. The control actions were the moments of the wheel motors. When visualizing the models under study, the built-in numerical methods of the Wolfram Mathematica system were used with a minimum accuracy of 10^{-6}.
Results. When building a mathematical model, the equations for the angular velocities of the wheels were determined. The authors took into account the presence of a contact site and derived the equations of dynamics of a differential drive robot. The elements of the system were force and moment projections, indicators of platform spin, masses, angular accelerations, and inertia of the wheels. It was shown how control actions were formed within the framework of nonholonomic mechanics. The model of engines that created a moment of control on the driving wheels was described. The solution was derived as the relationship between the inductance of the conductors of electric motors and the operation of the power supply. Three models describing the dynamics of a differential drive robot were examined in detail. The first model was nonholonomic. The second and third included a system of equations for the dynamics of a differential drive robot for a general case with a contact platform. At the same time, in the second model, the switching time in the engine was ignored and the Coulomb friction was involved. In the third model, a parameter to determine the speed of transients in the engine was introduced, and Pade decomposition was involved. This was a model with multicomponent friction. The calculation results were shown in the form of graphs. On them, the studied models were visualized in the form of curves of different colors. Comparison of the graphs showed in which cases, after the completion of transients, the control provided the required accuracy. These were models 1 and 2. In model 3, the software control generated an error in the angular velocity of rotation of the platform. This error could not be predicted within the framework of the 1st and 2nd models. In all the systems considered, the sliding speed of the wheels in the transverse direction dropped to zero. The condition of continuous motion of the support wheel was obtained and validated.
Discussion and Conclusion. Software control is acceptable in models that do not take into account wheel friction during simultaneous sliding, spinning and rolling (general case of spatial motion). However, it is important to consider the relationship bet ween these processes and multicomponent friction. This is required for the robot to perform program movements more accurately. It was established that software control in a model that takes into account the friction of

spinning and rolling caused deviations from the program values of the angular velocity of the platform. The results obtained can be used in the building of a control system with predictive models.

Keywords: software control of a robot, control in nonholonomic mechanics, Coulomb friction model, multicomponent friction, error in angular velocity of rotation

Acknowledgements. The authors appreciate the Department of Robotics, Mechatronics, Dynamics and Strength of Machines, National Research University MPEI, for assistance in preparing the article. We would like to thank the reviewers for their criticism and suggestions, which contributed to a significant improvement in the quality of the article.

For citation. Salimov MS, Merkuryev IV. Software Control of the Movement of a Differential Drive Robot for Different Friction Models. *Advanced Engineering Research (Rostov-on-Don)*. 2023;23(4):346–355. https://doi.org/10.23947/2687-1653-2023-23-4-346-355

Научная статья

Программное управление движением робота с дифференциальным приводом при разных моделях трения

М.С. Салимов ✉, **И.В. Меркурьев**
Национальный исследовательский университет «Московский энергетический институт»,
г. Москва, Российская Федерация
✉ SalimovMS@mpei.ru

Аннотация
Введение. Проектирование систем управления движением мобильных роботов требует построения математических моделей. Исследователи неоднократно обращались к этой теме. В частности, опубликованы работы, посвященные расчетам мультифизических процессов, моделированию движения различных видов колес в тех или иных условиях. Кроме того, рассматривались динамика деформируемых контактирующих тел при скольжении, качении и вращении, вопросы автономности и управляемости мобильных роботов. Отметим, что динамика и точность позиционирования колесных роботов во многом определяется трением. В литературе не представлены исследования динамики робота с дифференциальным приводом с учетом взаимосвязей эффектов трения скольжения, верчения и качения на основе теории поликомпонентного трения. Изыскания в этой области способны выявить новые динамические эффекты. Основываясь на полученных таким образом данных, можно заняться повышением точности позиционирования при построении математических моделей управления. Цель представленной работы — исследовать движение автоматического устройства с дифференциальным приводом с учетом трех моделей контакта: неголономного, кулоновского трения и поликомпонентного.
Материалы и методы. В качестве базовой приняли схему двухколесного робота с дифференциальным приводом и безотрывным движением по опорной поверхности. Перемещение устройства обеспечивалось программным управлением. Динамику описали в виде уравнений Аппеля. Для вычислений использовали математические модели, по-разному учитывающие трение. Координация действий механизма формировалась на динамическом уровне. Управляющие воздействия — моменты двигателей колес. При визуализации исследуемых моделей задействовали встроенные численные методы системы Wolfram Mathematica («Вольфрам математика») с минимальной точностью 10^{-6}.
Результаты исследования. При построении математической модели определили равенства для угловых скоростей колес. Учли наличие площадки контакта и вывели уравнения динамики робота с дифференциальным приводом. Элементами системы были проекции силы и момент, показатели верчения платформы, массы, угловые ускорения и инерция колес. Показали, как формируются управляющие воздействия в рамках неголономной механики. Описали модель двигателей, которые создают момент управления на ведущих колесах. Вывели решение как взаимосвязь индуктивности проводников электродвигателей и работы электропитания. Детально рассмотрели три модели, описывающие динамику робота с дифференциальным приводом. Первая — неголономная. Вторая и третья включали систему уравнений динамики робота с дифференциальным приводом для общего случая, при наличии площадки контакта. При этом во второй модели игнорируется время переключений в двигателе и задействуется трение Кулона. В третьей ввели параметр, определяющий скорость переходных процессов в двигателе, и задействовали разложения Паде. Это модель с поликомпонентным трением. Итоги расчетов показали в виде графиков. На них исследуемые модели визуализировали в виде кривых разного цвета. Сопоставление графиков показало, в каких случаях после завершения переходных процессов управление обеспечит требуемую точность.

Это модели 1 и 2. В модели 3 программное управление генерирует ошибку в угловой скорости вращения платформы. Данную ошибку нельзя спрогнозировать в рамках 1-й и 2-й модели. Во всех рассмотренных системах скорость скольжения колес в поперечном направлении падает до нуля. Получено и обосновано условие безотрывного движения опорного колеса.

Обсуждение и заключение. Программное управление допустимо в моделях, не учитывающих трение колес при одновременном скольжении, верчении и качении (общий случай пространственного движения). Однако важно учитывать взаимосвязь данных процессов и поликомпонентного трения. Это необходимо для более точного выполнения роботом программных движений. Установлено, что программное управление в модели, учитывающей трение верчения и качения, приводит к отклонениям от программных значений угловой скорости платформы. Полученные результаты можно использовать при построении системы управления с прогнозирующими моделями.

Ключевые слова: программное управление роботом, управление в неголономной механике, модель трения Кулона, поликомпонентное трение, ошибка угловой скорости вращения

Благодарности. Авторы выражают признательность кафедре «Робототехника, мехатроника, динамика и прочность машин» ФГБОУ ВО «НИУ «МЭИ» за помощь в подготовке статьи. Благодарим рецензентов за конструктивную критику и предложения, которые способствовали значительному повышению качества статьи.

Для цитирования. Салимов М.С., Меркурьев И.В. Программное управление движением робота с дифференциальным приводом при разных моделях трения. *Advanced Engineering Research (Rostov-on-Don)*. 2023;23(4):346–355. https://doi.org/10.23947/2687-1653-2023-23-4-346-355

Introduction. In the modern world, the demand for automatic mobile wheeled vehicles is growing, and the possibilities of coordinating their operation are being actively explored. Issues of autonomy and controllability of mobile robots are of considerable scientific and applied interest. In particular, approaches to the calculations of multiphysical processes, simulating the movement of specific types of wheels under different conditions are considered. Some studies focus on the dynamics of deformable contacting bodies during sliding, rolling and rotation. The results of these studies are used in robotics [1-3]. The control of mobile wheeled vehicles is considered on the example of electric scooters “Segway” [4].

Mobile mechanisms with simple and efficient wheel motion control systems are needed primarily for operating in narrow spaces [5], for conducting research under difficult industrial conditions [6].

In [7-11], the possibilities of accurate modeling of the dynamics of wheeled vehicles are shown, taking into account the sliding, spinning, and rolling of the wheels.

At the same time, the phenomena arising from the combination of friction effects are not described in the literature. The presented work aims at investigating the effect of multicomponent friction on the dynamics of a robot with a differential drive. Tasks involve building a mathematical model of robot movement with multicomponent friction and simulating program movements.

Materials and Methods. The scheme of a two-wheeled differential drive robot is considered (Fig. 1). The continuous movement of wheels of radius R along the support surface is assumed.

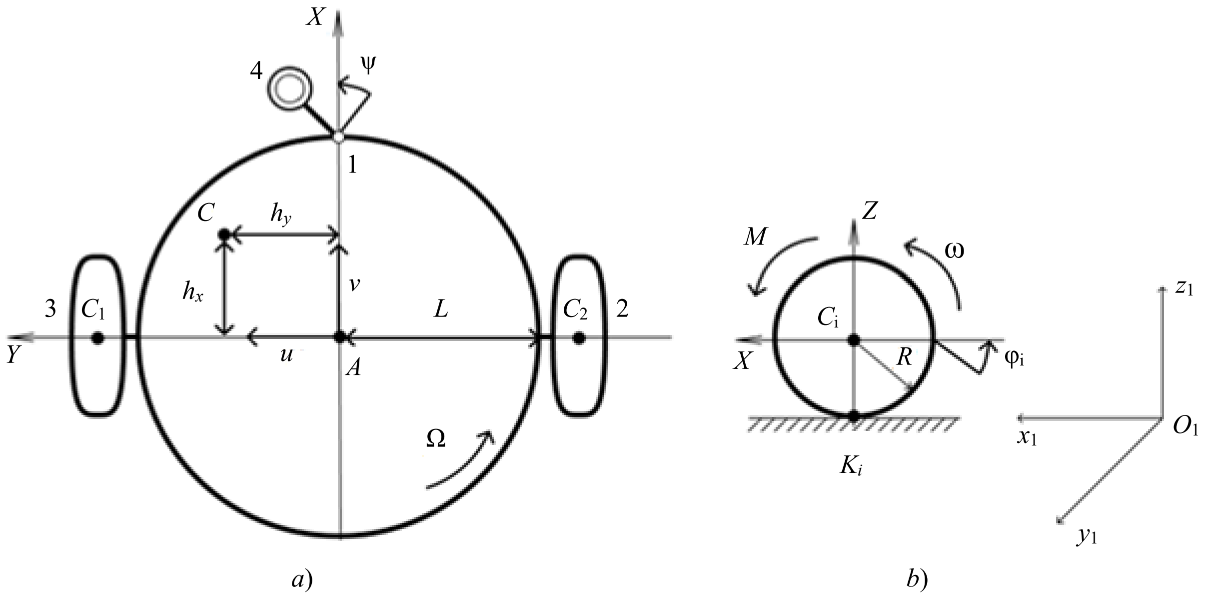

Fig. 1. Kinematic diagram of the robot: *a* — platform; *b* — one of the driving wheels

The gravity center of platform C is shifted relative to the geometric center of platform A along X axis by distance h_x, along Y — axis — by distance h_y. Points C_1 and C_2 — centers of mass of the wheels (index 1 corresponds to the left wheel, index 2 —to the right).

The following designations are introduced: m_1 — mass of the robot platform; J_{Cz} — moment of inertia of the platform relative to the center of mass C; O_1, x_1, y_1 — fixed coordinate system; x_A, y_A determine the position of point A in O_1, x_1, y_1; ψ — angle of the course of the platform; φ_i — wheel steering angles (index 1 corresponds to the left wheel, index 2 — to the right); $AC_1 = AC_2 = L$ — wheels width; M_1, M_2 — engine torques applied to the wheels.

It is assumed that only the normal bearing reaction acts on the support wheel 4 (Fig. 1). On the move, the support wheel is located on X axis at a distance R_0 from the center of the platform $(R_0 < L)$.

Research Results

Mathematical model of robot dynamics. When describing the movement of a differential drive robot in the framework of nonholonomic mechanics, expressions are used that take into account the limitations associated with zero wheel slip relative to the surface:

$$\upsilon_{K_1x} = 0, \upsilon_{K_2x} = 0, \upsilon_{K_1y} = 0, \upsilon_{K_2y} = 0, \tag{1}$$

where $\upsilon_{K_1x}, \upsilon_{K_2x}, \upsilon_{K_1y}, \upsilon_{K_2y}$ — projections on X and Y axes of velocities of points K_1 and K_2, which are centers of the contact areas of the wheels and the supporting surface.

Note that for a nonholonomic model, a point contact of the wheels and the surface is assumed, i.e., the contact area of each wheel degenerates into a single point of contact.

Consider the expressions:

$$\begin{aligned} \upsilon_{K_1x} &= \upsilon - \Omega L - R\omega_1, \\ \upsilon_{K_2x} &= \upsilon + \Omega L - R\omega_2, \\ \upsilon_{K_1y} &= \upsilon_{K_2y} = \upsilon_{Cy} = u. \end{aligned} \tag{2}$$

With their help, equality for the angular velocities of the wheels can be obtained:

$$\omega_1 = \frac{\upsilon - \Omega L}{R}, \omega_2 = \frac{\upsilon + \Omega L}{R}. \tag{3}$$

In the general case, when the presence of a contact platform is assumed, we obtain the equations of dynamics of a differential drive robot:

$$\begin{aligned} & m_1\left[\dot{\upsilon} - h_y\dot{\Omega} - \Omega\left(u + h_x\Omega\right)\right] + 2m_\kappa\left(\dot{\upsilon} - \Omega u\right) = F_{\|_1}\cos\alpha_1 + F_{\|_2}\cos\alpha_2 - F_{\perp_1}\sin\alpha_1 - F_{\perp_2}\sin\alpha_2, \\ & m_1\left[\dot{u} + h_x\dot{\Omega} + \Omega\left(\upsilon - h_y\Omega\right)\right] + 2m_\kappa\left(\dot{u} + \Omega\upsilon\right) = F_{\|_1}\sin\alpha_1 + F_{\|_2}\sin\alpha_2 - F_{\perp_1}\cos\alpha_1 - F_{\perp_2}\cos\alpha_2, \\ & \dot{\Omega}\left(J_{Cz} + 2J_{Kz} + m_1\left(h_x^2 + h_y^2\right) + 2m_\kappa L^2\right) + m_1\left[\left(\dot{u} + \Omega\upsilon\right)h_x - h_y\left(\dot{\upsilon} - \Omega u\right)\right] = \\ & M_{C_1} + M_{C_2} + \left(F_{\|_2}\cos\alpha_2 - F_{\perp_2}\sin\alpha_2 - F_{\|_1}\cos\alpha_1 + F_{\perp_1}\sin\alpha_1\right)L, \\ & J_{Ky}\dot{\omega}_1 = M_1 - M_{y_1} - \left(F_{\|_1}\cos\alpha_1 - F_{\perp_1}\sin\alpha_1\right)R, \\ & J_{Ky}\dot{\omega}_2 = M_2 - M_{y_2} - \left(F_{\|_2}\cos\alpha_2 - F_{\perp_2}\sin\alpha_2\right)R. \end{aligned} \tag{4}$$

Here, $F_{\|_1}, F_{\|_2}$ — projections of the friction force on the directions of the slip speeds of the centers of the wheel contact patches; $F_{\perp_1}, F_{\perp_2}$ — projections of the friction force in directions perpendicular to the speeds of the centers of the wheel contact patches; M_{c_1}, M_{c_2} — summands of the friction torque under spinning for two wheels; $\dot{\Omega}$ — angular acceleration of platform spinning; $\dot{\omega}_1, \dot{\omega}_2$ — angular accelerations of wheels projected onto their axis of rotation; m_K — weight of each wheel; J_{Ky} and J_{Kz} — inertia torques of the wheel relative to the corresponding axes.

To form the control actions, a model of the robot dynamics described in the framework of nonholonomic mechanics is used [12]:

$$m_1\left[\dot{\upsilon} - h_y\dot{\Omega} - \Omega h_x\Omega\right] + 2m_\kappa\dot{\upsilon} + \frac{2J_{Ky}}{R^2}\dot{\upsilon} = \frac{M_1 + M_2}{R},$$

$$m_1\left[\left(+h_x\dot{\Omega}+\Omega\left(\upsilon-h_y\Omega\right)\right)h_x-h_y\left(\dot{\upsilon}-h_y\dot{\Omega}-\Omega h_x\Omega\right)\right]+$$
$$\dot{\Omega}\left(J_{Cz}+2J_{Kz}+m_1\left(h_x^2+h_y^2\right)+2m_\kappa L^2\right)+2J_{Ky}\frac{L^2}{R^2}\dot{\Omega}=\frac{\left(M_2-M_1\right)L}{R}. \tag{5}$$

It can also be represented as:

$$F_\upsilon=\frac{M_1+M_2}{R},M_\Omega=\frac{\left(M_2-M_1\right)L}{R}, \tag{6}$$

where F_υ and M_Ω — left sides of the equation (5).

Model of engines on driving wheels. Let us describe a model of engines capable of generating control torque on driving wheels M_1, M_2.

The equations of motion of wheeled DC motors can be expressed by the formulas [13]:

$$L_e\frac{d\left(i_k\right)}{dt}+Ri_k=U_k-c_1\omega_k,$$
$$M_k=c_2 i_k,\ \left(k=1,2\right). \tag{7}$$

Here, L_e — inductance of electric motor conductors; R — resistance to electric current in the motor circuit; U_k — power supply for the engine k; i_k — current passing through the motor armature circuit; c_1, c_2 — structural constants of engines.

It is assumed that the drive wheel motors have the same characteristic. From (7), it can be seen that

$$i_k=\frac{M_k}{c_2}. \tag{8}$$

Given (8), in the first equation from system (7), we obtain a differential equation with respect to moment M_κ :

$$\frac{L_e}{c_2}\dot{M}_k+\frac{R}{c_2}M_k=U_k-c_1\omega_k. \tag{9}$$

Equation (9) is divided by multiplier $\frac{R}{c^2}$, and we get:

$$\frac{L_e c_2}{c_2 R}\dot{M}_k+M_k=\frac{c_2}{R}U_k-\frac{c_1 c_2}{R}\omega_k. \tag{10}$$

Let us introduce the notation:

$$T_1=\frac{L_e c_2}{c_2 R},K_1=\frac{c_1 c_2}{R},K_2=\frac{c_2}{R}\ . \tag{11}$$

In this case, the control moments can be described:

$$T_1\dot{M}_k+M_k=K_2U_k-K_1\omega_k, \tag{12}$$

where K_1, K_2 — constants; T_1 — parameter that determines the speed of transients in the electrical part of engines.

When ignoring the switching time in the electromechanical system of the engine:

$$M_k=K_2U_k-K_1\omega_k. \tag{13}$$

Авторы [14] получили похожие формулы.

The authors [14] obtained similar formulas.

Model under study. Let us consider models describing the dynamics of a differential drive robot.

Model 1 is described by equations (6) and (12), when the duration of transients is assumed to be vanishingly small $T_1=0$:

$$m_1\left[\dot{\upsilon}-h_y\dot{\Omega}-\Omega h_x\Omega\right]+2m_\kappa\dot{\upsilon}+\frac{2J_{Ky}}{R^2}\dot{\upsilon}=\frac{K_2U_1-K_1\omega_1+K_2U_2-K_1\omega_2}{R},$$
$$m_1\left[\left(+h_x\dot{\Omega}+\Omega\left(\upsilon-h_y\Omega\right)\right)h_x-h_y\left(\dot{\upsilon}-h_y\dot{\Omega}-\Omega h_x\Omega\right)\right]+2J_{Ky}\frac{L^2}{R^2}\dot{\Omega}+$$
$$+\dot{\Omega}\left(J_{Cz}+2J_{Kz}+m_1\left(h_x^2+h_y^2\right)+2m_\kappa L^2\right)=\frac{\left(\left(K_2U_2-K_1\omega_2\right)-\left(K_2U_1-K_1\omega_1\right)\right)L}{R}. \tag{14}$$

Here, ω_1, ω_2 are calculated by formulas (3).

Equations (4), (13), as well as the Coulomb friction model, are used to describe Model 2:

$$F_{\parallel_i}=-fN_i,F_{\perp_i}=0,M_{C_i}=0. \tag{15}$$

Model 3 is represented by equations (4), (12). In addition, multicomponent friction presented in [12] with the help of Pade decompositions is taken into account:

$$F_{\parallel_i} = -fN_i \frac{\sqrt{\upsilon^2_{K_ix}+\upsilon^2_{K_iy}} + k_r I_1 I_2 \Omega \dfrac{2I_1 - k_r I_2 \cos\left(\dfrac{\pi}{2}-\alpha\right)}{I_0}\cos\left(\dfrac{\pi}{2}-\alpha\right)}{\sqrt{\upsilon^2_{K_ix}+\upsilon^2_{K_iy}} + \dfrac{2I_1 - k_r I_2 \cos\left(\dfrac{\pi}{2}-\alpha\right)}{I_0}\left|\Omega\right|}, \tag{16}$$

$$F_{\perp_i} = -fN_i \frac{k_r \pi \Omega}{k_r I_1 I_2 \dfrac{2I_1 - k_r I_2 \cos\left(\dfrac{\pi}{2}-\alpha\right)}{I_0}\cos\left(\dfrac{\pi}{2}-\alpha\right)\sqrt{\upsilon^2_{K_ix}+\upsilon^2_{K_iy}} + \left|\Omega\right|}, \tag{17}$$

$$M_{C_i} = -2f\pi I_2 \frac{\dfrac{k_r I_3 \cos\left(\dfrac{\pi}{2}-\alpha\right)}{2I_2}\left(\dfrac{2I_2}{I_3} - k_r\cos\left(\dfrac{\pi}{2}-\alpha\right)\right)\sqrt{\upsilon^2_{K_ix}+\upsilon^2_{K_iy}} + \Omega}{\left(\dfrac{2I_2}{I_3} - k_r\cos\left(\dfrac{\pi}{2}-\alpha\right)\right)\sqrt{\upsilon^2_{K_ix}+\upsilon^2_{K_iy}} + \left|\Omega\right|}, \tag{18}$$

$$M_{\perp_i} = -k_r \pi I_3 \frac{\omega_i}{\left|\omega_i\right|}. \tag{19}$$

Here, I_1, I_2, I_3 constants that are found from the formulas in [12]; α — angle characterizing the direction of linear sliding speeds relative to the contact points of wheels K_1, K_2; k_r — coefficient whose sign depends on the rolling direction.

To determine the program control, the motion laws of the robot should be specified $\upsilon^d(t), \Omega^d(t)$. . By (5), it is possible to express values $F_\upsilon = F^d_\Omega(t)$, $F_\upsilon = F^d_\Omega(t)$, $M_\Omega = M^d_\Omega(t)$ depending on time. We use known values F_υ, M_Ω to calculate control voltages U_1 and U_2, supplied to the wheel drives:

$$U_2 = \frac{1}{K_2}\left(\frac{R}{2}\left(F_\upsilon + \frac{M_\Omega}{L}\right) + K_1\omega_2\right), U_1 = \frac{1}{K_2}\left(\frac{R}{2}\left(F_\upsilon - \frac{M_\Omega}{L}\right) + K_1\omega_1\right). \tag{20}$$

The motion of the system with the given initial conditions $\upsilon(0) = 0.5\frac{m}{s}$, $u(0) = 0.2\frac{m}{s}$, $\Omega(0) = 0.2\frac{1}{s}$ was modeled in the Wolfram Mathematica package.

Consider $\upsilon^d(t) = 0.5\ \frac{m}{s}$, $\Omega^d(t) = 0.3\frac{1}{s}$. To integrate the system, the integration step was automatically selected and the built-in numerical methods of Wolfram Mathematica were used with an accuracy of the results of at least 10^{-6}.

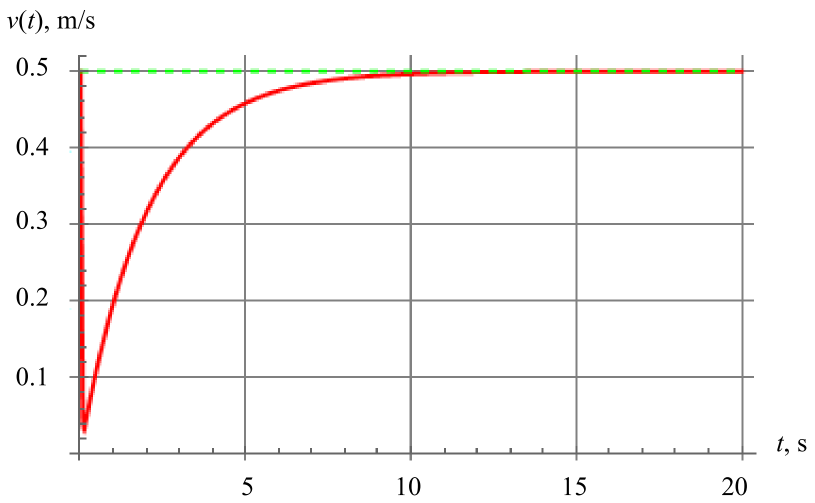

Fig. 2. Dependence of longitudinal velocity υ. Green curve — nonholonomic model 1; red curve — model 2 with Coulomb friction; blue curve — model 3 with multicomponent friction. Blue and red curves coincide

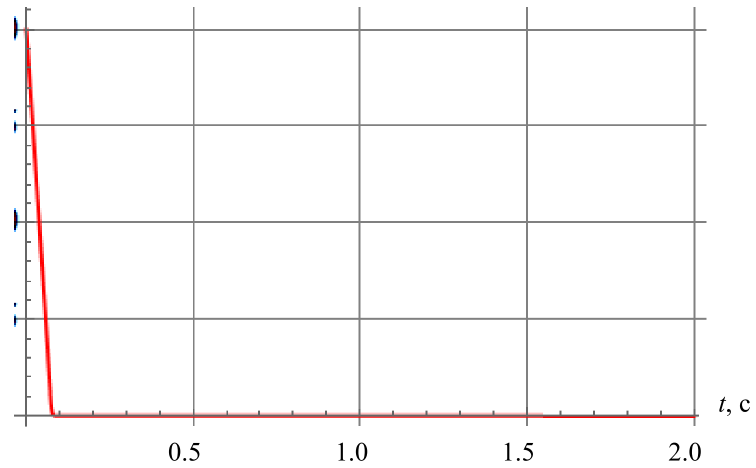

Fig. 3. Dependence of transverse velocity u. Green curve — nonholonomic model 1; red curve — model 2 with Coulomb friction; blue curve — model 3 with multicomponent friction. Green, blue and red curves coincide

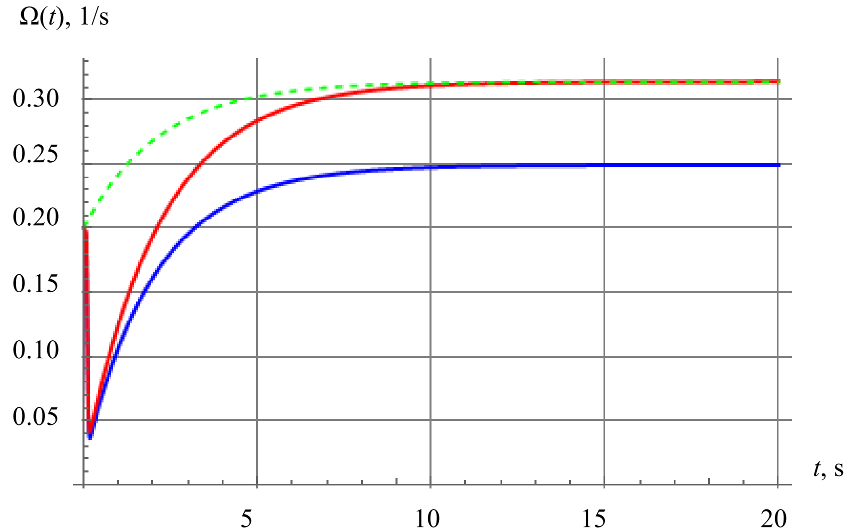

Fig. 4. Dependence of angular velocity of the robot. Green curve — nonholonomic model 1; red curve — model 2 with Coulomb friction, blue curve — model 3 with multicomponent friction

Figures 2 and 4 show that the control guarantees faithful realization of the program laws of motion after the completion of transients in models 1 (nonholonomic) and 2 (with Coulomb friction). In Model 3 (multicomponent sliding, rolling and twisting friction), after the completion of transients due to software control, a constant error occurs in the angular velocity of platform rotation. In all the models considered, the sliding speed of the wheels in the transverse direction quickly decreases to zero. The cases of matching dependences obtained for different models are shown in Figures 2 and 3.

To check the fulfillment of the conditions of continuous motion of the supporting wheel, we write down the theorem on the variation of the kinetic moment of the system in projections on Y axis:

$$J_{Ky}(\dot{\omega}_1+\dot{\omega}_2)=M_1+M_2-M_{y_1}-M_{y_2}-N_3R_0+m_1gh_x-\left(F_{\|_1}\cos\alpha_1-F_{\perp_1}\sin\alpha_1+F_{\|_2}\cos\alpha_2-F_{\perp_2}\sin\alpha_2\right)R.$$

According to (4):

$$M_1+M_2=-N_3R_0+m_1gh_x.$$

From the last equation, we obtain the condition of continuous motion of the supporting wheel:

$$m_1gh_x-(M_1+M_2)>0.$$

Considering (5):

$$m_1gh_x-R(m_1+2m_k+\frac{2J_{Ky}}{R^2})\dot{\upsilon}+Rm_1[h_y\dot{\Omega}+h_x\Omega^2]>0.$$

The robot's accelerations did not exceed 1 m/s^2; therefore, this inequality is fulfilled at every moment of time.

Discussion and Conclusion. The simulation results allowed for drawing a number of conclusions. Software control based on nonholonomic model 1 is acceptable for robots whose design does not take into account the contact friction of the wheels that occurs under a combination of sliding, spinning and rolling. However, when forming control actions, to achieve more accurate adherence to the program motion laws, it is required to take into account the model of multicomponent friction. The resulting solution can be used to build a control system with a model predictive control. Such a development will be the subject of further research.

References

1. Gerasimov KV, Zobova AA, Kosenko II. Omni-Vehicle Dynamical Models Mutual Matching for Different Roller-Floor Contact Models. In: *Proc. European Congress on Computational Methods in Applied Sciences and Engineering "Multibody Dynamics"*. Cham: Springer; 2019. P. 511–517. http://doi.org/10.1007/978-3-030-23132-3_61

2. Zobova AA, Habra T, Van der Noot N, Dallali H, Tsagarakis NG, Fisette P, et al. Multi-Physics Modelling of a Compliant Humanoid Robot. *Multibody System Dynamics*. 2017;39:95–114. https://doi.org/10.1007/s11044-016-9545-4

3. Gerasimov KV, Zobova AA. On the Motion of a Symmetrical Vehicle with Omniwheels with Massive Rollers. *Mechanics of Solids*. 2018;53:32–42. https://doi.org/10.3103/S0025654418050060

4. Corke P. Robot Arm Kinematics. In book: *Robotics, Vision and Control*, 2nd ed. Cham: Springer; 2017. P. 193–228. https://doi.org/10.1007/978-3-319-54413-7_7

5. Junjie Shen, Dennis Hong. OmBURo: A Novel Unicycle Robot with Active Omnidirectional Wheel. In: *Proc. IEEE Int. Conf. on Robotics and Automation* (*ICRA*). New York City: IEEE; 2020. P. 11–19. https://doi.org/10.1109/ICRA40945.2020.9196927

6. Munitsyn LV. Vibrations of a Rigid Body with Cylindrical Surface on a Vibrating Foundation. *Mechanics of Solids*. 2017;52:675–685. https://doi.org/10.3103/S0025654417060073

7. Goryacheva IG, Zobova AA. Dynamics of Deformable Contacting Bodies with Sliding, Rolling, and Spinning. *International Journal of Mechanical Sciences*. 2022;216:106981. https://doi.org/10.1016/j.ijmecsci.2021.106981

8. Zobova AA, Goryacheva IG. Effect of Contacting Bodies' Mechanical Properties on the Dynamics of a Rolling Cylinder. *Acta Mechanica*. 2020;232(5):1971–1982. http://doi.org/10.1007/s00707-020-02800-w

9. Kireenkov AA, Zhavoronok SI, Nushtaev DV. On Tire Models Accounting for Both Deformed State and Coupled Dry Friction in a Contact Spot. *Computer Research and Modeling*. 2021;13(1):163–173. https://doi.org/10.20537/2076-7633-2021-13-1-163-173

10. Kireenkov AA, Zhavoronok SI. Coupled Dry Friction Models in Problems of Aviation Pneumatics' Dynamics. *International Journal of Mechanical Sciences*. 2017;127:198–203. http://doi.org/10.1016/j.ijmecsci.2017.02.004

11. Kireenkov AA, Fedotenkov GV, Shiriaev A, Zhavoronok SI. Application of the Theory of the Multicomponent Dry Friction in Some of Control Robot Systems. *International Journal for Computational Civil and Structural Engineering*. 2022;18(1):14–23. https://doi.org/10.22337/2587-9618-2022-18-1-14-23

12. Salimov MS, Saypulaev GR, Merkuriev IV. Four-Dimensional Integral Model of Dry Friction on the Example of Wheel Movement. *Journal of Physics: Conference Series*. 2021;2096:012043. https://doi.org/10.1088/1742-6596/2096/1/012043

13. Alaci S, Ciornei FC, Pentiuc RD, Ciornei MC, Românu IC. Indetermination versus Incompatibility in Dynamic Systems with Dry Friction. *Journal of Physics: Conference Series*. 2020;1426:012011. https://doi.org/10.1088/1742-6596/1426/1/012011

14. Long Chen, Jun Liu, Hai Wang, Youhao Hu, Xuefeng Zheng, Mao Ye, et al. Robust Control of Reaction Wheel Bicycle Robot via Adaptive Integral Terminal Sliding Mode. *Nonlinear Dynamics*. 2021;104:2291–2302. https://doi.org/10.1007/s11071-021-06380-9

Список литературы

1. Gerasimov K.V., Zobova A.A., Kosenko I.I. Omni-Vehicle Dynamical Models Mutual Matching for Different Roller-Floor Contact Models. In: *Proc. European Congress on Computational Methods in Applied Sciences and Engineering "Multibody Dynamics"*. Cham: Springer; 2019. P. 511–517. http://doi.org/10.1007/978-3-030-23132-3_61

2. Zobova A.A., Habra T., Van der Noot N., Dallali H., Tsagarakis N.G., Fisette P., et al. Multi-Physics Modelling of a Compliant Humanoid Robot. *Multibody System Dynamics*. 2017;39:95–114. https://doi.org/10.1007/s11044-016-9545-4

3. Gerasimov K.V., Zobova A.A. On the Motion of a Symmetrical Vehicle with Omniwheels with Massive Rollers. *Mechanics of Solids*. 2018;53:32–42. https://doi.org/10.3103/S0025654418050060

4. Corke P. Robot Arm Kinematics. In book: *Robotics, Vision and Control*, 2nd ed. Cham: Springer; 2017. P. 193–228. https://doi.org/10.1007/978-3-319-54413-7_7

5. Junjie Shen, Dennis Hong. OmBURo: A Novel Unicycle Robot with Active Omnidirectional Wheel. In: *Proc. IEEE Int. Conf. on Robotics and Automation* (*ICRA*). New York City: IEEE; 2020. P. 11–19. https://doi.org/10.1109/ICRA40945.2020.9196927

6. Munitsyn L.V. Vibrations of a Rigid Body with Cylindrical Surface on a Vibrating Foundation. *Mechanics of Solids*. 2017;52:675–685. https://doi.org/10.3103/S0025654417060073

7. Goryacheva I.G., Zobova A.A. Dynamics of Deformable Contacting Bodies with Sliding, Rolling, and Spinning. *International Journal of Mechanical Sciences.* 2022;216:106981. https://doi.org/10.1016/j.ijmecsci.2021.106981

8. Zobova A.A., Goryacheva I.G. Effect of Contacting Bodies' Mechanical Properties on the Dynamics of a Rolling Cylinder. *Acta Mechanica*. 2020;232:1971–1982. http://doi.org/10.1007/s00707-020-02800-w

9. Киреенков А.А., Жаворонок С.И., Нуштаев Д.В. О моделях шины, учитывающих как деформированное состояние, так и эффекты сухого трения в области контакта. *Компьютерные исследования и моделирование*. 2021;13(1):163–173. https://doi.org/10.20537/2076-7633-2021-13-1-163-173

10. Kireenkov A.A., Zhavoronok S.I. Coupled Dry Friction Models in Problems of Aviation Pneumatics' Dynamics. *International Journal of Mechanical Sciences*. 2017;127:198–203. http://doi.org/10.1016/j.ijmecsci.2017.02.004

11. Kireenkov A.A., Fedotenkov G.V., Shiriaev A., Zhavoronok S.I. Application of the Theory of the Multicomponent Dry Friction in Some of Control Robot Systems. *International Journal for Computational Civil and Structural Engineering.* 2022;18(1):14–23. https://doi.org/10.22337/2587-9618-2022-18-1-14-23

12. Salimov M.S., Saypulaev G.R., Merkuriev I.V. Four-Dimensional Integral Model of Dry Friction on the Example of Wheel Movement. *Journal of Physics: Conference Series.* 2021;2096:012043. https://doi.org/10.1088/1742-6596/2096/1/012043

13. Alaci S., Ciornei F.C., Pentiuc R.D., Ciornei M.C., Românu I.C. Indetermination versus Incompatibility in Dynamic Systems with Dry Friction. *Journal of Physics: Conference Series*. 2020;1426:012011. https://doi.org/10.1088/1742-6596/1426/1/012011

14. Long Chen, Jun Liu, Hai Wang, Youhao Hu, Xuefeng Zheng, Mao Ye, et al. Robust Control of Reaction Wheel Bicycle Robot via Adaptive Integral Terminal Sliding Mode. *Nonlinear Dynamics*. 2021;104:2291–2302. https://doi.org/10.1007/s11071-021-06380-9

Received 20.09.2023
Revised 20.10.2023
Accepted 07.11.2023

About the Authors:

Maksim S. Salimov, Teaching assistant of Department of Robotics, Mechatronics, Dynamics and Strength of Machines, National Research University MPEI (14, Krasnokazarmennaya St., Moscow, 111250, RF), SPIN-code: 7721-7434, ORCID, SalimovMS@mpei.ru

Igor V. Merkuryev, Dr.Sci. (Eng.), Associate Professor, Head of the Department of Robotics, Mechatronics, Dynamics and Strength of Machines, National Research University MPEI (14, Krasnokazarmennaya St., Moscow, 111250, RF), SPIN-code: 1608-9638, ScopusID, ORCID, MerkuryevIV@mpei.ru

Claimed contributorship:
MS Salimov: research objectives and tasks formulation, text preparation, computational analysis.
IV Merkuryev: academic advising, analysis of the research results, revision of the text, correction of the conclusions.

Conflict of interest statement: the authors do not have any conflict of interest.

All authors have read and approved the final manuscript.

Поступила в редакцию 20.09.2023
Поступила после рецензирования 20.10.2023
Запланирована в номер 07.11.2023

Об авторах

Максим Сергеевич Салимов, ассистент кафедры робототехники, мехатроники, динамики и прочности машин Национального исследовательского университета «МЭИ» (111250, РФ, г. Москва, ул. Красноказарменная, 14), SPIN-код: 7721-7434, ORCID, SalimovMS@mpei.ru

Игорь Владимирович Меркурьев, доктор технических наук, доцент, заведующий кафедрой робототехники, мехатроники, динамики и прочности машин Национального исследовательского университета

«МЭИ» (111250, РФ, г. Москва, ул. Красноказарменная, 14), SPIN-код: 1608-9638, ScopusID, ORCID, MerkuryevIV@mpei.ru

Заявленный вклад соавторов

М.С. Салимов — формирование цели и задачи исследования, подготовка текста, расчеты.

И.В. Меркурьев — научное руководство, анализ результатов исследований, доработка текста, корректировка выводов.

Конфликт интересов: авторы заявляют об отсутствии конфликта интересов.

Все авторы прочитали и одобрили окончательный вариант рукописи.

MECHANICS

UDC 531.133.1
https://doi.org/10.23947/2687-1653-2023-23-4-356-364

Original article

Analysis of Positioning Accuracy in Case of Design Errors in the Installation of Mecanum Wheels of the Mobile Platform

EDN: IQHEGM

Galina V. Pankrateva, Anton E. Mordin, Gasan R. Saypulaev ✉
National Research University "Moscow Power Engineering Institute", Moscow, Russian Federation
✉ saypulaevgr@mail.ru

Abstract

Introduction. Mobile robots capable of omnidirectional movement are widely used in various fields of human activity. To provide high accuracy of positioning of omnidirectional platforms with mecanum wheels, it is required to develop their detailed mathematical models used in the construction of a motion control system. Due to the complicated design of the mecanum wheels, various errors may occur during the construction of omnidirectional platforms, including the error of installing such wheels on the platform. Its effect on the accuracy of the platform movement has not been studied before. This work aims at assessing the positioning errors that arise due to the presence of design errors in the installation of mecanum wheels, and analyzing the effect of these errors on the accuracy of program motion testing when using control at the kinematic level.

Materials and Methods. The analysis of positioning accuracy was based on mathematical modeling of the platform kinematics, taking into account structural errors in the installation of mecanum wheels. To describe the relationship between the angular speeds of rotation of the wheels and the speeds of the platform, the conditions of nonslip of the contact points on the support surface were used. Numerical calculations were carried out in the *Wolfram Mathematica* package.

Results. A formula was obtained for estimating errors in platform pseudovelocities under program control formed at the kinematic level. The estimation of the errors of the platform speeds for simple movements was carried out. According to the calculation results, it has been shown that the speed errors are significant for robots with mecanum wheels operating autonomously.

Discussion and Conclusion. The calculation results demonstrated the significant impact of wheel installation errors on the positioning accuracy of the mecanum-platform, and confirmed the need to take into account these design errors when creating autonomous mecanum-platforms. The constructed model of the robot's kinematics makes it possible to predict errors in platform speeds that arise under program control, as well as deviations of the coordinates of the geometric center of the platform from the program motion. The proposed kinematic model can be used to improve the positioning accuracy through forming a platform motion control that compensates for the influence of wheel installation errors.

Keywords: mecanum wheel, omnidirectional platform, kinematic model, design errors, program control

Acknowledgements. The authors would like to thank their colleagues for their help in conducting the research and working on the article.

For citation. Pankrateva GV, Mordin AE, Saypulaev GR. Analysis of Positioning Accuracy in Case of Design Errors in the Installation of Mecanum Wheels of the Mobile Platform. *Advanced Engineering Research (Rostov-on-Don).* 2023;23(4):356–364. https://doi.org/10.23947/2687-1653-2023-23-4-356-364

Научная статья

Анализ точности позиционирования при конструкционных погрешностях в установке меканум-колёс мобильной платформы

Г.В. Панкратьева, А.Е. Мордин, Г.Р. Сайпулаев
Национальный исследовательский университет «Московский энергетический институт»,
г. Москва, Российская Федерация
saypulaevgr@mail.ru

Аннотация

Введение. Мобильные роботы, способные осуществлять всенаправленное движение, широко применяются в различных областях человеческой деятельности. Для обеспечения высокой точности позиционирования всенаправленных платформ с меканум-колёсами требуется разработать их детальные математические модели, используемые при построении системы управления движением. Из-за непростой конструкции меканум-колёс при построении всенаправленных платформ могут возникать различные погрешности, включая погрешность установки таких колёс на платформу. Влияние ее на точность движения платформы ранее не исследовалось. Целью данной работы является оценка ошибок позиционирования, возникающих из-за наличия конструкционных погрешностей в установке меканум-колёс, и анализ влияния указанных погрешностей на точность отработки программного движения при использовании управления на кинематическом уровне.

***Материалы и методы*.** Анализ точности позиционирования основан на математическом моделировании кинематики платформы с учетом конструкционных погрешностей в установке меканум-колёс. Для описания взаимосвязи между угловыми скоростями вращения колес и скоростями платформы используются условия непроскальзывания точек контакта по опорной поверхности. Численные расчеты проведены в математическом пакете *Wolfram Mathematica*.

Результаты исследования. Получена формула для оценки погрешностей псевдоскоростей платформы при программном управлении, формируемом на кинематическом уровне. Проведена оценка погрешностей скоростей платформы для простых движений. По результатам расчетов показано, что погрешности скоростей являются значительными для роботов с меканум-колёсами, функционирующих автономно.

***Обсуждение и заключение*.** Результаты расчетов продемонстрировали существенное влияние погрешностей установки колес на точность позиционирования меканум-платформы и подтвердили необходимость учитывать указанные конструкционные погрешности при создании автономных меканум-платформ. Построенная модель кинематики робота позволяет прогнозировать ошибки отработки скоростей платформы, возникающие при программном управлении, а также отклонения координат геометрического центра платформы от программного движения. Кинематическая модель может быть использована для повышения точности позиционирования за счет формирования управления движением платформы, компенсирующего влияние неточностей установки меканум-колёс.

Ключевые слова: меканум-колесо, всенаправленная платформа, кинематическая модель, конструкционные погрешности, программное управление

Благодарности. Авторы выражают признательность коллегам за помощь в проведении исследования и работе над статьей.

Для цитирования. Панкратьева Г.В., Мордин А.Е., Сайпулаев Г.Р. Анализ точности позиционирования при конструкционных погрешностях в установке меканум-колёс мобильной платформы. *Advanced Engineering Research (Rostov-on-Don).* 2023;23(4):356–364. https://doi.org/10.23947/2687-1653-2023-23-4-356-364

Introduction. Mobile robots (or omnidirectional platforms) capable of moving in any direction are widely used in the military, medical, educational, and industrial fields of human activity [1, 2]. The possibility of omnidirectional movement can be achieved by equipping the mobile platform with omni-wheels of various types (mekanum wheels, classic omni-wheels). To provide high accuracy of positioning omnidirectional platforms, it is required to develop their detailed mathematical models for the construction of a motion control system. The need for maintaining high accuracy of movement is associated with the demand to make omnidirectional platforms operate autonomously.

Often, when mathematically modeling the kinematics of mecanum wheels, assumptions are made that simplify the description of the movement of such wheels. Specifically, this is discussed in [3–5]. Thus, in [3, 4], the dynamics of the mecanum platform is considered, taking into account the rolling dry friction forces and the conditions of non-slip contact points, expressed by non-holonomic bonds. In [5], it is emphasized that studying the influence of the finite linear dimensions of the rollers and vibrations associated with this effect on the dynamics of the mecanum platform is of interest.

The urgently needed lines of research on omnidirectional wheels are modeling the effect of the design of the mekanum wheel rollers, and optimizing the shape of rollers [6–9]. The requirement to optimize the shape of rollers is due to the fact that with some forms of omni-wheel rollers, vertical vibrations of contact points may occur when moving omnidirectional platforms (for more information, see the patent review [10]).

Another factor that significantly affects the positioning accuracy of the mecanum platform is the slippage of the contact points of the mecanum wheels with the supporting surface. One of the ways to account for the slippage of contact points when describing kinematics is to use the assumption that the sliding speed is proportional to the product of the angular velocity of rotation of the wheel and the radius of the mecanum wheel, and the proportionality coefficient is considered constant [11, 12]. This assumption allows for reducing the kinematics equations to a problem with nonholonomic connections. However, the experimental results show that the specified coefficient changes with the movement of the platform [13, 14].

It is worth noting that due to the complicated design of the mekanum wheels, various manufacturing errors may occur during the construction of the mekanum platforms. They include the error of installing the mekanum wheels on the platform, small deviations in the shape of the rollers, etc. The influence of inaccuracies in the installation of mekanum wheels on the accuracy of the platform movement has not been studied before. As part of this work, the impact of errors in the installation of mekanum wheels on the positioning accuracy of the omnidirectional platform and its kinematics are investigated.

The article is aimed at assessing positioning errors arising from structural inaccuracies in the installation of mekanum wheels, and analyzing their impact on the precision in movement of an omnidirectional mekanum platform. To do this, it is required to build a mathematical model of the movement of such a platform, taking into account structural errors in the installation of mekanum wheels. The resulting mathematical model can provide for investigation of the influence of these wheels on the positioning accuracy of the mobile platform. This model can be used to form a control that compensates for platform positioning errors.

Materials and methods. Robot design description. As the basis for this study, a robot model in the form of a rectangular platform with four mecanum wheels when moving along a horizontal plane, is considered (Fig. 1). Errors associated with the non-orthogonality of the axes of rotation of the wheels and the longitudinal axis of the platform are taken into account.

To describe the kinematics of the robot, movable coordinate system $Cxyz$, is introduced, associated with the robot platform and the origin in the geometric center of the platform.

The following designations are used in mathematical modeling: h — половина расстояния между осями колёсных пар (при ортогональных осях колёс); l — half the width of the platform; x_i and y_i — abscissa and ordinate of point D_i of fastening the *i*-th wheel drive to the platform; O_i — — geometric center of the *i*-th mecanum wheel; V_L, V_T — longitudinal and transverse velocities of the geometric center of the platform; $s = |D_iO_i|$ — drive shaft length; Ω — angular velocity of the platform spinning; α_i — angle between Cx axis and axis of rotation of the *i*-th wheel (parallel to vector $\overrightarrow{D_iO_i}$) (Fig. 1). Numbers of the platform wheels are indicated in the diagram in Figure 1, and the ellipses on the wheels show the location of the contacting rollers of each wheel.

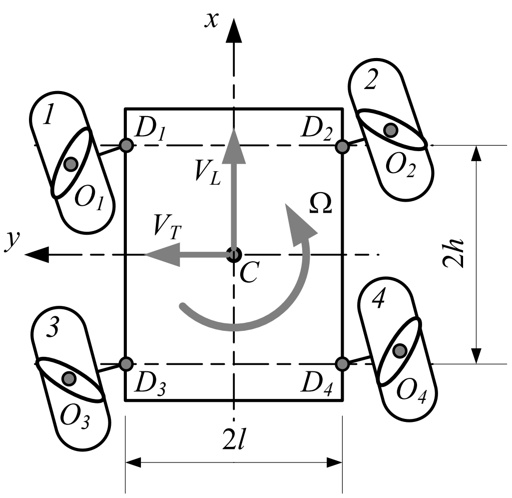

Fig. 1. Kinematic scheme of the platform

Description of the kinematic model construction method. We describe the movement of the platform within the framework of a nonholonomic formulation of the problem using a simplified model of mecanum wheels: the wheel is modeled by a disk with radius R, and the contact point can slip relative to the direction perpendicular to the axis of the contacting roller. At the same time, if there is no error in the arrangement of the wheel axles, there is a relationship between the angular speeds of rotation of the wheels around its own axis $\dot{\varphi}_i$ and the speeds of the platform V_L, V_T, Ω [15]:

$$\dot{\varphi}_i = \frac{1}{R}\left[V_L + V_T \tan\delta_i - \left(y_i - x_i \tan\delta_i\right)\Omega\right], \tag{1}$$

where δ_i — angle between the direction of the axis of the contacting roller and the plane of the mecanum wheel.

To study the influence of structural errors, it is needed to describe the relationship between angular velocities of the wheels $\dot{\varphi}_i$ and speeds of the platform V_L, V_T, Ω taking into account the errors associated with the location of the wheel axles. The parameters of the platform design and wheel arrangement are given in Table 1.

Table 1

Platform design parameters

i	x_i	y_i	δ_i	α_i	d_i
1	h	l	–45°	$90° + \Delta\alpha_1$	s
2	h	–l	45°	$-90° + \Delta\alpha_2$	–s
3	–h	l	45°	$90° + \Delta\alpha_3$	s
4	–h	–l	–45°	$-90° + \Delta\alpha_4$	–s

Here, $\Delta\alpha_i$ — angle characterizing the nonorthogonality of the wheel axes and the longitudinal axis of platform Cx; d_i — vector $\overrightarrow{D_iO_i}$ projection onto the own axis of rotation of the *i*-th wheel.

Research Results. Describing the kinematics of the mecanum platform within the framework of nonholonomic mechanics, as was done in [3–5], in the absence of structural errors ($\Delta\alpha_i = 0$), , we determine the condition of nonslip of the contact point along the axis of the contacting roller:

$$V_{K_ix}\cos\left(\delta_i + \Delta\alpha_i\right) + V_{K_iy}\sin\left(\delta_i + \Delta\alpha_i\right) = 0, \tag{2}$$

where V_{K_ix}, V_{K_iy} — projections of the velocity of point K_i of contact of the *i*-th wheel with the supporting surface, which are determined from the vector equation:

$$V_{K_i} = V_C + \Omega_P \times \overrightarrow{CO_i} + \omega_i \times \overrightarrow{O_iK_i}. \tag{3}$$

Here, $V_{K_i} = \begin{bmatrix} V_{K_ix} & V_{K_iy} & 0 \end{bmatrix}^{\mathrm{T}}$ — velocity vector of point K_i of contact of the *i*-th wheel with the supporting surface in projections on the axis of the movable coordinate system $Cxyz$; $V_C = \begin{bmatrix} V_L & V_T & 0 \end{bmatrix}^{\mathrm{T}}$ — velocity vector of the geometric center of the platform in projections on axis $Cxyz$; $\Omega_P = \begin{bmatrix} 0 & 0 & \Omega \end{bmatrix}^{\mathrm{T}}$ —— angular velocity vector of the platform in projections on axis $Cxyz$; $\overrightarrow{CO_i} = \overrightarrow{CO_i} + \overrightarrow{O_iD_i} = \begin{bmatrix} x_i - d_i\sin\Delta\alpha_i & y_i + d_i\cos\Delta\alpha_i & 0 \end{bmatrix}^{\mathrm{T}}$ — radius-vector connecting the geometric centers of platform C and the *i*-th wheel O_i, in projections on axis $Cxyz$; $\omega_i = \begin{bmatrix} \dot{\varphi}_i\sin\Delta\alpha_i & \dot{\varphi}_i\cos\Delta\alpha_i & \Omega \end{bmatrix}^{\mathrm{T}}$ — angular velocity vector in projections on axis $Cxyz$; $\overrightarrow{O_iK_i} = \begin{bmatrix} 0 & 0 & -R \end{bmatrix}^{\mathrm{T}}$ — radius-vector connecting the geometric centers of the *i*-th wheel O_i and the contact point of roller K_i.

Rewriting vector equation (3) and using skew-symmetric matrices to calculate vector products, we rewrite equation (3) in matrix form:

$$\begin{bmatrix} V_{K_ix} \\ V_{K_iy} \\ 0 \end{bmatrix} = \begin{bmatrix} V_L \\ V_T \\ 0 \end{bmatrix} + \begin{bmatrix} 0 & -\Omega & 0 \\ \Omega & 0 & 0 \\ 0 & 0 & 0 \end{bmatrix}\begin{bmatrix} x_i - d_i\sin\Delta\alpha_i \\ y_i + d_i\cos\Delta\alpha_i \\ 0 \end{bmatrix} + \begin{bmatrix} 0 & -\Omega & \dot{\varphi}_i\cos\Delta\alpha_i \\ \Omega & 0 & -\dot{\varphi}_i\sin\Delta\alpha_i \\ -\dot{\varphi}_i\cos\Delta\alpha_i & \dot{\varphi}_i\sin\Delta\alpha_i & 0 \end{bmatrix}\begin{bmatrix} 0 \\ 0 \\ -R \end{bmatrix}. \tag{4}$$

After performing calculations:

$$V_{K_i x} = V_L - \Omega\left(y_i + d_i \cos\Delta\alpha_i\right) - R\dot{\varphi}_i \cos\Delta\alpha_i,$$
$$V_{K_i y} = V_T + \Omega\left(x_i - d_i \sin\Delta\alpha_i\right) - R\dot{\varphi}_i \sin\Delta\alpha_i. \tag{5}$$

After transferring the platform parameters from Table 1 to relationship equations (2) taking into account (5), they can be represented as:

$$\begin{aligned}
\dot{\varphi}_1 &= \frac{1}{R}\left[V_L - V_T - (h+l)\Omega\right]\cos\Delta\alpha_1 + \frac{1}{R}\left[V_L + V_T + (h-l)\Omega\right]\sin\Delta\alpha_1 - \frac{s}{R}\Omega,\\
\dot{\varphi}_2 &= \frac{1}{R}\left[V_L + V_T + (h+l)\Omega\right]\cos\Delta\alpha_2 - \frac{1}{R}\left[V_L - V_T - (h-l)\Omega\right]\sin\Delta\alpha_2 + \frac{s}{R}\Omega,\\
\dot{\varphi}_3 &= \frac{1}{R}\left[V_L + V_T - (h+l)\Omega\right]\cos\Delta\alpha_3 - \frac{1}{R}\left[V_L - V_T + (h-l)\Omega\right]\sin\Delta\alpha_3 - \frac{s}{R}\Omega,\\
\dot{\varphi}_4 &= \frac{1}{R}\left[V_L - V_T + (h+l)\Omega\right]\cos\Delta\alpha_4 + \frac{1}{R}\left[V_L + V_T - (h-l)\Omega\right]\sin\Delta\alpha_4 + \frac{s}{R}\Omega.
\end{aligned} \tag{6}$$

Note that in the absence of errors in fixing the axles of the wheel motors $\left(\Delta\alpha_i = 0\right)$, equations (6) take the form:

$$\begin{aligned}
\dot{\varphi}_1^{ideal} &= \frac{1}{R}\left[V_L - V_T - (h+l)\Omega\right], \quad \dot{\varphi}_2^{ideal} = \frac{1}{R}\left[V_L + V_T + (h+l)\Omega\right],\\
\dot{\varphi}_3^{ideal} &= \frac{1}{R}\left[V_L + V_T - (h+l)\Omega\right], \quad \dot{\varphi}_4^{ideal} = \frac{1}{R}\left[V_L - V_T + (h+l)\Omega\right].
\end{aligned} \tag{7}$$

and coincide with the known results [6].

In matrix form, equations (6) and (7) can be represented as:

$$\dot{q} = H\left(\Delta\alpha_i\right)\dot{\pi}, \tag{8}$$

$$\dot{q} = H_0\dot{\pi}, \tag{9}$$

where $\dot{\pi} = \begin{bmatrix} V_L & V_T & \Omega \end{bmatrix}^{\mathrm{T}}$ — vector of pseudovelocities of the platform; $\dot{q} = \begin{bmatrix} \dot{\varphi}_1 & \dot{\varphi}_2 & \dot{\varphi}_3 & \dot{\varphi}_4 \end{bmatrix}^{\mathrm{T}}$ — vector of angular velocities of wheels; $H\left(\Delta\alpha_i\right)$ — matrix of coefficients at pseudovelocities in equations (6); and $H_0 = H\left(\Delta\alpha_i = 0\right)$.

When forming the control at the kinematic level, the values of the angular velocities of platform $\dot{\pi}^d$ are calculated according to the desired values of the pseudovelocities of the platform according to the formula:

$$\dot{q}^d = H_0\dot{\pi}^d, \tag{10}$$

where superscript d indicates the desired (program) speed values. The obtained values of angular velocities are fed to the input of the wheel motor control system.

However, if there are inaccuracies in the fastening of the axles of the wheel motors, according to the results of testing the program values of the angular velocities of the wheels, the movement of the platform is realized in the form:

$$\dot{\pi} = \left(H^{\mathrm{T}}\left(\Delta\alpha_i\right)H\left(\Delta\alpha_i\right)\right)^{-1} H^{\mathrm{T}}\left(\Delta\alpha_i\right)\dot{q}^d = \left(H^{\mathrm{T}}\left(\Delta\alpha_i\right)H\left(\Delta\alpha_i\right)\right)^{-1} H^{\mathrm{T}}\left(\Delta\alpha_i\right)H_0\dot{\pi}^d. \tag{11}$$

According to the found expression, it is possible to estimate the error of developing the program movement of the platform, specified by the presence of inaccuracies in fixing the axles of the wheel motors, according to the formula:

$$\Delta\dot{\pi} = \dot{\pi} - \dot{\pi}^d = \left[\left(H^{\mathrm{T}}\left(\Delta\alpha_i\right)H\left(\Delta\alpha_i\right)\right)^{-1} H^{\mathrm{T}}\left(\Delta\alpha_i\right)H_0 - E_3\right]\dot{\pi}^d, \tag{12}$$

where E_3 — unit matrix of order 3.

Since the pseudovelocities of the platform are related to the coordinates of the geometric center in a fixed reference frame by the relations [15],

$$\begin{aligned}
\dot{x}_C &= V_L\cos\psi - V_T\sin\psi,\\
\dot{y}_C &= V_L\sin\psi + V_T\cos\psi,\\
\dot{\psi} &= \Omega,
\end{aligned} \tag{13}$$

then, taking into account the errors of the pseudovelocities, we can rewrite the indicated expressions in the form:

$$\begin{aligned} &\dot{x}_C = \dot{x}_C^d \cos\Delta\psi - \dot{y}_C^d \sin\Delta\psi + \Delta V_L \cos\left(\psi^d + \Delta\psi\right) - \Delta V_T \sin\left(\psi^d + \Delta\psi\right), \\ &\dot{y}_C = \dot{x}_C^d \sin\Delta\psi + \dot{y}_C^d \cos\Delta\psi + \Delta V_L \sin\left(\psi^d + \Delta\psi\right) + \Delta V_T \cos\left(\psi^d + \Delta\psi\right), \\ &\psi = \psi^d + \Delta\psi, \end{aligned} \tag{14}$$

where $\dot{x}_C^d = V_L^d \cos\psi^d - V_T^d \sin\psi^d$, $\dot{y}_C^d = V_L^d \sin\psi^d + V_T^d \cos\psi^d$ — laws of velocity variation of the platform geometric center in a fixed reference frame corresponding to the program movement; $\psi^d = \psi^d(0) + \int\limits_0^t \Omega^d(t_1)dt_1$ — law of the angle variation of the platform course corresponding to the program movement; $\Delta\psi = \int\limits_0^t \Delta\Omega(t_1)dt_1$ — course angle error.

Taking into account the entered designations, we obtain formulas for positioning errors in the form:

$$\begin{aligned} &\Delta\dot{x}_C = \dot{x}_C^d \left(\cos\Delta\psi - 1\right) - \dot{y}_C^d \sin\Delta\psi + \Delta V_L \cos\left(\psi^d + \Delta\psi\right) - \Delta V_T \sin\left(\psi^d + \Delta\psi\right), \\ &\Delta\dot{y}_C = \dot{x}_C^d \sin\Delta\psi + \dot{y}_C^d \left(\cos\Delta\psi - 1\right) + \Delta V_L \sin\left(\psi^d + \Delta\psi\right) + \Delta V_T \cos\left(\psi^d + \Delta\psi\right). \end{aligned} \tag{15}$$

As a numerical example for error estimation, consider the parameters of the robot KUKA youBot [16]:

$$h = 0.235\, m, \quad l = 0.14\, m, \quad R = 0.05\, m, \quad s = 0.01\, m.$$

As an example, let us take the errors of fixing the axles of the motor wheels equal to:

$$\Delta\alpha_1 = \Delta\alpha_2 = 1°, \quad \Delta\alpha_3 = \Delta\alpha_4 = 2°.$$

Below are the results of calculating the errors of the platform velocities with simple movements of the platform. As examples of simple platform movements, consider:

– forward movement: $V_L = 1$ m/s, $V_T = 0$ m/s, $\Omega = 0$ rad/s;

– forward movement to the left: $V_L = 0$ m/s, $V_T = 1$ m/s, $\Omega = 0$ rad/s;

– rotation around a vertical axis passing through the geometric center of the platform: $V_L = 0$ m/s, $V_T = 0$ m/s, $\Omega = 1$ rad/s.

The errors of the pseudovelocities of the platform with these movements are calculated using the formulas:

– moving forward:

$\Delta V_L = 1.35 \cdot 10^{-4}$ m/s, $\Delta V_T = -8.73 \cdot 10^{-3}$ m/s, $\Delta\Omega = 6.8 \cdot 10^{-2}$ rad/s;

– lateral movement to the left:

$\Delta V_L = 8.72 \cdot 10^{-3}$ m/s, $\Delta V_T = -3.81 \cdot 10^{-4}$ m/s, $\Delta\Omega = 1.46 \cdot 10^{-4}$ rad/s;

– rotation around a vertical axis passing through the geometric center of the platform:

$\Delta V_L = -2.49 \cdot 10^{-3}$ m/s, $\Delta V_T = -4.22 \cdot 10^{-5}$ m/s, $\Delta\Omega = 1.97 \cdot 10^{-4}$ rad/s.

The obtained values of pseudovelocity errors are significant for mobile robots with mecanum wheels, since they cause deviations in coordinates of the order of 10 cm in 2 minutes of robot movement. This makes it unacceptable for the mekanum platform to function offline in the absence of compensation for these positioning errors. Note that occurrence of a non-zero error in the angular velocity of rotation of the platform causes a nonlinear increase in the positioning error of the platform (formulas (15)) when considering control at the kinematic level.

These results allow us to conclude that it is required to take into account the inaccuracies of fixing the wheel axles when building a control system. It should be noted that since the mounting errors of the wheel motor axles are unknown quantities, it is required to develop methods for identifying the parameters of the mathematical model of robot movement to determine them [16].

The application of the developed kinematic model of the mecanum platform, which takes into account the inaccuracies of fixing the axles of the wheel motors, makes it possible to build control at the kinematic level with greater positioning accuracy.

Thus, within the framework of this study, a model of the kinematics of a mobile platform with mecanum wheels is presented with an error in the installation of the axes of the wheel motors. A formula is obtained for estimating the errors of the pseudovelocities of the platform with software control formed at the kinematic level. Errors in the development of program motion for simple movements of the mecanum platform (forward movement, lateral movement to the left, and rotation in place) have been estimated.

Discussion and Conclusion. The resulting kinematic model of a mobile platform with mecanum wheels can be used to improve positioning accuracy by forming a platform motion control that compensates for the impact of wheel installation inaccuracies. To use the obtained model in the control tasks of the mecanum platform, it is required to develop methods for identifying the parameters of the mathematical model in the future.

The task for further research in this area is to develop a mathematical model of the dynamics of the mecanum platform, taking into account the errors in the installation of the axes of the wheel motors.

References

1. Adascalitei F, Doroftei I. Practical Applications for Mobile Robots Based on Mecanum Wheels – a Systematic Survey. *The Romanian Review Precession Mechanics, Optics & Mechatronics*. 2011;40:21–29.

2. Safar MJA. Holonomic and Omnidirectional Locomotion Systems for Wheeled Mobile Robots: A Review. *Jurnal Teknologi (Sciences & Engineering).* 2015;77(28):91–97. https://doi.org/10.11113/jt.v77.6799

3. Hendzel Z, Rykała Ł. Modeling of Dynamics of a Wheeled Mobile Robot with Mecanum Wheels with the Use of Lagrange Equations of the Second Kind. *International Journal of Applied Mechanics and Engineering.* 2017;22(1):81–99. https://doi.org/10.1515/ijame-2017-0005

4. Hendzel Z, Rykała Ł. Description of Kinematics of a Wheeled Mobile Robot with Mecanum Wheels. *Modeling in Engineering.* 2015;57:5–12.

5. Zeidis I, Zimmermann K. Dynamics of a Four-Wheeled Mobile Robot with Mecanum Wheels. *Journal of Applied Mathematics and Mechanics.* 2019;99(12):e201900173. https://doi.org/10.1002/zamm.201900173

6. Adamov BI. Influence of Mecanum Wheels Construction on Accuracy of the Omnidirectional Platform Navigation (on Example of KUKA youBot Robot). In: *Proc. 25th Saint Petersburg Int. Conf. on Integrated Navigation Systems (ICINS).* New York City: IEEE; 2018. P. 1–4. https://doi.org/10.23919/ICINS.2018.8405889

7. Palacin J, Martinez D, Rubies E, Clotet E. Suboptimal Omnidirectional Wheel Design and Implementation. *Sensors*. 2021;21(3):865. https://doi.org/10.3390/s21030865

8. Kyung-Lyong Han, Oh-Kyu Choi, Jinwook Kim, Hyosin Kim, Jin S Lee. Design and Control of Mobile Robot with Mecanum Wheel. In: *Proc. Int. Conf. on Control, Automation and Systems* (*ICCAS-SICE)*. New York City: IEEE; 2009. P. 2932–2937.

9. Sun Wencheng, Li Shuge, Wang Weiqiang, Zhao Pengju, Yang Renqiang. Design of Chassis and Kinematics Research of Wheeled Robot. In: *Proc. IEEE 4th Information Technology, Networking, Electronic and Automation Control Conference.* New York City: IEEE; 2020. P. 2405–2408. https://doi.org/10.1109/ITNEC48623.2020.9085044

10. Junpeng Shao, Tianhua He, Jingang Jiang, Yongde Zhang. Recent Patents on Omni-Directional Wheel Applied on Wheeled Mobile Robot. *Recent Patents on Mechanical Engineering.* 2016;9(3):215–221. https://doi.org/10.2174/2212797609666160616091009

11. Dianfeng Zhang, Guangcang Wang, Zhaojing Wu. Reinforcement Learning-Based Tracking Control for a Three Mecanum Wheeled Robot. In: *Proc. IEEE Transactions on Neural Networks and Learning Systems.* New York City: IEEE; 2022. P. 1–8. https://doi.org/10.1109/TNNLS.2022.3185055

12. Danwei Wang, Chang Boon Low. Modeling and Analysis of Skidding and Slipping in Wheeled Mobile Robots: Control Design Perspective. *IEEE Transactions on Robotics and Automation*. 2008;24(3):676–687. https://doi.org/10.1109/TRO.2008.921563

13. Yunwang Li, Shirong Ge, Sumei Dai, Lala Zhao, Xucong Yan, Yuwei Zheng, et al. Kinematic Modeling of a Combined System of Multiple Mecanum-Wheeled Robots with Velocity Compensation. *Sensors*. 2019;20(1):75. https://doi.org/10.3390/s20010075

14. Li Xie, Christian Henkel, Karl Stol, Weiliang Xu. Power-Minimization and Energy-Reduction Autonomous Navigation of an Omnidirectional Mecanum Robot via the Dynamic Window Approach Local Trajectory Planning. *International Journal of Advanced Robotics Systems*. 2018;15(1):1–12. https://doi.org/10.1177/1729881418754563

15. Adamov BI. A Study of the Controlled Motion of a Four-Wheeled Mecanum Platform. *Russian Journal of Nonlinear Dynamics.* 2018;14(2):265–190. https://doi.org/10.20537/nd180209

16. Adamov BI, Kobrin AI. Parametric Identification of the Mathematical Model of the Omnidirectional Mobile Robot KUKA youBot. *Mechatronics, Automation, Control*. 2018;19(4):251–258. https://doi.org/10.17587/mau.19.251-258

Received 17.09.2023
Revised 15.10.2023
Accepted 29.10.2023

About the Authors:

Galina V. Pankrateva, Cand.Sci. (Phys.-Math.), Associate Professor of the Department of Robotics, Mechatronics, Dynamics and Strength of Machines, National Research University MPEI (14, Krasnokazarmennaya St., Moscow, 111250, RF), SPIN-code: 3872-1911, ORCID, gvpankr@gmail.com

Anton E. Mordin, student of the Department of Robotics, Mechatronics, Dynamics and Strength of Machines, National Research University MPEI (14, Krasnokazarmennaya St., Moscow, 111250, RF), SPIN-code: 1953-8416, ORCID, ToxaM_99@mail.ru

Gasan R. Saypulaev, postgraduate student, teaching assistant of the Department of Robotics, Mechatronics, Dynamics and Strength of Machines, National Research University MPEI (14, Krasnokazarmennaya St., Moscow, 111250, RF), SPIN-code: 4156-3048, ScopusID, ORCID, saypulaevgr@mail.ru

Claimed contributorship:

AE Mordin: basic concept formulation, research objectives and tasks, computational analysis, formulation of conclusions.

GV Pankrateva: academic advising, analysis of the research results, revision of the text.

GR Saypulaev: computational analysis, text preparation, correction of the conclusions.

Conflict of interest statement: the authors do not have any conflict of interest.

All authors have read and approved the final manuscript.

Поступила в редакцию 17.09.2023
Поступила после рецензирования 15.10.2023
Принята к публикации 29.10.2023

Об авторах:

Галина Витальевна Панкратьева, кандидат физико-математических наук, доцент кафедры робототехники, мехатроники, динамики и прочности машин Национального исследовательского университета «МЭИ» (111250, РФ, г. Москва, ул. Красноказарменная, 14), SPIN-код: 3872-1911, ORCID, gvpankr@gmail.com

Антон Евгеньевич Мордин, студент кафедры робототехники, мехатроники, динамики и прочности машин Национального исследовательского университета «МЭИ» (111250, РФ, г. Москва, ул. Красноказарменная, 14), SPIN-код: 1953-8416, ORCID, ToxaM_99@mail.ru

Гасан Русланович Сайпулаев, аспирант и ассистент кафедры робототехники, мехатроники, динамики и прочности машин Национального исследовательского университета «МЭИ» (111250, РФ, г. Москва, ул. Красноказарменная, 14), SPIN-код: 4156-3048, ScopusID, ORCID, saypulaevgr@mail.ru

Заявленный вклад соавторов:

А.Е. Мордин — формирование основной концепции, цели и задачи исследования, проведение расчетов, формирование выводов.

Г.В. Панкратьева — научное руководство, анализ результатов исследований, корректировка текста.

Г.Р. Сайпулаев — проведение расчетов, подготовка текста, корректировка выводов.

Конфликт интересов: авторы заявляют об отсутствии конфликта интересов.

Все авторы прочитали и одобрили окончательный вариант рукописи.

MECHANICS
МЕХАНИКА

UDC 539.42
https://doi.org/10.23947/2687-1653-2023-23-4-365-375

Original article

EDN: JBOFSU

Application of the Double Approximation Method for Constructing Stiffness Matrices of Volumetric Finite Elements

Peter P. Gaidzhurov , Nina A. Saveleva
Don State Technical University, Rostov-on-Don, Russian Federation
✉ gpp-161@yandex.ru

Abstract

Introduction. When numerically solving problems of elasticity theory in a three-dimensional formulation by the finite element method, finite elements (FE) in the form of parallelepipeds, prisms and tetrahedra are used. Regularly, the construction of stiffness matrices of volumetric FE is based on the principle of isoparametricity, which involves the Lagrange polynomials to approximate the geometry and displacements. In computational practice, the most widespread FE are the so-called multilinear isoparametric FE with a linear law of approximation of displacements. The main disadvantage of these elements lies in the "locking" effect when modulating bending deformations. Moreover, the error of the numerical solution increases drastically in the case when the structure, in comparison to conventional deformations, undergoes significant displacements as a rigid whole. Long-term experience in solving problems of deformable solid mechanics by the finite element method has shown that existing volumetric FE have slow convergence, specifically, when modeling bending deformations of plates and shells. This study aims at constructing stiffness matrices of multilinear volumetric FE of increased accuracy allowing for rigid displacements based on the double approximation method.

Materials and Methods. The mathematical apparatus of the double approximation method based on the principle of a separate representation of the distribution functions of displacements and deformations inside the element, was used to construct the stiffness matrices of volumetric FE. The storage and processing of the resulting system of equations was implemented in algorithmic terms of sparse matrices. Software development and computational experiments were carried out using the Microsoft Visual Studio 2013 64-bit computing platform and the Intel ® Parallel Studio XE 2019 compiler with the integrated Intel ® Visual Fortran Composer XE 2019 text editor. Visualization of the calculation results was performed using the descriptor graphics of the MATLAB computer mathematics package. A large eight-node SOLID185 CE of the ANSYS Mechanical software complex was used as a test sample.

Results. Mathematical tool and software were developed to study the stress-strain state of massive structures under various types of external actions. The authorized application software package was verified on test examples with known analytical solutions. It has been shown that the constructed FE accurately satisfy the basic requirements for finite element modeling of spatial problems of elasticity theory.

Discussion and Conclusion. The performed testing of the developed mathematical and program toolkit has shown that the finite elements constructed on the basis of the double approximation method can successfully compete with similar SOLID185 volumetric elements of the ANSYS Mechanical software complex. The proposed elements can be integrated into domestic import-substituting software systems that implement the finite element method in the form of the displacement method.

Keywords: finite element method, moment scheme of finite element method, double approximation method, volumetric finite elements, finite element testing

Acknowledgements. The authors appreciate the reviewers, whose critical assessment of the submitted materials and suggestions helped to significantly improve the quality of this article.

For citation. Gaidzhurov PP, Saveleva NA. Application of the Double Approximation Method for Constructing Stiffness Matrices of Volumetric Finite Elements. *Advanced Engineering Research (Rostov-on-Don).* 2023;23(4):365–375. https://doi.org/10.23947/2687-1653-2023-23-4-365-375

Научная статья

Применение метода двойной аппроксимации для построения матриц жесткости объемных конечных элементов

П.П. Гайджуров ✉, **Н.А. Савельева**
Донской государственный технический университет, г. Ростов-на-Дону, Российская Федерация
✉ gpp-161@yandex.ru

Аннотация
Введение. При численном решении задач теории упругости в трехмерной постановке методом конечных элементов применяются конечные элементы (КЭ) в форме параллелепипедов, призм и тетраэдров. Обычно построение матриц жесткости объемных КЭ базируется на принципе изопараметричности, суть которого состоит в использовании для аппроксимации геометрии и перемещений полиномов Лагранжа. В расчетной практике наибольшее распространение получили так называемые полилинейные изопараметрические КЭ с линейным законом аппроксимации перемещений. Главный недостаток данных элементов кроется в эффекте «*locking*» («запирания») при моделировании изгибных деформаций. Причем погрешность численного решения существенно возрастает в случае, когда конструкция, по сравнению с обычными деформациями, претерпевает значительные смещения как жесткое целое. Многолетний опыт решения задач механики деформируемого твердого тела методом конечных элементов показал, что существующие объемные КЭ обладают медленной сходимостью при моделировании изгибных деформаций пластин и оболочек. Цель настоящего исследования состоит в построении на основе метода двойной аппроксимации матриц жесткости полилинейных объемных КЭ повышенной точности, позволяющих учитывать жесткие смещения.
Материалы и методы. Для построения матриц жесткости объемных КЭ применен математический аппарат метода двойной аппроксимации, суть которого состоит в раздельном представлении функций распределения перемещений и деформаций внутри элемента. Хранение и обработка результирующей системы уравнений реализованы в алгоритмических терминах разреженных матриц. Разработка программного обеспечения и проведение вычислительных экспериментов осуществлены с использованием 64-х разрядной вычислительной платформы Microsoft Visual Studio 2013 и компилятора Intel® Parallel Studio XE 2019 со встроенным текстовым редактором Intel® Visual Fortran Composer XE 2019. Визуализация результатов расчетов выполнена с помощью дескрипторной графики пакета компьютерной математики Matlab. В качестве тестового образца использован объемный восьмиузловой КЭ SOLID185 программного комплекса ANSYS Mechanical.
Результаты исследования. Разработано математическое и программное обеспечение для исследования напряженно-деформированного состояния массивных конструкций при различных видах внешнего воздействия. На тестовых примерах с известными аналитическими решениями выполнена верификация авторизированного пакета прикладных программ. Показано, что построенные КЭ по точности удовлетворяют основным требованиям, предъявляемым к конечно-элементному моделированию пространственных задач теории упругости.
Обсуждение и заключение. Проведенное тестирование разработанного математического и программного обеспечения показало, что построенные на основе метода двойной аппроксимации конечные элементы успешно конкурируют с аналогичными объемными элементами SOLID185 программного комплекса ANSYS Mechanical. Предлагаемые элементы могут быть интегрированы в отечественные импортозамещающие программные комплексы, реализующие метод конечных элементов в форме метода перемещений.

Ключевые слова: метод конечных элементов, моментная схема метода конечных элементов, метод двойной аппроксимации, объемные конечные элементы, тестирование конечных элементов

Благодарности. Авторы выражают благодарность рецензентам, чья критическая оценка представленных материалов и высказанные предложения по их совершенствованию способствовали значительному повышению качества настоящей статьи.

Для цитирования. Гайджуров П.П., Савельева Н.А. Применение метода двойной аппроксимации для построения матриц жесткости объемных конечных элементов. *Advanced Engineering Research (Rostov-on-Don).* 2023;23(4):365–375. https://doi.org/10.23947/2687-1653-2023-23-4-365-375

Introduction. In finite element modeling of the stress-strain state of massive bodies, volumetric finite elements (FE) in the form of parallelepipeds (hexahedra), prisms and tetrahedra are used, the construction of stiffness matrices of which is usually performed using isoparametric technology [1-5]. At the same time, it is known that multilinear isoparametric FE, when using a single-layer scheme, do not satisfactorily model bending deformations even with a significant thickening of the mesh [6, 7]. The core of this problem is the effect of "locking" the element due to the so-called deformation of the "false shift" [8, 9]. To "improve" isoparametric FE, an apparatus of incompatible elements created through introducing additional out-of-node degrees of freedom, or auxiliary approximating polynomials, is used [8]. At the same time, the most effective way to solve the problem of "jamming" of the FE is the use of the moment scheme of the finite element method, whose theoretical foundations were developed by A.S. Sakharov [7]. Subsequently, this approach was called the double approximation method (DAM) [6]. Conceptually, the DAM is based on a separate representation of the distribution functions of displacements and deformations inside the element. The objective of this study is to construct on the basis of MDA and test new volumetric multilinear FE that allow simulating the behavior of various structures under different types of external actions.

Materials and Methods. Let us consider a family of volumetric FE consisting of eight-node and six-node elements in global Cartesian axes z_m, m = 1, 2, 3 (Fig. 1). Geometry and displacements of the FE are presented in the following form:

$$z_m = \sum_{k=1}^{n_e} z_m^{(k)} \varphi(x_1, x_2, x_3)\,;\; u_m = \sum_{k=1}^{n_e} u_m^{(k)} \varphi(x_1, x_2, x_3)\,,$$

where $z_m^{(k)}$, $u_m^{(k)}$ — nodal coordinates and displacements; $\varphi_k(x_1, x_2, x_3)$ — "shape functions" representing the product of one-dimensional Lagrange linear polynomials; x_1, x_2, x_3 — — local, in general, nonorthogonal coordinates of FE; n_e — number of element nodes. For the basic eight-node element (Fig. 1 *a*) n_e = 8, "shape functions" are defined by formula:

$$\varphi_k\,(x_1, x_2, x_3) = \frac{1}{8}\prod_{r=1}^{3}(1 + p_{rk}\, x_r)\,, \tag{1}$$

Here, p_{rk} — coordinates of nodes in local axes. We set values p_{rk} in matrix form:

$$\left[\begin{array}{c:c:c:c:c:c:c:c} 1 & 1 & -1 & -1 & 1 & 1 & -1 & -1 \\ \hdashline -1 & 1 & 1 & -1 & -1 & 1 & 1 & -1 \\ \hdashline -1 & -1 & -1 & -1 & 1 & 1 & 1 & 1 \end{array}\right].$$

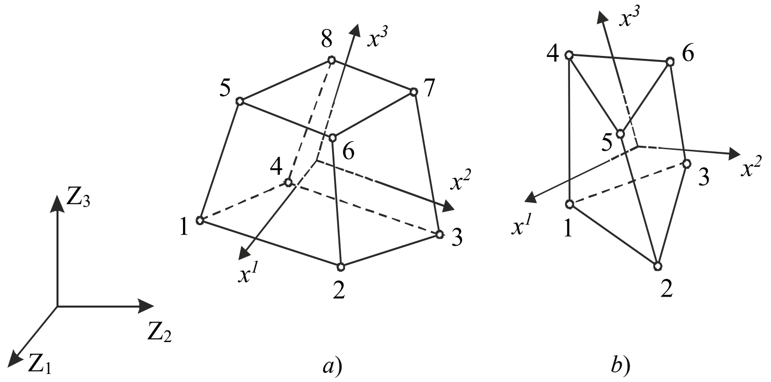

Fig. 1. Volumetric FE:
a — eight-node; *b* — six-node

The relationship between the covariant components of the strain tensor in the local basis and displacements in the global axes has the form [7]:

$$\varepsilon_{ij} = \frac{1}{2}\Big(z_{m,j}\, u_{m,i} + z_{m,i}\, u_{m,j} \Big),$$

(summation over repeated index)

where $z_{m,s} = \partial z_m / \partial x_s$; $u_{m,s} = \partial u_m / \partial x_s$, $s = i, j$.

Mechanics

The relationship between vector of deformations $\{\varepsilon\}$ and vector of nodal displacements $\{w\}$ is represented in matrix form: $\{\varepsilon\}=[D]\{w\}$,

where block matrix: $\underset{(6\times n_e)}{[D]}=\left[[D]_1\,[D]_2\ldots[D]_{n_e}\right]$;

submatrix:

$$\underset{(6\times 3)}{[D]_k}=\left[\{D^{(1)}\}_k\,\{D^{(2)}\}_k\,\{D^{(3)}\}_k\right],\ k=1,2,\ldots,n_e\,.$$

Expressions for the vector columns of the considered FE have the following form [10]: an eight-node element (Fig. 1 *a*)

$$\{D^{(m)}\}_k=\frac{1}{8}\left\{\begin{array}{c} p_{1k}\left[\tilde z_{m,1}+(\tilde z_{m,12}+\tilde z_{m,1}\,p_{2k})x_2+(\tilde z_{m,13}+\tilde z_{m,1}\,p_{3k})x_3+\right.\\ \left.+(\tilde z_{m,123}+\tilde z_{m,12}\,p_{3k}+\tilde z_{m,13}\,p_{2k}+\tilde z_{m,1}\,p_{2k}\,p_{3k})\,x_2\,x_3\right]\\ \hdashline p_{2k}\left[\tilde z_{m,2}+(\tilde z_{m,12}+\tilde z_{m,2}\,p_{1k})x_1+(\tilde z_{m,23}+\tilde z_{m,2}\,p_{3k})x_3+\right.\\ \left.+(\tilde z_{m,123}+\tilde z_{m,12}\,p_{3k}+\tilde z_{m,23}\,p_{1k}+\tilde z_{m,2}\,p_{1k}\,p_{3k})\,x_1\,x_3\right]\\ \hdashline p_{3k}\left[\tilde z_{m,3}+(\tilde z_{m,13}+\tilde z_{m,3}\,p_{1k})x_1+(\tilde z_{m,23}+\tilde z_{m,3}\,p_{2k})x_2+\right.\\ \left.+(\tilde z_{m,123}+\tilde z_{m,13}\,p_{2k}+\tilde z_{m,23}\,p_{1k}+\tilde z_{m,3}\,p_{1k}\,p_{2k})\,x_1\,x_2\right]\\ \hdashline \tilde z_{m,1}\,p_{2k}+\tilde z_{m,2}\,p_{1k}+(\tilde z_{m,13}\,p_{2k}+\tilde z_{m,1}\,p_{2k}\,p_{3k}+\tilde z_{m,23}\,p_{1k}+\\ +\tilde z_{m,2}\,p_{1k}\,p_{3k})\,x_3\\ \hdashline \tilde z_{m,1}\,p_{3k}+\tilde z_{m,3}\,p_{1k}+(\tilde z_{m,12}\,p_{3k}+\tilde z_{m,1}\,p_{2k}\,p_{3k}+\tilde z_{m,23}\,p_{1k}+\\ +\tilde z_{m,3}\,p_{1k}\,p_{2k})\,x_2\\ \hdashline \tilde z_{m,2}\,p_{3k}+\tilde z_{m,3}\,p_{2k}+(\tilde z_{m,12}\,p_{3k}+\tilde z_{m,2}\,p_{1k}\,p_{3k}+\tilde z_{m,13}\,p_{2k}+\\ +\tilde z_{m,3}\,p_{1k}\,p_{2k})\,x_1 \end{array}\right\};\qquad(2)$$

Six-node element (Fig. 1 *b*)

$$\{D^{(m)}\}_k=\frac{1}{8}\left\{\begin{array}{c} \tilde z_{m,1}\,\tilde\varphi_{k,1}+(\tilde z_{m,13}\,\tilde\varphi_{k,1}+\tilde z_{m,1}\,\tilde\varphi_{k,13})\,x_3\\ \hdashline \tilde z_{m,2}\,\tilde\varphi_{k,2}+(\tilde z_{m,23}\,\tilde\varphi_{k,2}+\tilde z_{m,2}\,\tilde\varphi_{k,23})\,x_3\\ \hdashline \tilde z_{m,3}\,\tilde\varphi_{k,3}+(\tilde z_{m,13}\,\tilde\varphi_{k,3}+\tilde z_{m,3}\,\tilde\varphi_{k,13})\,x_1+\\ +(\tilde z_{m,23}\,\tilde\varphi_{k,3}+\tilde z_{m,3}\,\tilde\varphi_{k,23})\,x_2\\ \hdashline \tilde z_{m,1}\,\tilde\varphi_{k,2}+\tilde z_{m,2}\,\tilde\varphi_{k,1}+(\tilde z_{m,13}\,\tilde\varphi_{k,2}+\tilde z_{m,1}\,\tilde\varphi_{k,23}+\\ +\tilde z_{m,23}\,\tilde\varphi_{k,1}+\tilde z_{m,2}\,\tilde\varphi_{k,13})\,x_3\\ \hdashline \tilde z_{m,1}\,\tilde\varphi_{k,3}+\tilde z_{m,3}\,\tilde\varphi_{k,1}\\ \hdashline \tilde z_{m,2}\,\tilde\varphi_{k,3}+\tilde z_{m,3}\,\tilde\varphi_{k,2} \end{array}\right\}.\qquad(3)$$

The notation is introduced here:

$$\tilde z_{m,\alpha}=\left.\frac{\partial z_m}{\partial x_\alpha}\right|_{x_1=x_2=x_3=0},\ \tilde z_{m,\alpha\beta}=\left.\frac{\partial^2 z_m}{\partial x_\alpha\,\partial x_\beta}\right|_{x_1=x_2=x_3=0};$$

$$\tilde z_{m,123}=\left.\frac{\partial^3 z_m}{\partial x_1\,\partial x_2\,\partial x_3}\right|_{x_1=x_2=x_3=0}.$$

$$\tilde\varphi_{k,\alpha}=\left.\frac{\partial\tilde\varphi_k}{\partial x_\alpha}\right|_{x_1=x_2=x_3=0};\ \tilde\varphi_{k,\alpha\beta}=\left.\frac{\partial^2\tilde\varphi_k}{\partial x_\alpha\,\partial x_\beta}\right|_{x_1=x_2=x_3=0};\ \alpha,\beta=1,2,3\,.$$

Expressions for “shape functions $\tilde\varphi_k(x_1,x_2,x_3)$ of a six-node FE obtained on the basis of the polynomial (1) using the degeneration principle have the following form:

$$\tilde\varphi_1=\frac{1}{8}(1+p_{11}x_1)(1+p_{21}x_2)(1+p_{31}x_3);$$

$$\tilde\varphi_2=\frac{1}{8}(1+p_{12}x_1)(1+p_{22}x_2)(1+p_{32}x_3);$$

$$\tilde{\varphi}_3 = \frac{1}{8}\Big[(1+p_{13}x_1)(1+p_{23}x_2)(1+p_{33}x_3)+(1+p_{14}x_1)(1+p_{24}x_2)(1+p_{34}x_3)\Big];$$

$$\tilde{\varphi}_4 = \frac{1}{8}(1+p_{15}x_1)(1+p_{25}x_2)(1+p_{35}x_3);$$

$$\tilde{\varphi}_5 = \frac{1}{8}(1+p_{16}x_1)(1+p_{26}x_2)(1+p_{36}x_3);$$

$$\tilde{\varphi}_6 = \frac{1}{8}\Big[(1+p_{17}x_1)(1+p_{27}x_2)(1+p_{37}x_3)+(1+p_{18}x_1)(1+p_{28}x_2)(1+p_{38}x_3)\Big].$$

Formulas (2) and (3) were the basis for constructing stiffness matrices of the FE under study. The corresponding software was developed on the basis of the Microsoft Visual Studio computing platform and the Intel® Parallel Studio XE compiler with the built-in Intel® Visual Fortran Composer XE text editor. The processes of storing and processing the global stiffness matrix were implemented in terms of sparse matrices [11]. To visualize the results of calculations, the descriptor graphics of the MATLAB computer system was used.

Research Results. The investigation on the accuracy and convergence of the developed finite element algorithm was carried out on test examples with an analytical solution. The test examples show numerical solutions obtained using the developed elements and the SOLID185 element of the ANSYS Mechanical software package similar in dimension [5, 11]. Below are examples selected so that they contain a combination of bending deformations and rigid displacements of FE.

Example 1. A spliced ring rigidly fixed in one section and loaded with concentrated force at the free end. The design scheme of the ring is shown in Figure 2. Initial data: average radius R = 0.2 m; cross-sectional dimensions 0.2×0.2 cm; modulus of elasticity $E = 10^{11}$ H/m^2; Poisson's ratio ν = 0.3; concentrated force F = 10 H.

The deflection at the point of application of force according to the theory of curved rods (exact solution) is [7]:

$$f = \frac{F\pi R^3}{EJ} = \frac{10\cdot 3.14\cdot 0.2^3}{1\cdot 10^{11}\cdot 8.333\cdot 10^{-10}} = -0.00302 \text{ m}.$$

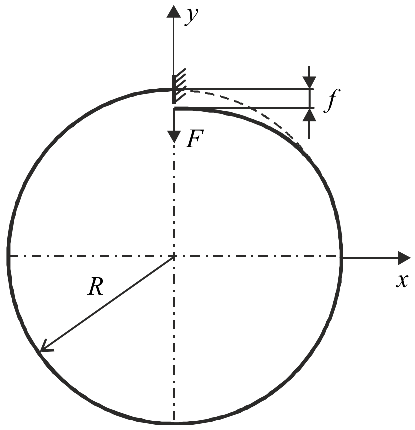

Fig. 2. Calculation scheme of the spliced ring

The convergence results are presented in Table1.

Table 1

Convergence results for the spliced ring

Grid	f/δ, м / %	
	DAM	ANSYS
2×2×32	–0.00170 / 44	–0.000433 / 86
2×2×64	–0.00292 / 3.3	–0.00125 / 59
2×2×128	–0.00293 / 3	–0.00251 / 17

Table 1 shows the value of deflection f in the numerator, and relative error δ in the denominator.

The visualization of displacements u_y, obtained on the basis of DAM and ANSYS on a 2×2×64 grid is shown in Figures 3 and 4. Note that the field of vertical displacements obtained using ANSYS does not reflect the zones with extreme value u_y = –0.00314 m shown in Figure 3 by the arrow.

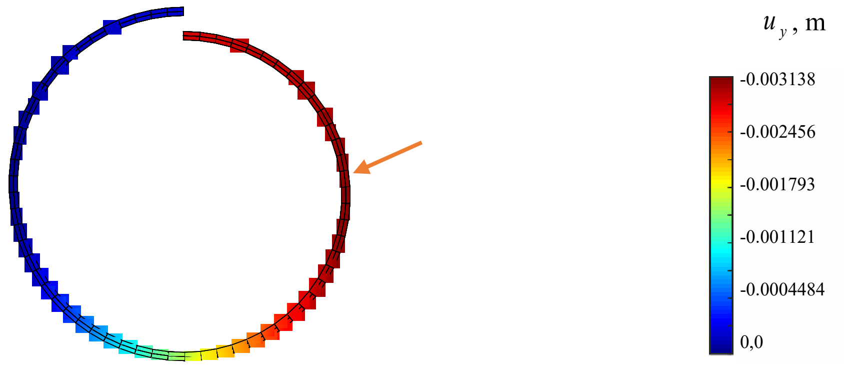

Fig. 3. Distribution pattern u_y (DAM)

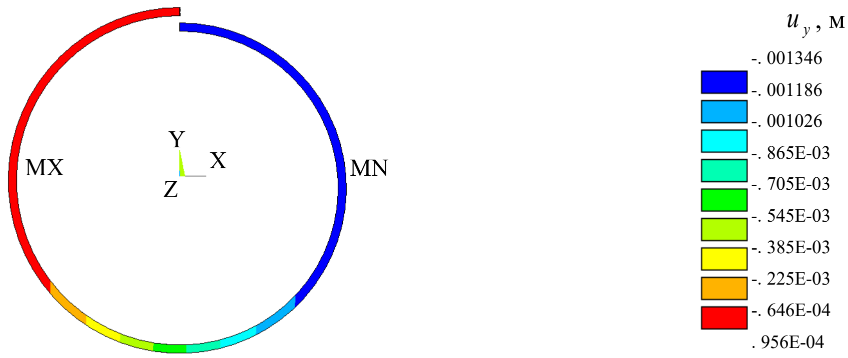

Fig. 4. Distribution pattern u_y (ANSYS)

In this example, the importance of taking into account rigid displacements is particularly clearly seen.

Example 2. A square plate, rigidly pinched along the contour and loaded with a uniformly distributed load. Source data: side length стороны $a = 1$ m; thickness $h = 0.01$ m; elasticity modulus $E = 10^5$ H/m^2; Poisson's ratio $\nu = 0.25$.

The exact value of the deflection in the center of the plate is determined by formula [12]:

$$u_q = \alpha \frac{q\,a^4}{D},$$

where $\alpha = 0.00126$; $D = \dfrac{E\,h^3}{12\,(1-\nu^2)}$ —— cylindrical stiffness; $q = 0.00888889$ H/m^2 — distributed load intensity. Exact value u_q (in meters) is equal to coefficient α.

In this example, ¼ part of the plate was considered taking into account the conditions of symmetry. The convergence results in the form of graphs $u_q \sim s$ for single-layer and double-layer models are shown in Figures 5 and 6. Here and further, layers mean the breakdown of the plate into FE by thickness. In these figures, values 1, 2, 3, 4 of parameter s 1, 2, 3, 4 correspond to the grids: 4×4, 8×8, 16×16, 32×32. The graphs below show the results of the solution obtained using ANSYS (line 1) and DAM (line 2). The horizontal line indicated by the number 3 corresponds to the exact solution.

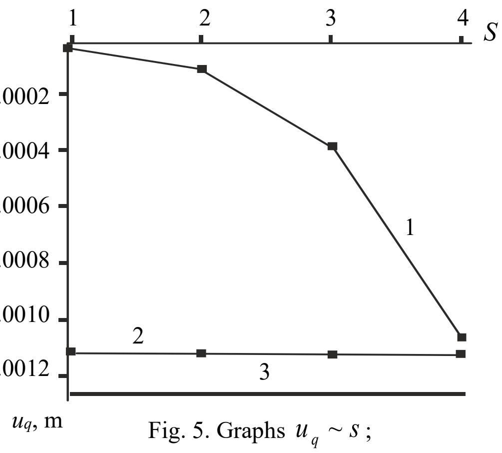

Fig. 5. Graphs $u_q \sim s$;
single-layer scheme

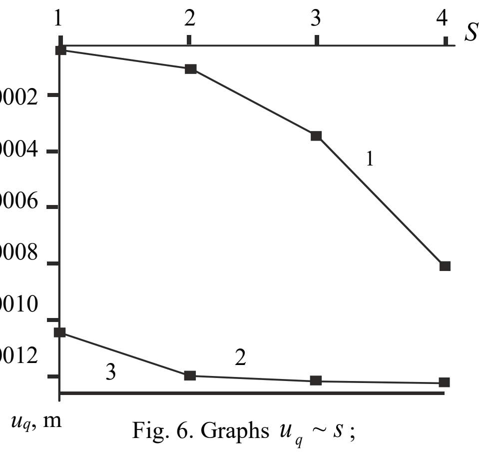

Fig. 6. Graphs $u_q \sim s$;
two-layer scheme

It follows from Figure 5 that with a single-layer breakdown scheme, the relative error values on a 32×32 grid are: SOLID185 — 16%; DAM - 10.5%. When using a two-layer scheme (Fig. 6) on a 32×32 grid, we have: SOLID185 — 36%; DAM — 2.8%.

FE patch testing was performed for the 16×16×2 breakdown scheme with grid distortion (Fig. 7). The patch test results in the form of deflection distribution patterns u_z are shown in Figures 8 and 9.

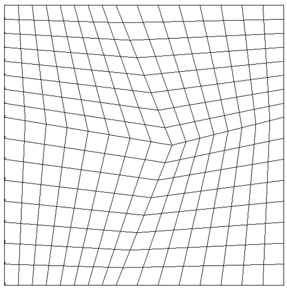

Fig. 7. Scheme of plate breakdown for patch test

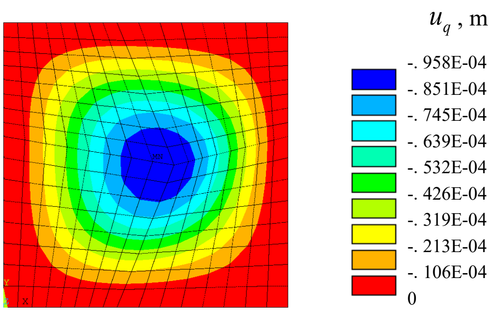

Fig. 8. Distribution u_q (SOLID185)

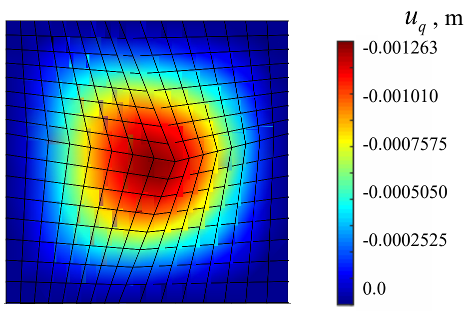

Fig. 9. Distribution u_q (МДА)

As can be seen from the Figures, the distortion of the grid, when using SOLID185, causes a more noticeable asymmetry of field u_z, than when using DAM. At the same time, the value of the maximum deflection for FE DAM u_q = 0,001263 m coincides with the exact solution.

Example 3. A round plate, rigidly pinched along the contour and loaded with a uniformly distributed load. Radius and thickness of the plate: $R = 1$ m; $h = 0.01$ m. The mechanical constants are similar to the data in Example 2.

The exact value of the deflection in the center of the plate is determined by formula [12]:

$$u_q = \frac{1}{64}\frac{q a^4}{D}.$$

At the value of the intensity of distributed load $q = 0.00888889$ H/m^2 value $u_q = 0.01563$ m.

In the testing process, two versions of sampling the ¼ part of the plate (sector) on FE were used. In the first version, the

Mechanics

three sides of the sector were divided into an equal number of segments. The second version was based on a radial regular pattern of sector breakdown. In this case, the number of elements along the radius and the circular part of the sector was assumed to be the same. The considered sector discretization versions for a 32×32 grid are shown in Figure 10.

Fig. 10. Sampling versions for the circular plate sector on FE:
1 — uniform breakdown of the three sides of the sector;
2 — radial regular breakdown

The convergence results in the form of graphs $u_q \sim s$ for sampling the ¼ part of the plate according to version 1 with single-layer and two-layer breakdown schemes are presented in Figures 11, 12, and Figures 13, 14, respectively.

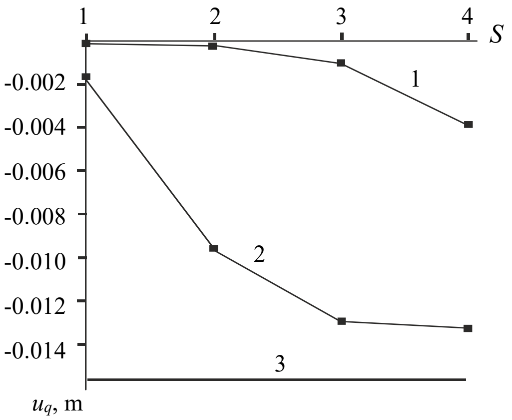

Fig. 11. Graphs $u_q \sim s$ for version 1;
single-layer scheme

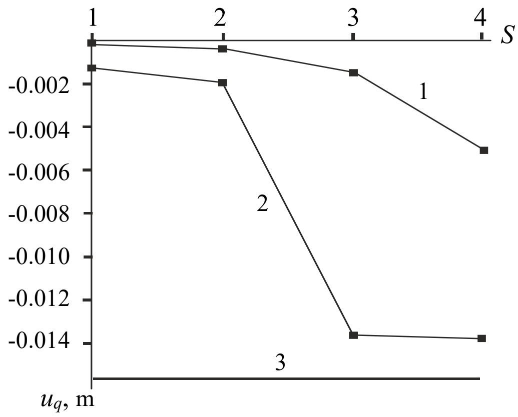

Fig. 12. Graphs $u_q \sim s$ for version 2;
single-layer scheme

In these figures, values 1, 2, 3, 4 of parameter s 1, 2, 3, 4 correspond to the grids: 4×4, 8×8, 16×16, 32×32. As in Example 1, line 1 corresponds to a SOLID185-based solution, and line 2 corresponds to DAM. The horizontal line indicated by the number 3 corresponds to the exact solution.

It follows from the above graphs that an element constructed according to the moment scheme on a 32×32×2 grid of version 2 has a relative error of 4 %.

Visualization patterns of the field of distribution of vertical displacements u_z for DAM and SOLID185 with a radial layout of the ¼ plate (32×32×2 grid) are shown in Figures 15 and 16, respectively.

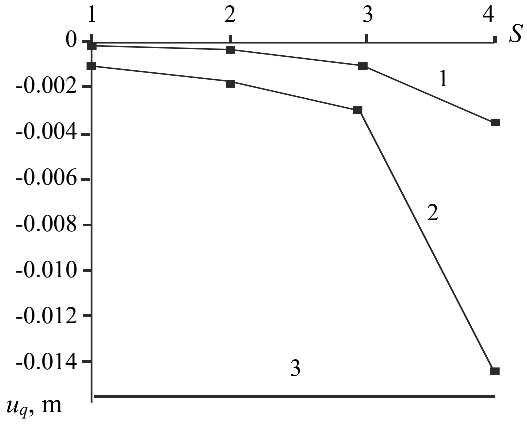

Fig. 13. Graphs $u_q \sim s$ for version 1; two-layer scheme

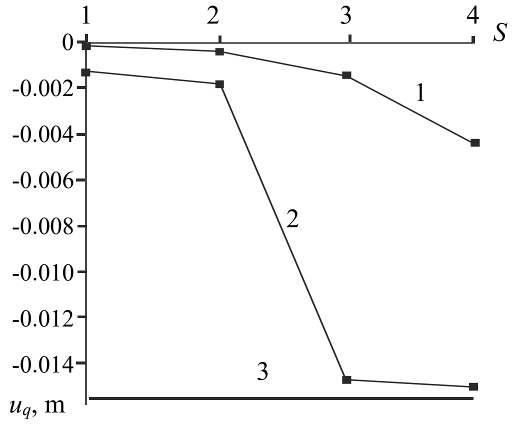

Fig. 14. Graphs $u_q \sim s$ for version 2; two-layer scheme

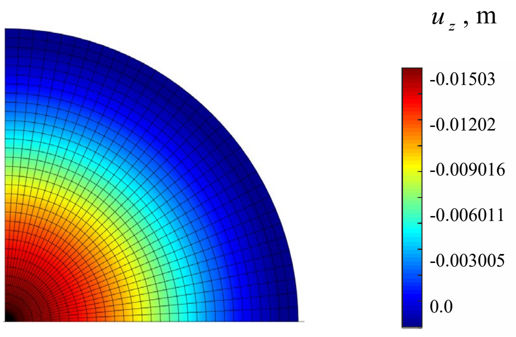

Fig. 15. Distribution u_z (МДА)

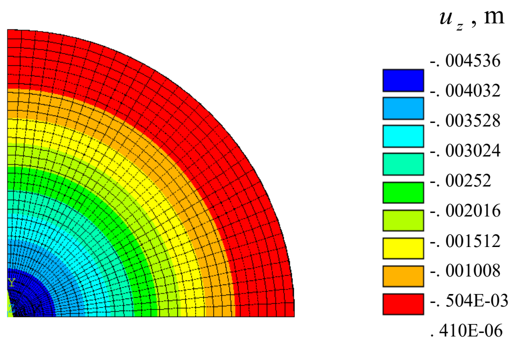

Fig. 16. Distribution u_z (SOLID185)

From the above figures, it can be seen that despite the qualitative coincidence of patterns u_z, relative errors for the maximum deflection are: DAM — 3.8%; SOLID185 — 71%. Such a significant error, when using SOLID185, is because the developers applied "shape functions" similar to the functions used for the eight-node element to approximate the geometry and displacements of the six-node element, i.e., without the "degeneration" principle [7].

Discussion and Conclusion. Stiffness matrices of volumetric multilinear finite elements constructed on the basis of the double approximation method make it possible to simulate the stress-strain state of building structures of arbitrary geometry under various types of external actions. The fundamental difference between the proposed concept and the previously known finite element technologies is that the displacements, in this case, are set in global coordinates, and the components of the strain tensor are determined in local, in general, nonorthogonal axes.

The test examples show that the volumetric finite elements, constructed by the double approximation method, have stable convergence and compete successfully with an element of a similar type SOLID185 of the ANSYS Mechanical computing complex.

The developed mathematical software can be introduced into domestic import-substituting software complexes implementing the finite element method in the form of the displacement method.

References

1. Zienkiewicz OC, Taylor RL. *The Finite Element Method,* Fifth edition. Oxford, UK: Butterworth-Heinemann; 2000. 708 p.

2. David V Hutton. *Fundamentals of Finite Element Analysis*. New York, NY: The McGraw Hill Companies; 2004. 494 p. URL: https://wp.kntu.ac.ir/fz_kalantary/Source/Finite%20element%20method/BooksNumerical/Fundamentals%20of%20Finite%20Element%20Analysis,%20Hutton%20(2004).pdf (accessed: 15.08.2023).

3. Daryl L Logan. *A First Course in the Finite Element Method*. New York, NY: CL Engineering; 2011. 836 p. URL: https://kntu.ac.ir/DorsaPax/userfiles/file/Mechanical/OstadFile/dr_nakhodchi/DarylL.LoganAFirstCourse.pdf (accessed: 15.08.2023).

4. Carlos A Felippa. *Introduction to Finite Element Methods*. Boulder, CO: University of Colorado; 2004. 791 p. URL: https://vulcanhammernet.files.wordpress.com/2017/01/ifem.pdf (accessed: 15.08.2023).

5. Saeed Moaveni. *Finite Element Analysis. Theory and Application with ANSYS*. Hoboken, NJ: Prentice Hall; 1999. 527 p. URL: http://ftp.demec.ufpr.br/disciplinas/TM738/Livros/Finite%20Element%20Analysis,%20Theory%20and%20application%20with%20ANSYS,%20.pdf (accessed: 15.08.2023).

6. Golovanov AI, Tyuleneva ON, Shigabutdinov AF. *Finite Element Method in Statics and Dynamics of Thin-Walled Structures.* Moscow: Fizmatlit; 2006. 391 p. (In Russ.)

7. David V Hutton. *Fundamentals of Finite Element Analysis*. New York, NY: McGraw-Hill; 2004. 505 p. URL: https://wp.kntu.ac.ir/fz_kalantary/Source/Finite%20element%20method/BooksNumerical/Fundamentals%20of%20Finite%20Element%20Analysis,%20Hutton%20(2004).pdf (accessed: 15.08.2023).

8. Miguel Luiz Bucalem, Klaus-Jürgen Bathe. *The Mechanics of Solids and Structures – Hierarchical Modeling and the Finite Element Solution*. New York, NY: Springer; 2011. 597 p.

9. Jacob Fish, Ted Belytschko. *A First Course in Finite Elements*. Hoboken, NJ: Wiley; 2007. 319 p.

10. Gaidzhurov PP. Finite Elements of Increased Accuracy for Solving 3D Problems of Elasticity Theory. *University News. North-Caucasian Region. Technical Sciences Series.* 2003;(1):54–57. URL: https://cyberleninka.ru/article/n/konechnye-elementy-povyshennoy-tochnosti-dlya-resheniya-trehmernyh-zadach-teorii-uprugosti/viewer (accessed: 15.08.2023). (In Russ.)

11. Chigarev AV, Kravchuk AS, Smalyuk AF. *ANSYS for Engineers. Moscow*: Mashinostroenie; 2004. 512 p. URL: https://www.researchgate.net/profile/AKravchuk/publication/262729610_ANSYS_dla_inzenerov/links/0f31753b4294b13fc9000000/ANSYS-dla-inzenerov.pdf (accessed: 15.08.2023). (In Russ.)

12. Madenci E, Guven I. *The Finite Element Method and Applications in Engineering Using ANSYS*. New York, NY: Springer; 2015. 664 p.

Received 29.09.2023
Revised 31.10.2023
Accepted 18.11.2023

About the Authors:

Peter P. Gaidzhurov, Dr.Sci. (Eng.), Professor of the Structural Mechanics and Theory of Structures Department, Don State Technical University (1, Gagarin sq., Rostov-on-Don, 344003, RF), SPIN-code: 6812-9718, ORCID, gpp-161@yandex.ru

Nina A. Saveleva, Senior lecturer of the Structural Mechanics and Theory of Structures Department, Don State Technical University (1, Gagarin sq., Rostov-on-Don, 344003, RF), SPIN-code: 8437-8080, ORCID, ninasav86@mail.ru

Claimed contributorship:

PP Gaidzhurov: problem statement, selection of solution method and building of mathematical and computer model, discussion of the results.

NA Saveleva: conducting a review, computational analysis, discussion of the results.

Conflict of interest statement: the authors do not have any conflict of interest.

All authors have read and approved the final manuscript.

Поступила в редакцию 29.09.2023
Поступила после рецензирования 31.10.2023
Принята к публикации 18.11.2023

Об авторах:

Петр Павлович Гайджуров, доктор технических наук, профессор кафедры строительной механики и теории сооружений Донского государственного технического университета (344003, РФ, г. Ростов-на-Дону, пл. Гагарина, 1), ORCID, SPIN-код: 6812-9718, gpp-161@yandex.ru

Нина Александровна Савельева, старший преподаватель кафедры строительной механики и теории сооружений Донского государственного технического университета, (344003, РФ, г. Ростов-на-Дону, пл. Гагарина, 1), SPIN-код: 8437-8080, ORCID, ninasav86@mail.ru

Заявленный вклад соавторов

П.П. Гайджуров — постановка задачи, выбор метода решения и построение математической и компьютерной модели, обсуждение результатов.

Н.А. Савельева — проведение обзора, проведение расчетов, обсуждение результатов.

Конфликт интересов: авторы заявляют об отсутствии конфликта интересов.

Все авторы прочитали и одобрили окончательный вариант рукописи.

MACHINE BUILDING AND MACHINE SCIENCE

UDC 621.791.14
https://doi.org/10.23947/2687-1653-2023-23-4-376-386

Original article

EDN: LFCYNM

Advantages of Friction Welding of Fittings with Small Diameter Conical Contact Form

Yuri V. Poletaev, Viktor V. Shchepkin
Don State Technical University, Rostov-on-Don, Russian Federation
shepkinviktor@rambler.ru

Abstract

Introduction. As numerous production tests show, the use of manual arc welding (MAW) of thick-walled fittings of small diameter (up to 80 mm) does not provide a high-quality weld joint that meets the requirements of regulatory and technical documents of nuclear power plants (NPP). The solution to this problem is possible on the basis of research and development of welding technology with optimal heat input instead of MAW. Existing fusion welding technologies do not allow for optimal regulated heat input. However, this can be realized during the development and further use of the friction welding (FW) method. Therefore, this work aimed at developing a technology based on an automated technique of friction welding, which could provide the enhancing of the quality of weld joints of small diameter fittings of power equipment to the level of regulatory requirements.

Materials and Methods. Small diameter fittings with a conical contact surface made of low-alloy steel 10GN2MFA were used. The experimental study was performed on a friction welding machine MST–41. Methods of non-destructive and destructive quality control were used in accordance with the regulatory and technical documentation of nuclear power engineering.

Results. A methodology was developed, and the optimal dimensions of the conical contacting surface under welding were determined. It was shown that optimal heat input during friction welding was achieved by preparing a conical contacting surface in the angle range $\alpha = 30^\circ$–40°. The methodology and parameters of the friction welding mode for models of small diameter fittings were experimentally tested. In the course of the research, a cyclogram of the friction welding process was obtained and described, which confirmed the stage-by-stage formation of the weld joint due to the sequential inclusion of annular sections of the conical surface of the connected parts in the heating stage. The results of non-destructive and destructive testing were obtained, confirming the presence of a high-quality weld joint at the level of the requirements of the regulatory and technical documents of the NPP.

Discussion and Conclusion. The obtained research results can be used to develop the technology of friction welding of pipes, as well as products made of carbon and low-alloy steels.

Keywords: fitting simulator, manual arc welding, friction welding, conical surface, cyclogram, mode parameters, optimal heat input, mechanical properties

Acknowledgements. The authors would like to thank the Editorial board and the reviewers for their attentive attitude to the article and for the specified comments that improved the quality of the article.

For citation. Poletaev YuV, Shchepkin VV. Advantages of Friction Welding of Fittings with Small Diameter Conical Contact Form. *Advanced Engineering Research (Rostov-on-Don)*. 2023;23(4):376–386. https://doi.org/10.23947/2687-1653-2023-23-4-376-386

Научная статья

Преимущества сварки трением штуцеров с конической контактирующей формой малого диаметра

Ю.В. Полетаев, В.В. Щепкин ✉
Донской государственный технический университет, г. Ростов-на-Дону, Российская Федерация
✉ shepkinviktor@rambler.ru

Аннотация

Введение. По свидетельствам многочисленных производственных испытаний, применение ручной дуговой сварки (РДС) толстостенных штуцеров малого диаметра (до 80 мм) не обеспечивает получения качественного сварного соединения, удовлетворяющего требованиям нормативно-технических документов атомных электрических станций (АЭС). Решение указанной проблемы возможно на основе разработки технологии сварки с оптимальным тепловложением и применения ее взамен РДС. Существующие технологии сварки плавлением не позволяют обеспечить оптимальное регулируемое тепловложение. Однако это может быть реализовано при разработке и дальнейшем использовании способа сварки трением (СТ). Поэтому цель данной работы заключалась в разработке технологии на основе автоматизированного способа сварки трением, позволяющей повысить качество сварных соединений штуцеров малого диаметра энергетического оборудования до уровня нормативных требований.

Материалы и методы. Использовали штуцеры малого диаметра с конусной контактирующей поверхностью из низколегированной стали 10ГН2МФА. Экспериментальное исследование выполняли на машине сварки трением МСТ–41. Использованы методы неразрушающего и разрушающего контроля качества в соответствии с нормативно-технической документацией атомного энергетического машиностроения.

Результаты исследования. Разработана методика и определены оптимальные размеры конусной контактирующей поверхности при сварке. Показано, что оптимальное тепловложение при сварке трением достигается при подготовке конусной контактирующей поверхности в диапазоне углов $\alpha = 30^{\circ}$–40°. Экспериментально отработана методика и параметры режима сварки трением моделей штуцеров малого диаметра. В ходе исследований получена и описана циклограмма процесса сварки трением, подтвердившая стадийное формирование сварного соединения за счет последовательного включения в стадию нагрева кольцевых участков конической поверхности соединяемых деталей. Получены результаты неразрушающего и разрушающего контроля, подтвердившие наличие качественного сварного соединения на уровне требований нормативно-технических документов АЭС.

Обсуждение и заключение. Полученные результаты исследований могут быть использованы для разработки технологии сварки трением патрубков, а также изделий из углеродистых и низколегированных сталей.

Ключевые слова: имитатор штуцера, ручная дуговая сварка, сварка трением, коническая поверхность, циклограмма, параметры режима, оптимальное тепловложение, механические свойства

Благодарности. Авторы выражают благодарность редакции и рецензентам за внимательное отношение к статье и указанные замечания, которые позволили повысить ее качество.

Для цитирования. Полетаев Ю.В., Щепкин В.В. Преимущества сварки трением штуцеров с конической контактирующей формой малого диаметра. *Advanced Engineering Research (Rostov-on-Don)*. 2023;23(4):376–386. https://doi.org/10.23947/2687-1653-2023-23-4-376-386

Introduction. The key problem of welding small diameter fittings is short weld length, which does not allow for full control of the quality of the manual arc welding process. Supplying welding equipment to the welding site is also not always technologically possible.

Weld-in and weld-on fittings are connected to the basic part by a fillet seam through manual arc welding with a coated electrode. Weld-in fittings are welded from the outside or from the inside with a constructive faulty fusion. In any case, the presence of non-welded gaps in the joints, which are stress concentrators, reduces the operability of the structure, as it can cause cracks. A more perfect connection is one that has no unwelded gap. Sometimes, to obtain a guaranteed penetration of the entire wall of the fitting and to exclude the possibility of cracking from faulty fusion, a moulding back ring removable after welding is used, or a thick-walled pipe blank is soldered in. After welding, it is drilled out to the internal diameter specified in the drawing (Fig. 1). This is quite time-consuming, but justified in critical structures, e.g., in the manufacture of equipment for nuclear power plants [1]. This method is shown in Figure 1, where the fitting assembly is shown before (*a*) and after welding (*b*). Here: *D* — inner diameter of fitting; *h, b* — welded joint legs; *S* — fitting wall thickness. According to the normative document[1], from which the drawing is borrowed, the permissible size for the wall thickness of the fitting should be ≥2 mm; bluntness of the welded joint — 4±1 mm; included angle — 50°±5°.

h, b — катеты сварного соединения; *S* — толщина стенки штуцера. Согласно нормативному документу[2], из которого заимствован рисунок, допускаемый размер на толщину стенки штуцера должен быть ≥2 мм; притупление сварного соединения — 4±1 мм; угол разделки кромок под сварку — 50°±5°.

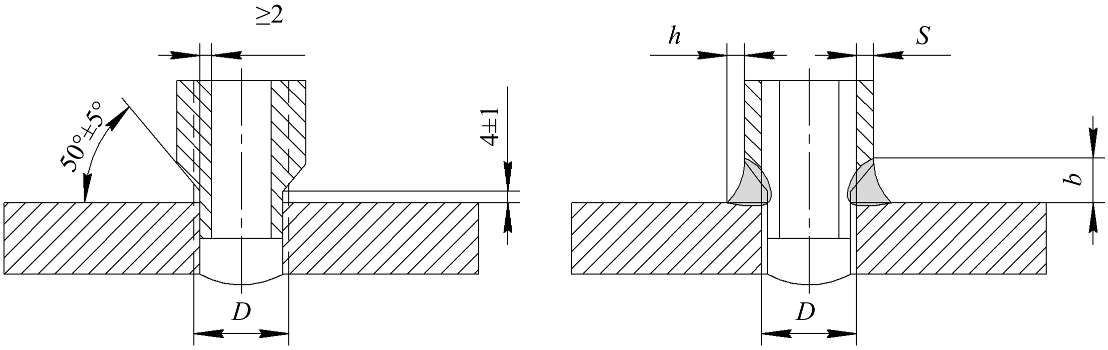

a) *b)*

Fig. 1. Fitting unit: *a* — before welding; *b* — after welding and removing the weld root

To weld the fitting, the following process operations are performed: turning the hole in the housing, grooving on the fitting, assembly of the unit maintaining perpendicularity, tacking the fitting, multilayer welding, removal of the weld root through boring the inner diameter to the standard dimensions.

The known disadvantages of the MAW do not allow for stable quality of the welded joint and are characterized by a large volume of cast weld metal in a limited space. This causes overheating and high residual stresses, which requires additional operations of heat treatment. The cost of repairing equipment in the event of a breakdown is high. This results in time and economic expenditures [2–6].

The analysis of the results of the literature review and production experience indicate the technical and economic feasibility of abandoning the use of the MAW method for obtaining welded thick-walled connections of fittings and pipes of small diameter (up to 80 mm) [7, 8].

In this regard, it was decided to investigate the effect of the grooving shape and the method of friction welding instead of MAW to provide optimal minimum heat input and stable quality of welds. Friction welding is characterized by optimal heat input (compared to fusion welding methods), in which a fine-grain structure is formed with a low level of residual welding stresses and a high level of mechanical properties [9, 10].

The objective of the work is to raise the quality of welds of small diameter fittings of power equipment to the level of regulatory requirements based on the development of an automated friction welding method.

Materials and Methods. Theoretical and experimental studies were carried out on welds made of low-alloy steel 10GN2MFA, used as the basic structural material for the manufacture of a steam generator, pressure compensator, and other critical NPP equipment[3].

[1] *Basic Provisions on Welding and Surfacing of Components and Structures of Nuclear Power Plants, Experimental and Research Nuclear Reactors and Installations 1513-72.* URL: https://docs.cntd.ru/document/564412851 (accessed: 02.08.2023). (In Russ.)

[2] *Основные положения по сварке и наплавке узлов и конструкций атомных электростанций, опытных и исследовательских ядерных реакторов и установок* ОП 1513-72. URL: https://docs.cntd.ru/document/564412851 (дата обращения: 02.08.2023).

In the work, a computational and experimental method was used to select the optimal shape of the joined surfaces under welding.

The developed friction welding technology was implemented when performing welded joints of fittings on the MST-41 installation.

Methods and volumes of non-destructive (radiographic, ultrasonic, visual-measuring, hardness determination) and destructive (static strength and impact bending tests, metallographic studies of the welded joint) control used in the manufacture of welded structures of NPP were applied to assess the quality of welds.

Research Results. Taking into account the process capabilities of the FW, at the first stage, the assembly technique was tested without grooving preparation in the form of a "classic" T-joint (Fig. 2 *a*) [11]. Parameters of the welding mode were selected according to the recommendations given in [11].

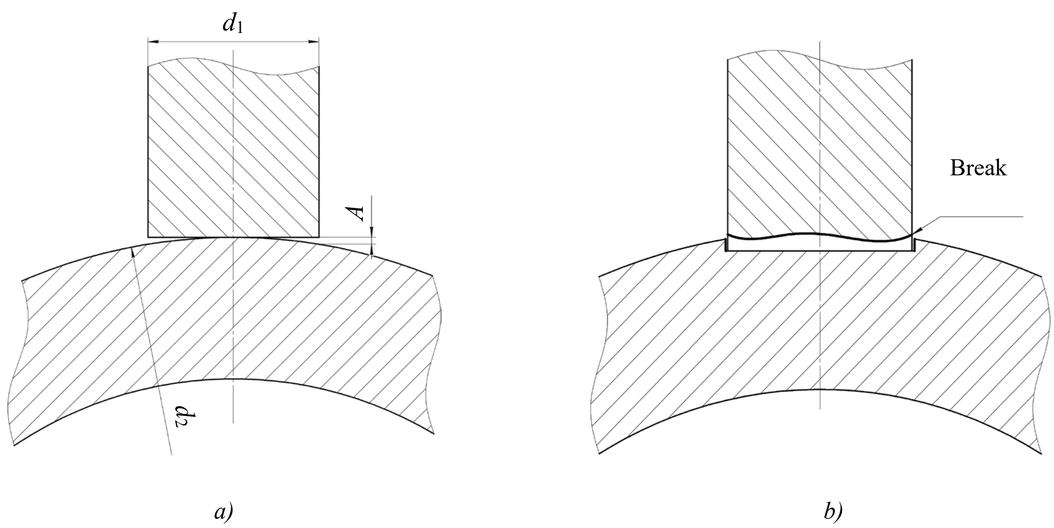

Fig. 2. Fitting unit simulators: *a* — T-joint simulator;
b — connection with pre-grooving: d_1 — fitting simulator diameter; d_2 — housing simulator diameter; A — gap

Quality control showed that the assembly of the fitting and the cylindrical housing of the equipment provided that gap A, whose value varied depending on the diameter of housing d_2 and fitting d_1. This form of joint did not provide uniform heating of the contacting surface, which caused the formation of sections of plastic material and their slippage with violation of the weld.

Taking into account the negative results of FW at the first stage, at the second stage, a friction welding procedure with preliminary grooving on the body (Fig. 2 *b*) was proposed and worked out. As the experimental results showed, at the initial stage of welding, the annular part was heated, the alignment was disturbed, and the subsequent separation of the lower part of the fitting simulator occurred, which ultimately caused the formation of a shapeless welded joint.

In the course of the experimental studies, it has been established that to obtain a high-quality weld of a large thickness base with a certain radius of curvature and a thick-walled fitting of small diameter obtained through friction welding, it is required:

– to develop a design of the connected surfaces that provides a reliable connection and high mechanical characteristics of the welded connection of small diameter fittings in a state without subsequent heat treatment or with heat treatment to lower temperatures;

– to provide optimal heating of the joining surfaces through the use of reasonable values of the welding mode parameters.

The analysis of the experimental data obtained indicates the need to develop a design of the connected surfaces to provide more uniform heating and the formation of a high-quality connection under FW. The conical shape of the surfaces was chosen as one of the options for obtaining such a compound [12–15].

[3] *Federal norms and rules in the field of the use of atomic energy. Welding and surfacing of equipment and pipelines of nuclear power plants NP-104-18. Order of the Federal Service for Environmental, Technological and Nuclear Supervision No. 554, dated 14.11.2018.* URL: https://sudact.ru/law/prikaz-rostekhnadzora-ot-14112018-n-554-ob/np-104-18/ (accessed: 02.08.2023). (In Russ.)

In the process of selecting the optimal contact surface, a verification calculation of the strength of welds of cylindrical and conical shapes was performed (Fig. 3). Calculations for the cylindrical surface were performed according to formula [16]:

$$N_ц = \left[\sigma_p\right] \cdot L \cdot S, \quad (1)$$

Where $\left[\sigma_p\right]$ — tensile strength, MPa; L — weld length, mm; S — weld thickness, mm.

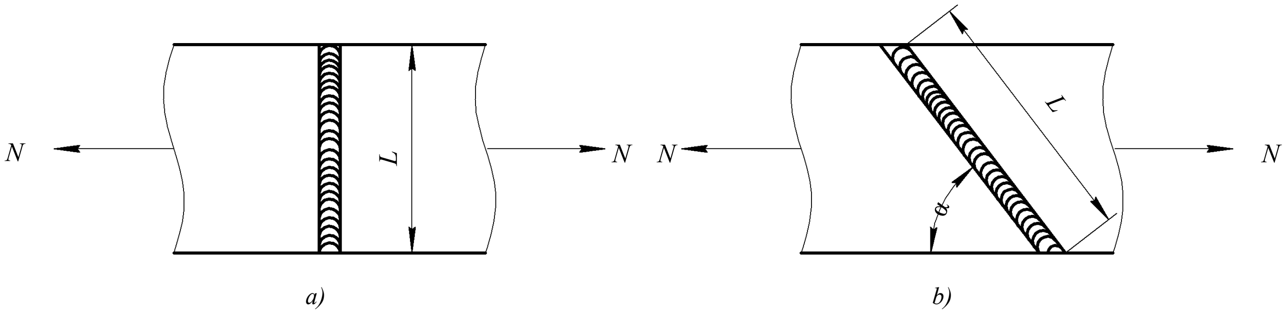

Fig. 3. Types of weld joints: *a* — cylindrical connectable surface; *b* — conical connectable surface:
N — load; L — weld length; α — angle of connectable surfaces

Calculations for the conical surface were performed according to formula:

$$N_к = \frac{\left[\sigma_P\right] \cdot L \cdot S}{\sin\alpha} \quad (2)$$

It can be seen that the shortest weld joint and the destructive load rate is characteristic of a model with a cylindrical contact surface. When moving to the conical contact surface, the length of the weld joint and the destructive load rate N naturally increase. These characteristics depend directly on angle α, whose optimal range, according to the calculation results, is presented in Table 1.

Table 1

Influence of angle of inclination α on strength indicators

Connection type	Angle of inclination, α,º	Load N, N
Cylindrical	–	59,283
Conical	30	118,566
	32.5	110,396
	35	101,609
	37.5	97,396
	40	94,959

Note that an unreasonable change in value α both up and down causes a decrease in strength (with a decrease in the weld length), or an increase in overheating and the amount of welding deformations (with an increase in the weld length).

In this regard, it is proposed to use a conical contacting surface on the one hand — on the fitting, on the other — a reciprocal conical surface on the housing (Fig. 4 *a*)

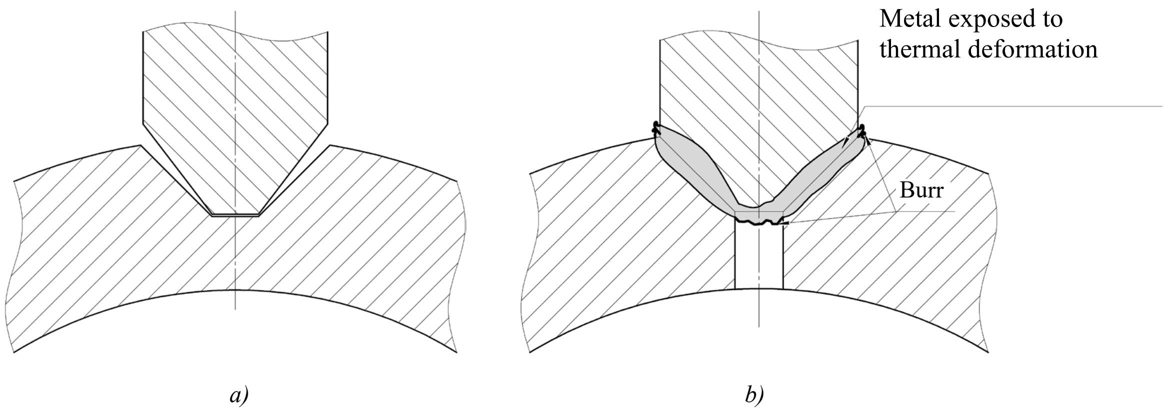

Fig. 4. Fitting unit: *a* — shape of the contact surface; *b*— ompleted weld

This design provides performing welds regardless of the diameter of the housing, since ductile metal fills the connected surface evenly under welding (Fig. 4 *b*).

Since the developed design provides uniform filling of the weld preparation regardless of the shape of the housing, it was proposed to use a flat surface of the housing for further experimental studies. The design and manufacture of models of fittings with different angles of the conical surface was carried out (Fig. 5).

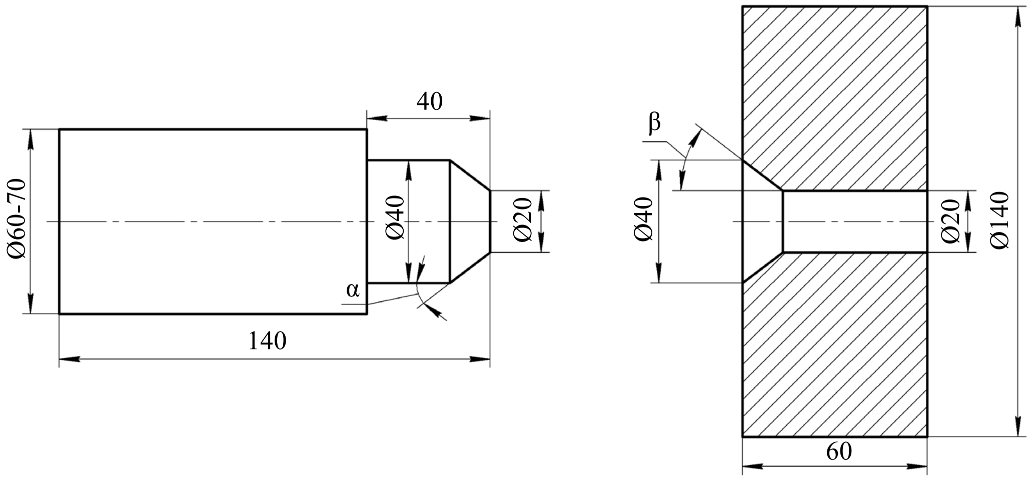

Fig. 5. Fitting unit model: α — fitting cone angle; β — housing cone angle

The dimensions of the angles of the mating surfaces of the joint were selected taking into account the calculation results, as well as the energy capacity of the MST-41 welding machine and the expected dimensions of the weld [18].

When preparing the surfaces of model elements for welding with cone angles α = 30.0°; 32.5°; 35.0°; 37.5° and 40.0°, welds were formed qualitatively with reasonably selected parameters of the FW mode. At the same time, the highest quality connection was obtained with a surface angle of 37.5°.

In the course of experimental studies, a pattern was established in the formation of a weld, namely, a gradual process of friction, heating, and plastic deformation took place on the surface of the welded joint. These differences from the known methods of forming joints in FW did not allow using the classical cyclogram of the welding process [11]. This required a more detailed study of the sequence of formation of the compound and the description of the cyclogram of the process in accordance with the specifics (Fig. 6).

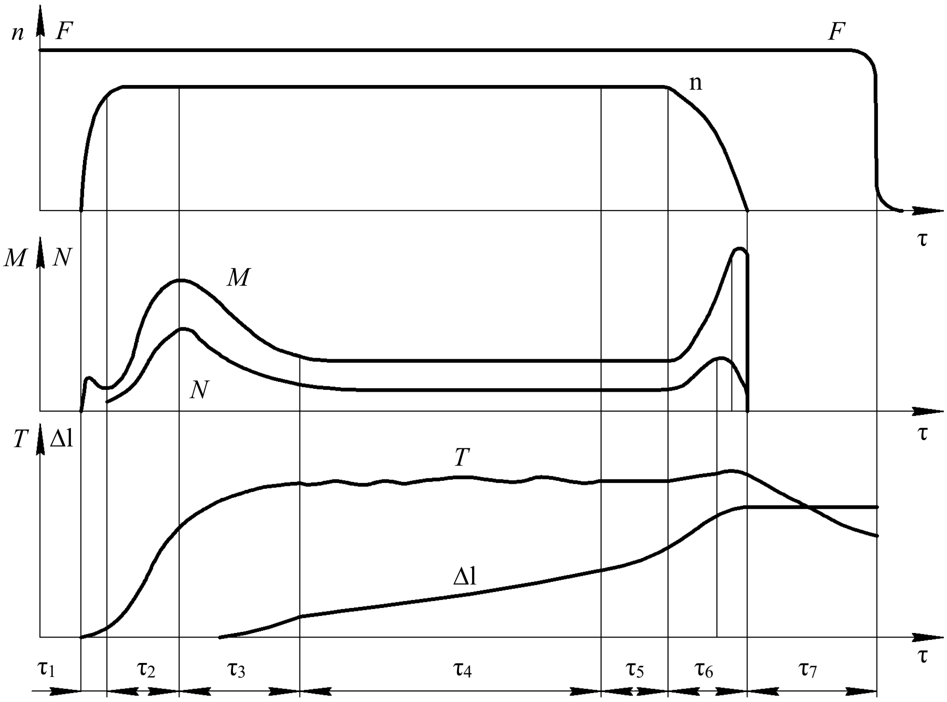

Fig. 6. FW process cyclogram:
n — angular velocity; F — heating pressure; M — friction moment; N — heat generation power;
T — temperature in the connection zone; Δl — upsetting; τ_1–τ_7 — cycle phases

In the welding process, phases τ_1, τ_2, τ_3 are similar to the initial phases of the FW cylindrical surfaces. In the first phase, the surface is lapped with separate microirregularities, but, unlike the classical methods, lapping does not go over the entire surface, but only on the area in contact with the cone. In the second phase, there is an increase in the area of the contacting surfaces and, as a result, temperature rise. The third phase is characterized by a rise in temperature and the release of plasticized metal (burr). The fourth phase τ_4 — phase of sequential heating of the entire cone surface. In this phase, there is a partial repetition of the processes occurring in the second and third phases. The difference is that the areas entering the heating process are already partially warmed up. In the fifth phase τ_5, a process of uniform heating of the entire welded surface occurs, close to a quasi-stationary state. The sixth τ_6 and seventh τ_7 — the braking and forging phases, in which the process of complete stop of rotation and compression occurs.

The implementation of this cyclogram is possible using the developed technique for calculating the parameters of the friction welding mode [17]. The basic parameters include: welding time t_c, heating pressure $P_н$, rotation speed V, and forging pressure $P_п$. The calculation results are shown in Table 2.

Table 2

Parameters of FW process of fitting model

Material	Sample number	Heating pressure, MPa	Forging pressure, MPa	Rotation speed, rpm	Welding time, sec.
10GN2MFA Steel	10–1	0.323	0.539	1,200	27
	10–2	0.367	0.539	1,200	32
	10–3	0.340	0.539	1,200	30

It is possible to significantly reduce the heating pressure and increase the welding time due to the sequential inclusion of annular sections of the conical surface of the connected parts in the heating stage.

The proposed process solutions make it possible to obtain high-quality connections with lower operating parameters, which reduces heat input in the weld, providing a reliable connection and minimal grain growth. In addition, with this method of welding, the annular sections entering into heating at the point of friction have a layer of ductile metal from the previous layer, which acts as a lubricant. This reduces the friction coefficient, and thereby reduces the required power of the welding machine.

The authors carried out the control of welds by non-destructive and destructive methods. The quality control results and mechanical properties of welds are shown in Table 3. The results of hardness measurement (Fig. 7) and microstructure (Fig. 8) of the welds meet the requirements of regulatory and technical documents.[4]

The hardness values in all samples indicate a fairly uniform structure over the entire weld section. Hardness values corresponding to the hardness of quenching structures were not revealed. Figure 7 shows a slight increase in hardness along the fusion line. To align the values along the cross-section of the weld, it is recommended to carry out heat treatment — thermofixation.

Table 3

Results of mechanical tests, radiographic and ultrasonic inspection of the fitting welds

Steel grade	Sample number	Stress limit σ_B, MPa	Yield strength $\sigma_{0.2}$, MPa	Relative elongation δ, %	Relative narrowing ψ, %	Bend angle	Impact strength KCV, J/m^2	Control	
								MAW	UT
10GN2MFA	10–1	635	595	14–17	70–78	123	251	sat	sat
	10–2	510	425	12–16	67–71	127	195	sat	sat
	10–3	770	650	15	68–70	125	273	sat	sat

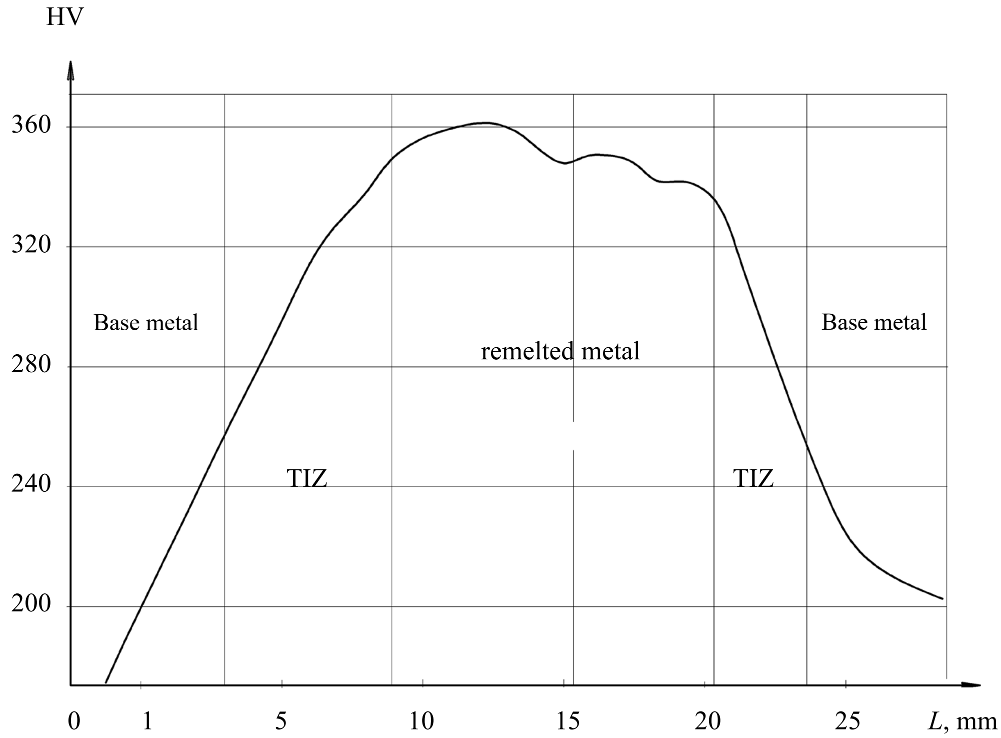

Fig. 7. Hardness distribution over the width of the weld joint made of 10GN2MFA steel (TIZ — thermal impact zone)

[4] *Testing rules of metal for equipment and pipelines of nuclear power plants during manufacture and installation. NP-105-18*. Order of the Federal Service for Environmental, Technological and Nuclear Supervision No. 553, dated 14.11.2018. (In Russ.)

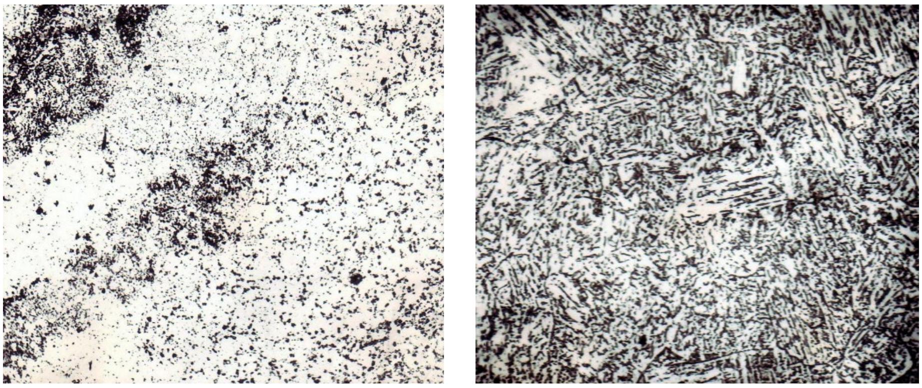

a) *b)*

Fig. 8. Microstructure of various zones of a weld from 10GN2MFA steel made by friction welding (×500): *a* — thermal impact zone; *b* — fusion line

Discussion and Conclusion. High and stable quality of the weld is obtained due to optimal heat input under friction welding of the contacting surfaces through the sequential including of the annular sections of the conical welds in the heating and friction process. This contributes to the metal structure refinement of the weld and the thermal impact zone, and obtaining high mechanical properties of the metal of the weld.

As a result of the experimental study, the positive effect of the basic structural and processing factors and, above all, the conical shape of the connected surfaces, on the quality of thick-walled welds of small diameter fittings (up to 80 mm) was established. The obtained positive results of destructive and non-destructive testing confirm the required quality and prospects for the use of friction welding of fitting welds with a conical surface in the manufacture of NPP equipment.

References

1. Sabitov MKh, Ponikarov SI, Valeev SI. Assessment of the Resource of Safe Operation of Gas Separators with Defects in Fillet Weld Fitting Welding. *Herald of Kazan Technological University*. 2013;16(15):118–120. https://cyberleninka.ru/article/n/otsenka-resursa-bezopasnoy-ekspluatatsii-g-azoseparatorov-s-defektami-uglovyh-svarnyh-shvov-privarki-shtutserov/viewer (accessed: 20.08.2023). (In Russ.)

2. Ermolaev VV, Zhuchenko LA, Lyubimov AA, Gladshtein VI, Kremet VL. Experience in Reconstructing the PT-60-90 Turbine Reconstruction of the Turbine PT-60-90 by Reconditioning Heat Treatment of the High-Pressure Cylinder Shell. *Thermal Engineering*. 2018;(6):5–14. https://doi.org/10.1134/S004036361806005X

3. Mironova LI, Fedik II. Local Thermal Loading of Two Intersecting Cylindrical Rotational Shells with a Variable Wall Thickness. *Engineering and Automation Problems*. 2015;(1):83–87.

4. Elchaninov AA, Korchagin IB. Design of a Device for Welding Fittings to a Heat Exchanger. In: *Collection of Works of the Winners of the Competition of Research Works of Students and Graduate Students of VSTU in Priority Areas for the Development of Science and Technology*. Voronezh: Voronezh State Technical University; 2020. P. 224–226. https://studfile.net/preview/16729056/page:23/ (accessed: 28.08.2023). (In Russ.)

5. Dolgachev YuV, Pustovoit VN. Interaction of Ferromagnetically Ordered Clusters with Dislocations in Austenite and Twinning. *Materials Science Forum*. 2022;1052:134–139. https://doi.org/10.4028/p-a8jty9

6. Assaulenko SS, Lyudmirsky YG, Kharchenko VY, Chernogorov AL. Computer-Digital Technique for Evaluating the Geometry of the Interface of the Weld with the Base Metal. *IOP Conference Series: Materials Science and Engineering*. 2020;1001:012038. https://doi.org/10.1088/1757-899X/1001/1/012038

7. Cleiton Carvalho Silva, Arlindo Braga de Souza Neto, Francisco Diego Araruna da Silva, Francisco Edval Sampaio de Freitas Júnior, Jesualdo Pereira Farias. Welding of ASTM A106 Gr. B Steel Pipes for High-Temperature Service — Part 1 — Residual Stress Analysis. *Welding International*. 2009;23(4):270–281. https://doi.org/10.1080/09507110802543476

8. Maodong Kang, Ming Jiang, Soumya Sridar, Wei Xiong, Zhixiong Xie, Jun Wang. Effect of Multiple Repair Welding on Crack Susceptibility and Mechanical Properties of Inconel 718 Alloy Casting. *Journal of Materials Engineering and Performance*. 2022;31(1):254–261. https://doi.org/10.1007/s11665-021-06173-6

9. Kaimeng Wang, Hongyang Jing, Lianyong Xu, Lei Zhao, Yongdian Han, Kai Song, et al. Fracture Mechanism of a Ni-Base Alloy under High-Temperature Cyclic Deformation: Experiments and Microstructure Characterization. *Materials Characterization*. 2022;189:111944. https://doi.org/10.1016/j.matchar.2022.111944

10. Lyudmirskii YuG, Assaulenko SS, Ageev SO. Constructive and Technological Method of Increasing Durability of "Choke Connections". *Journal of Physics: Conference Series*. 2021;2131:042061. https://doi.org/10.1088/1742-6596/2131/4/042061

11. Gnyusov SF, Khazanov IO, Sovetchenko BF, Degtyarenko EA, Kiselev AS, Trushchenko EA, et al. *Application of the Effect of Superplasticity of Steels in Tool Production*. Monograph. Tomsk: NTL Publishing House; 2008. 240 p. (In Russ.)

12. Poletaev YuV, Poletaev VYu, Shchepkin VV. Friction Welding of Fittings and Nozzles from Low-Alloy Steel 15X2HMFA. *Welding International*. 2020;34(1–3):29–33. https://doi.org/10.1080/09507116.2021.1919446

13. Shchepkin V, Poletaev Yu. Friction Welding of Fasteners from Austenite Steels. *E3S Web of Conferences*. 2020;210:08012. https://doi.org/10.1051/e3sconf/202021008012

14. Schepkin V, Poletaev Yu. Friction Welding of Carbon Quality Steel. *Journal of Physics: Conference Series*. 2021;2131:042062. https://doi/org/10.1088/1742-6596/2131/4/042062

15. Poletaev YuV, Poletaev VYu, Shchepkin VV. Friction Welding of Fittings and Branch Pipes from Low-Alloy Steel 15Kh2NMFA. *Welding Production*. 2018;(7):13–18. (In Russ.)

16. Konovalov AV, Kurkin AS, Makarov EL, Nerovnyi VM, Yakushkin BF. *Theory of Welding Processes*. VM Nerovnyi (ed). Moscow: Bauman University Publ. House; 2007. 752 p. (In Russ.)

17. Shchepkin VV, Poletaev YuV, Rogozin DV. Method for Calculating the Parameters of the Friction Welding Mode of Conical Connections. In: *Proc. XXIV Int. Sci.-Pract. Conf. within the Framework of the Agro-Industrial Forum of the South of Russia, Exhibitions "Interagromash", "Agrotechnologies"*. Rostov-on-Don: DSTU-PRINT; 2021. P. 490–493. https://doi.org/10.23947/interagro.2021.490-493 (In Russ.)

Received 02.09.2023
Revised 30.09.2023
Accepted 17.10.2023

About the Authors:

Yuri V. Poletaev, Dr.Sci. (Eng.), Senior Research Fellow, Professor of the Welding Fabrication Machines and Automation, Don State Technical University (1, Gagarin sq., Rostov-on-Don, 344003, RF), SPIN-code: 7763-3543, ScopusID, ORCID, anclav51@mail.ru

Viktor V. Shchepkin, Teaching assistant of the Welding Fabrication Machines and Automation, Don State Technical University (1, Gagarin sq., Rostov-on-Don, 344003, RF), SPIN-code: 2093-6094, ScopusID, ORCID, shepkinviktor@rambler.ru

Claimed contributorship:

VV Shchepkin: basic concept formulation, research objective and tasks, calculations, text preparation, formulation of conclusions.

YuV Poletaev: academic advising, analysis of research results, revision of the text, correction of the conclusions.

Conflict of interest statement: the authors do not have any conflict of interest.

All authors have read and approved the final manuscript.

Поступила в редакцию 02.09.2023

Поступила после рецензирования 30.09.2023

Принята к публикации 17.10.2023

Об авторах:

Юрий Вениаминович Полетаев, доктор технических наук, старший научный сотрудник, профессор кафедры машин и автоматизации сварочного производства Донского государственного технического университета (344003, РФ, г. Ростов-на-Дону, пл. Гагарина, 1), SPIN-код: 7763-3543, ScopusID, ORCID, anclav51@mail.ru

Виктор Викторович Щепкин, ассистент кафедры машин и автоматизации сварочного производства Донского государственного технического университета (344003, РФ, г. Ростов-на-Дону, пл. Гагарина, 1), SPIN-код: 2093-6094, ScopusID, ORCID, shepkinviktor@rambler.ru

Заявленный вклад соавторов:

В.В. Щепкин — формирование основной концепции, цели и задачи исследования, проведение расчетов, подготовка текста, формирование выводов.

Ю.В. Полетаев — научное руководство, анализ результатов исследований, доработка текста, корректировка выводов.

Конфликт интересов: авторы заявляют об отсутствии конфликта интересов.

Все авторы прочитали и одобрили окончательный вариант рукописи.

MACHINE BUILDING AND MACHINE SCIENCE

UDC 673.7
https://doi.org/10.23947/2687-1653-2023-23-4-387-397

Original article

EDN: LRSXPY

Effect of Glass Fiber Reinforcement on the Mechanical Properties of Polyester Composites

Imad Rezakalla Antypas
Don State Technical University, Rostov-on-Don, Russian Federation
✉ Imad.antypas@mail.ru

Abstract
Introduction. Glass fibers significantly improve the quality of composite materials, make them lighter, stronger, more corrosion resistant and thermally stable. Strengths and weaknesses of specific composites are actively discussed in the scientific and applied literature. At the same time, the effect of the ratio of fibers and matrix material on the mechanical characteristics of composites has not been sufficiently investigated. The presented study is intended to fill this gap. The work is aimed at manufacturing a composite material on a polymer basis reinforced with glass fiber, and investigating the influence of weight ratios of elements on the mechanical characteristics of the composite. For the first time, a report on the comparison of the characteristics of composites (with different fiber content) to each other and to steel is published.
Materials and Methods. Fiberglass and polyester were used as starting materials with the addition of a mediator to speed up the molding process. The samples were made manually and tested for tensile strength, hardness, and impact strength using standard equipment. The results were summarized in the form of tables, visualized in the form of graphs, and processed by comparative analysis.
Results. The technique of creating samples and methods of their testing were described. The research showed that hardness, tensile strength and impact resistance increased with a growth in the percentage of randomly distributed fiberglass to 50% with 50% unsaturated polyester. In this case, the maximum values of tensile strength — 175.4 MPa, hardness — 38 HV and impact resistance — 1.56 J/mm^2 were obtained. The inexpediency of exceeding the proportion of fiberglass by more than 50% was experimentally proven, since mechanical properties deteriorated. This was due, in particular, to the fragility of the glass, which, if the proportions were violated, was transmitted to the entire composite. In addition, with an excessively high volume of reinforcing fibers, the resin was not enough for high-quality bonding of the elements, which significantly reduced the strength of the material. Most of the mechanical characteristics of a composite made of 50% polyester and 50% fiberglass are better than those of steel.
Discussion and Conclusion. It has been proved that the properties of the composite material depend significantly on the glass fiber content. The resulting composite was compared to steel. It turned out that it had better mechanical characteristics and less weight. This allows us to recommend the material for boat hulls.

Keywords: glass fiber reinforcement, ratio of polyester to glass fiber in a composite, mechanical characteristics of a composite, comparison of composite and steel samples

Acknowledgements. The author would like to thank the Editorial board of the journal and the reviewers for their attentive attitude to the article, and comments that helped to improve the quality of the article.

For citation. Antypas IR. Effect of Glass Fiber Reinforcement on the Mechanical Properties of Polyester Composites. *Advanced Engineering Research* (*Rostov-on-Don*). 2023;23(4): 387–397. https://doi.org/10.23947/2687-1653-2023-23-4-387-397

Научная статья

Влияние армирования стекловолокном на механические свойства полиэстерных композитов

И.Р. Антибас
Донской государственный технический университет, г. Ростов-на-Дону, Российская Федерация
✉ Imad.antypas@mail.ru

Аннотация
Введение. Стекловолокна существенно улучшают качество композитных материалов, делают их легче, прочнее, устойчивее к коррозии и термически стабильнее. В научной и прикладной литературе активно обсуждаются сильные и слабые стороны конкретных композитов. При этом недостаточно исследовано влияние соотношения волокон и материала матрицы на механические характеристики композитов. Представленная работа призвана восполнить этот пробел. Цели исследования — изготовление композиционного материала на полимерной основе, армированного стекловолокном, а также изучение влияния весовых соотношений элементов на механические характеристики композита. Впервые публикуется отчет о сопоставлении характеристик композитов (с различным содержанием волокна) друг с другом и со сталью.
Материалы и методы. В качестве исходных материалов использовались стекловолокно и полиэстер с добавлением медиатора для ускорения процесса формования. Образцы изготавливались вручную и при помощи стандартного оборудования испытывались на растяжение, твердость и ударную прочность. Результаты обобщали в виде таблиц, визуализировали в виде графиков и обрабатывали методом сравнительного анализа.
Результаты исследования. Показаны способ создания образцов и методы их испытаний. Изыскания позволили установить, что твердость, прочность на разрыв и устойчивость к удару возрастают с увеличением процентного содержания случайно распределенного стекловолокна до 50 % при 50 % ненасыщенного полиэстера. В этом случае достигаются максимальные значения прочности на разрыв — 175,4 МПа, твердости — 38 HV и ударопрочности — 1,56 Дж/мм^2. Экспериментально доказана нецелесообразность превышения доли стекловолокна более чем на 50 %, т. к. механические свойства ухудшаются. Это объясняется, в частности, хрупкостью стекла, которая при нарушении пропорций передается всему композиту. Кроме того, при чрезмерно высоком объеме армирующих волокон смолы будет недостаточно для качественного скрепления элементов, что существенно снизит прочность материала. Большинство механических характеристик композита из 50 % полиэстера и 50 % стекловолокна лучше, чем у стали.
Обсуждение и заключение. Доказано, что свойства композитного материала существенно зависят от содержания стекловолокна. Полученный композит сравнили со сталью. Выяснилось, что он обладает лучшими механическими характеристиками и меньшим весом. Это позволяет рекомендовать использовать данный материал для изготовления корпусов лодок.

Ключевые слова: армирование стекловолокном, соотношение полиэстера и стекловолокна в композите, механические характеристики композита, сравнение композитных и стальных образцов

Благодарности. Автор выражает благодарность редакции и рецензентам за внимательное отношение к статье и замечания, которые позволили повысить ее качество.

Для цитирования: Антибас И.Р. Влияние армирования стекловолокном на механические свойства полиэстерных композитов. *Advanced Engineering Research* (*Rostov-on-Don*). 2023;23(4):387–397. https://doi.org/10.23947/2687-1653-2023-23-4-387-397

Introduction. Polymers are attractive as composite matrices due to their relatively low density, ease of processing, and excellent mechanical properties. High-temperature resins are used for the production of aircraft, rockets, boats, and other equipment. Reinforcement (glass fiber) takes the major load, specifically, if the composite consists of fibers dispersed in a weak matrix (e.g., a carbon-epoxy composite). Thus, the strength and stiffness of the material are determined by the strength and stiffness of the fibers [1–4].

Major advantages of glass fiber-reinforced composites are high strength and modulus of elasticity. Due to their low specific gravity, good strength-to-weight ratio, these materials out-perform metals. In addition, the verified ratio of fatigue strength and weight significantly increases the resistance of many composite laminates to fatigue damage [5, 6].

The authors [7] have proved that the mechanical properties of fiber-reinforced composites depend on the properties of the materials included in their composition (type, quantity, distribution and orientation of fibers, voids). The character of interfacial connections and load transfer mechanisms at the phase interface also play an important role.

Studies [8] have shown that the tensile strength of plates from glass fiber varies depending on environmental conditions. In [9], two types of composites with different glass fiber reinforcement were considered: chopped and mixed with unsaturated polyester resin (glass fiber 0/90). It was found that the composite reinforced with chopped glass fiber had a higher modulus of elasticity, maximum stress, and yield strength than the composite reinforced with glass fiber 0/90.

The authors of scientific papers focused on the features of various types of glass fiber and matrix materials. At the same time, the dependence of the quality of the composite on the ratio of the volumes of fibers and the matrix material has not been sufficiently investigated.

In the presented article, the quality of materials is compared in two directions. The first parallel is composites with different ratios of fibers and matrices. The second is composite and steel. The data is published for the first time.

The study aimed at investigating the effect of the glass fiber content on the mechanical properties of the material, i.e., on its behavior under load. Hardness, tear and impact resistance were evaluated.

Materials and Methods. For the production of samples, resin (polyester) with the addition of substances that promote the reaction, and glass fiber were used as starting materials (Fig. 1).

Fig. 1. Glass fiber

The obtained samples were tested for tension, hardness, and shock load. Similar experiments were carried out on steel parts. Each experiment was repeated five times. From test to test, the percentage of glass fiber was increased, and then the average results were taken.

Table 1 shows the mechanical-physical properties of the glass fiber used.

Таблица 1

Mechanical-physical properties of glass fiber [10]

Indicator	Value
Density, kg/m^3	2,500
Tensile strength, MPa	2,400
Modulus of elasticity, GPa	85
Elongation, %	0.01

Unsaturated polyester, which is a viscous liquid at room temperature, was used as the basic material. Its mechanical properties are shown in Table 2.

Table 2

Mechanical properties of polyester [10]

Indicator	Value
Density, kg/m^3	1,200
Tensile strength, MPa	42
Modulus of elasticity, GPa	2.8
Elongation, %	3.2

Auxiliary materials. The following substances were added to unsaturated polyester [11]:

– cobalt liquid material for hardening (3–4 %);

– mediator — a stimulating substance used to accelerate precipitation (1.5 –3 %).

Measurement of glass fiber density. To determine the density of glass fiber, it was immersed in water in a standard container. The obtained value ρ = 2,500 kg/m^3 coincided with the reference value.

Tensile testing of glass fiber. The average diameter of the fibers was determined using a microscope — 20.14 µm. After calculating the cross-section of one fiber, their average number in the bundle was determined through comparing the masses of the fibers and the bundle from which they were taken. The average number of fibers in the bundle turned out to be 2,200. Then, depending on the number of fibers, the bundle cross-section was calculated A = 0.7 mm^2.

Experiments were hampered by breaks in the attachment points due to the fragility of the fibers. The pressure of the clamps of the stretching device on the ends of the fibers was reduced as follows. Special paper with good absorbency was filled with resinous material, fibers were placed in it and left at room temperature until complete dry-out. Then the paper was cut, and samples were obtained from fiber bundles ready for testing (Fig. 2).

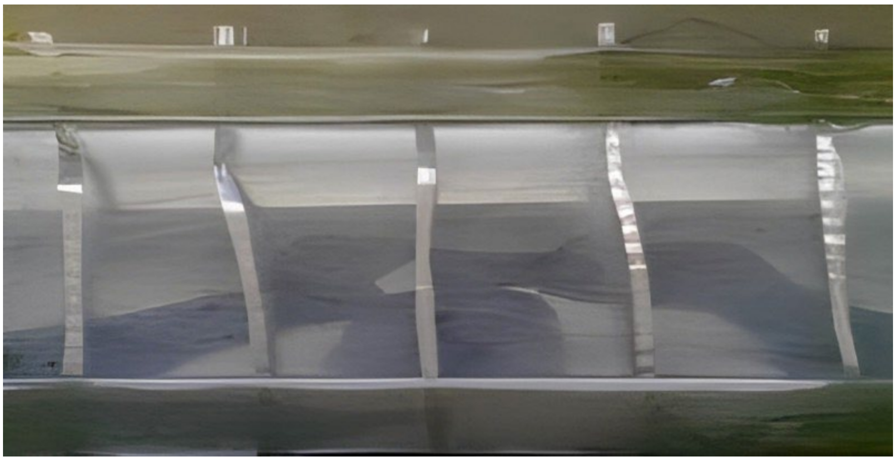

Рис. 2. Образцы волокон на растяжение

The dimensions of the tensile samples were determined in accordance with the international standard requirements ASTM D 2343–95[1] for such tests. Experimental parameters were as follows: the length of the fibers between mandrels was 25 cm, the length of the mandrels at both ends — 5 cm, the speed of application of the tensile load — 12.7 m/s, laboratory temperature — 23ºC.

Research Results

Sampling. Samples with different mass content of glass fiber were prepared (10%, 20%, 30%, 40%, 50%, and 60%). To do this, a mixture of 5% polyester, cobalt, and a catalyst was prepared at room temperature. A certain amount of it was evenly distributed with a brush over the inner surface of the mold. Then, a layer with randomly distributed glass fibers was applied. Next, the layers of fibers were impregnated with the mixture and superimposed on each other until a final sample of the appropriate proportions was obtained (Fig. 3, 4).

a) *b)*

Fig. 3. Sample forms: *a* — preparation; *b* — ready-made

[1] Standard Test Method for Tensile Properties of Glass Fiber Strands, Yarns, and Rovings Used in Reinforced Plastics. URL: https://cdn.standards.iteh.ai/samples/3930/2180b1c23fb041fe88bcfd3fba3fe2f6/ASTM-D2343-95.pdf (accessed: 27.09.2023).

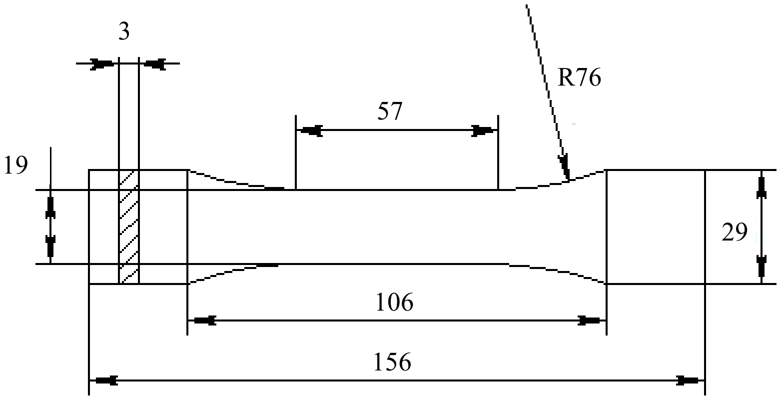

Fig. 4. Standard sample form

Finished samples were taken out of the mold, cleaned and placed in a dry environment for 24 hours.

Tensile testing. Tensile tests were carried out in accordance with ISO 326 ASTMD 638[2], as shown in Figure 5. The sample was firmly fixed at both ends of the stretching device. A tensile load from zero to 20 N/min was gradually applied to it until the sample was destroyed.

Fig. 5. Stretching device

The stretching process was divided into three areas. In the first one, there was sliding between the clamping jaws and the sample surfaces; therefore, the samples were clamped well. In the second area, due to the elastic behavior of the contacting surfaces of materials, a direct relationship between stress and deformation was observed. The third area was after the destruction of the sample. It was neither complete nor sudden, because it went evenly depending on the orientation angles of the fibers in the layers of glass-fiber mat. As a result, the indicators of maximum tensile strength and elastic deformation of the samples were obtained.

Tensile strength σ_C^R, which expresses the fracture stress of the composite material, was calculated by ratio [12]:

$$\sigma_C^R = \frac{F_{\max}}{B \cdot e},$$

where F_{max} — maximum force that caused the destruction of the sample, H; B — sample thickness, mm, e — sample thickness, mm.

[2] Standard Test Method for Tensile Properties of Plastics. URL: https://tienda.aenor.com/norma-astm-d638-99-017910 (accessed: 27.09.2023).

Figure 6 shows the results of tensile testing of glass fiber.

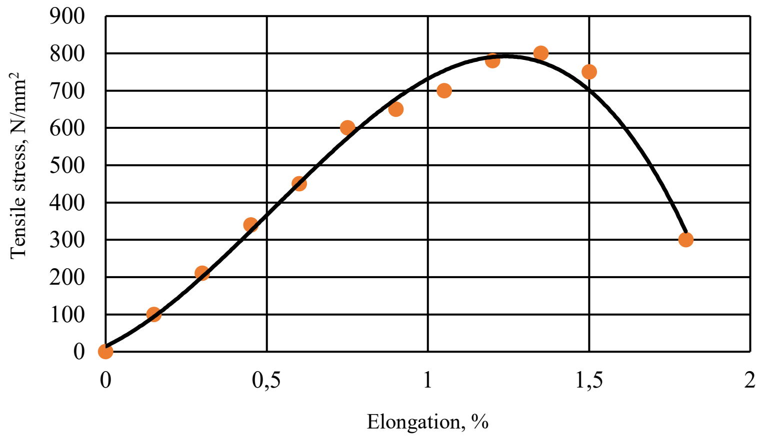

Fig. 6. Behavior of fibers under tension

According to Figure 6, the value of the elastic modulus under tension was calculated. Its average value E = 80,000 MPa, was established, which was accepted for further testing.

Figure 7 and Table 3 show the results of the effect of the fiber percentage on the strength under tensile tests.

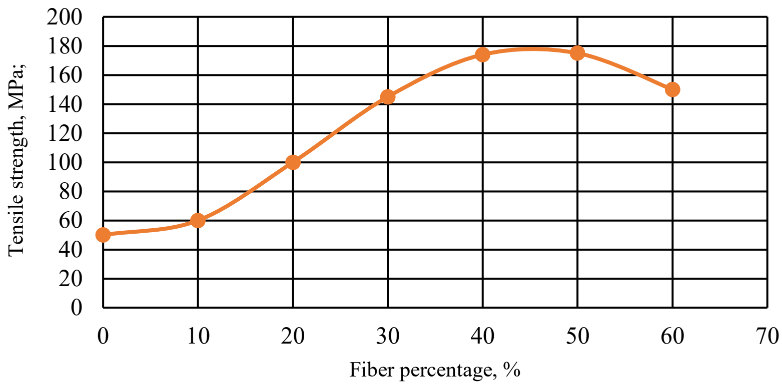

Fig. 7. Fiber percentage effect on the sample strength under tensile testing

The decrease in the value of tensile strength at a fiber content of 60% is due to the fact that polyester becomes insufficient to bind such a mass of fibers. Consequently, the adherence between the base and reinforcing materials is reduced.

Table 3

Tensile strength values depending on the percentage of fiber content for each sample

Fiber content in the sample, %	Tensile strength values, MPa
0	50
10	63.3
20	101.5
30	145.7
40	174.3
50	175.4
60	150.2

Figure 8 and Table 4 show how the glass fiber content affects the elastic deformation of the samples. It should be noted that with an increase in the fiber content, the elastic deformation index grows and reaches a maximum value (2.71%) at 50%. With a further increase in the mass of the fibers, the elastic deformation decreases, which is due to the high tensile strength of the glass fiber.

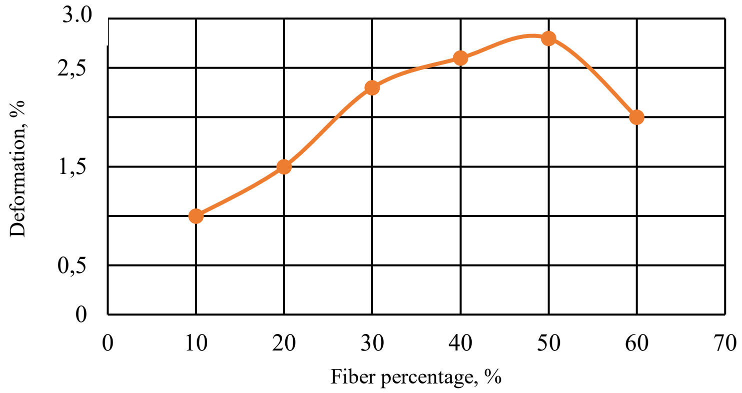

Fig. 8. Fiber content effect on elastic deformation

Table 4

Effect of fiber content in samples on elastic deformation

Fiber content in samples, %	Elastic deformation values, %
10	1.04
20	1.3
30	2.32
40	2.6
50	2.71
60	2.1

Impact tests. The experiments involved a Charpy device in accordance with ISO 179[3]. Samples with dimensions (80×10×4 mm) similar to those shown in Figure 9 were used.

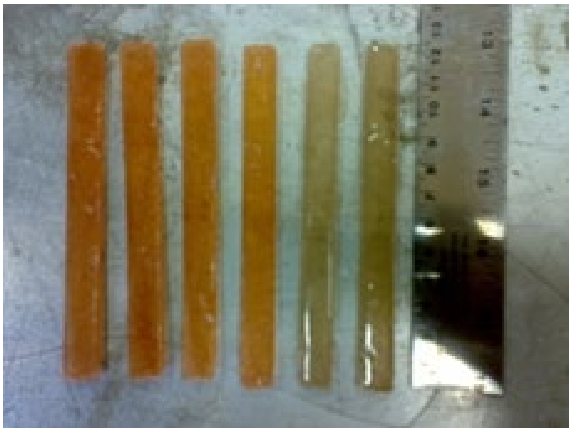

Fig. 9. Impact test samples

The strength was calculated by dividing the value of the energy expended by the cross-sectional area of the sample:

$$R = \frac{E}{A},$$

where R — impact resistance, J/mm^2; E — energy expended, J; A — sample cross-sectional area, mm^2.

Figure 10 and Table 5 show how the fiber content affects impact resistance.

[3] ISO 179-1:2010. Plastics. Determination of Charpy impact properties. Part 1: Non-instrumented impact test. URL: https://www.gostinfo.ru/catalog/Details/?id=4569214 (accessed: 27.09.2023). (In Russ.)

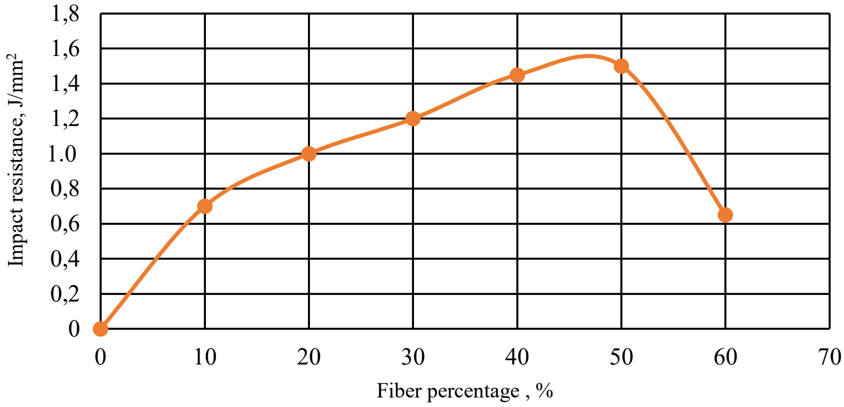

Fig. 10. Effect of fiber content on impact resistance

Impact resistance increases with a growth of fiber content up to 50%. This is due to the increase in the adherence as a result of the saturation of polyester fibers in the composite material. If the weight of the fibers exceeds 50%, the impact resistance is reduced. This is due to the fragility of the glass [7, 13].

Table 5

Effect of fiber content on impact resistance

Fiber content in samples, %	Impact resistance values, J/mm^2
10	0.75
20	1.27
30	1.37
40	1.45
50	1.56
60	0.7

Hardness testing. The hardness of the samples was tested on a durometer, and the Vickers number was calculated by the ratio:

$$HV = 1,854\frac{P}{D^2},$$

where P — applied load, kN; D — impact diameter, mm.

The tests showed an increase in hardness with a growth of the glass fiber content up to 50 % (Fig. 11 and Table 6).

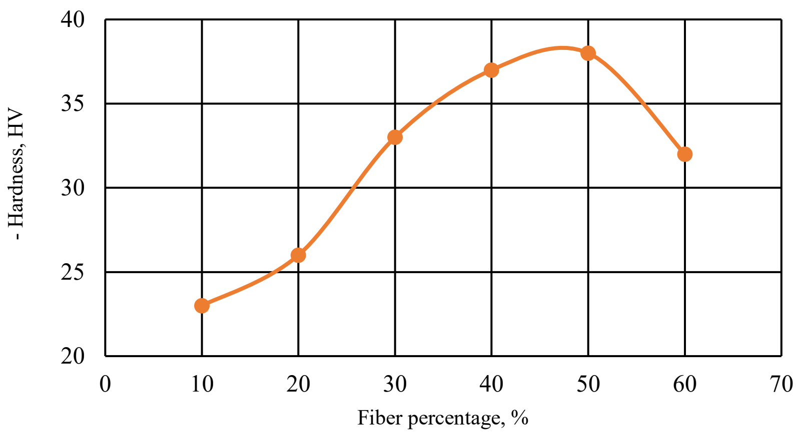

Fig. 11. Effect of glass fiber content on hardness

Table 6

Effect of fiber percentage on hardness values

Fiber content in samples, %	Hardness values, HV
10	23
20	26
30	33
40	37.2
50	38
60	32

With a growth of the percentage of glass fiber up to 50%, the hardness of the composite increases. Fibers and polymer chains are connected in a random order. As a result, the penetration resistance of the composite increases, i.e., the hardness [7, 13]. If the fiber content exceeds 50%, the hardness is reduced due to the disproportion of fibers and polyester (in this case, it is not enough to complete the connection of the reinforcing and base materials).

It should also be noted that in the course of the study, the inaccuracy of the conclusions in work [14] was proved. Polyester composites with a mass of reinforcing E glass fiber of 15%, 30%, 45%, and 60% were considered. The effect of the glass fiber content on such mechanical properties as tensile and bending strength, impact strength was investigated. The hardness of the composites was evaluated using the Brinell hardness tester. The results showed a significant improvement in the mechanical properties of the composite with an increase in the mass of glass fiber, specifically, at 60%. However, the authors used too wide range of glass fiber content in the composite, which complicated the assessment of the accuracy of the results obtained. In addition, the processes of destruction of fibers were not taken into account, their properties were not checked.

Steel sample testing. In accordance with ASTM[4] standard, the samples were made of A36 sheet steel. Tensile, impact and hardness tests were carried out in the same way as for glass fiber reinforced polyester samples.

Table 7 shows the results of mechanical tests of steel samples and their comparison to samples made of composite material with 50% glass fiber (this composite makeup showed the best results).

Table 7

Comparison of the results of mechanical tests of steel samples and samples made of composite material with a glass fiber content of 50 %

Mechanical testing	Samples made of A36 grade steel	Samples from composite materials with a glass fiber content of 50 %
Tensile strength, MPa	400	175.4
Impact resistance, J/mm^2	0.61	1.56
Elastic deformation, %	0.11	2.71
Hardness, HV	135.5	38

Discussion and Conclusion. Thus, tensile strength of a polyester composite increases significantly with a growth of the mass of glass fiber and reaches a maximum value of 175.4 MPa with a reinforcing material content of 50%. The insignificant content of fibers (they are gradually destroyed) causes the weakness of the composite.

Mechanical characteristics of the material made of 50% polyester and 50% glass fiber are better than those of steel (except for tensile strength). This allows for the use of composite for the production of boats, because in this case, tensile strength is not the basic characteristic [15]. Boats made of unsaturated polyester reinforced with glass fiber are 75% lighter than steel ones. Steel is not resistant to corrosion, which makes composite boats more durable.

The deterioration of the composite quality has been experimentally established if the content of reinforcing fibers exceeds 50%. Two main reasons for this phenomenon are indicated. First: with an excessive mass of glass, its fragility is transmitted to the entire material. Second: with a disproportionately large volume of resin fibers, it is not enough to bond them, which negatively affects the strength.

[4] ASTM (American Society for Testing and Materials). The name of a set of standards and an organization in the United States that issues regulations for use in various industries. ASTM standards regulate the chemical composition, mechanical, physical and electrical properties of materials, types of processing, manufacturing methods, testing and testing methods, as well as requirements for rolled metal. URL: https://almet.ru/directory/standards/astm.html (accessed: 27.09.2023). (In Russ.)

References

1. Kumar SN, Kumar VG, Kumar VC, Prabhu M. Experimental Investigation on Mechanical Behavior of E-Glass and S-Glass Fiber Reinforced with Polyester Resin. *SSRG International Journal of Mechanical Engineering*. 2018;5(5):19–26. https://doi.org/10.14445/23488360/IJME-V5I5P104

2. Bhowmick AK. Mechanical Properties of Polymers*. Material Sciences & Engineering*. 2016;1:453–461. URL: https://www.eolss.net/sample-chapters/c05/E6-36-01-03.pdf (accessed: 06.09.2023).

3. Hinton MJ, Soden PD, Kaddour AS. (eds) *Failure Criterion Fibre-Reinforced-Polymer Composites: The World-Wide Failure Exercise*, 1st ed. Amsterdam: Elsevier; 2004. 1269 p.

4. Ravi Jain, Luke Lee. (eds) *Fiber Reinforced Polymer (FRP) Composites for Infrastructure Applications. Focusing on Innovation, Technology Implementation and Sustainability*. New York, NY: Springer; 2012. 280 p. http://doi.org/10.1007/978-94-007-2357-3

5. Meijer HE, Govaert LE. Mechanical Performance of Polymer Systems: The Relation between Structure and Properties. *Progress in Polymer Science.* 2005;30(8–9);915–938. http://doi.org/10.1016/j.progpolymsci.2005.06.009

6. Lewin M (ed). *Handbook of Fiber Chemistry. International Fiber Science and Technology Series,* 3rd ed. Boca Raton, FL: CRC Press; 2006. 1056 p. https://doi.org/10.1201/9781420015270

7. Varga Cs, Miskolczi N, Bartha L, Lipóczi G. Improving the Mechanical Properties of Glass-Fibre-Reinforced Polyester Composites by Modification of Fibre Surface. *Materials and Design.* 2010;31(1):185–193. https://doi.org/10.1016/j.matdes.2009.06.034

8. Agarwel A, Garg S, Rakesh PK, Singh I, Mishra BK. Tensile Behaviour of Glass Fiber Reinforced Plastics Subjected to Different Environmental Conditions. *Indian Journal of Engineering & Materials Sciences.* 2010;17(6):471–476. URL: https://nopr.niscpr.res.in/bitstream/123456789/10873/1/IJEMS%2017%286%29%20471-476.pdf (accessed: 06.09.2023).

9. Estabraq T Abdullah. A Study of Bending Properties of Unsaturated Polyester/Glass Fiber Reinforced Composites. *Al-Nahrain Journal of Science.* 2013;16(3):129–132. http://doi.org/10.22401/JNUS.16.3.18

10. Gornet L. *Généralités sur les matériaux composites*. Nantes, France: ECN; 2008. 51 p. URL: https://cel.hal.science/file/index/docid/470296/filename/MatComposites.pdf (accessed: 06.09.2023).

11. Noorshashillawati Azura Binti Mohammad. *Characterization and Properties of the New Unsaturated Polyester Resins for Composite Application.* Gelugor, MYS: School of Industrial Technology; 2007. 125 p. URL: https://core.ac.uk/reader/32600400 (accessed: 06.09.2023).

12. Yilmaz H. Tensile Strength Testing of Thin Spray-on Liner Products (TSLs) and Shotcrete. *The Journal of The Southern African Institute of Mining and Metallurgy*. 2010;110(10):559–569. URL: http://www.scielo.org.za/pdf/jsaimm/v110n10/01.pdf (accessed: 06.09.2023).

13. Aramide FO, Atanda PO, Olorunniwo OO. Mechanical Properties of a Polyester Fibre Glass Composite. *International Journal of Composite Materials.* 2012;2(6):147–151. https://doi.org./10.5923/j.cmaterials.20120206.06

14. El-Wazerya MS, El-Elamy MI, Zoalfakar SH. Mechanical Properties Of Glass Fiber Reinforced Polyester Composites. *International Journal of Applied Science and Engineering.* 2017;14(3):121–131. https://doi.org/10.6703/IJASE.2017.14(3).121

15. Shenoi RA, Dulieu-Barton J, Quinn S. Composite Materials for Marine Applications: Key Challenges for the Future. In book: Nicolais L, Meo M, Milella E. (eds) *Composite Materials*. London: Springer; 2011. С. 69–89. http://doi.org/10.1007/978-0-85729-166-0_3

Received 29.09.2023
Revised 31.10.2023
Accepted 22.11.2023

About the Author:

Imad Rizakalla Antipas, Cand.Sci. (Eng.), Associate Professor of the Fundamentals of Machinery Design Department, Don State Technical University (1, Gagarin sq., Rostov-on-Don, 344003, RF), SPIN-code: 7371-0223, ScopusID, ResearchID, ORCID, imad.antypas@mail.ru

Conflict of interest statement: the author does not have any conflict of interest.

The author has read and approved the final manuscript.

Поступила в редакцию 29.09.2023
Поступила после рецензирования 31.10.2023
Принята к публикации 22.11.2023

Об авторе:

Имад Ризакалла Антибас, кандидат технических наук, доцент кафедры основ конструирования машин Донского государственного технического университета (344003, РФ, г. Ростов-на-Дону, пл. Гагарина, 1), SPIN-код: 7371-0223, ScopusID, ResearchID, ORCID, imad.antypas@mail.ru

Конфликт интересов: автор заявляет об отсутствии конфликта интересов.

Автор прочитал и одобрил окончательный вариант рукописи.

INFORMATION TECHNOLOGY, COMPUTER SCIENCE AND MANAGEMENT

UDC 004.942, 004.02, 519.622, 544.3, 544.2
https://doi.org/10.23947/2687-1653-2023-23-4-398-409

Original article

EDN: PDPGGO

Automation of the Formation of a Mathematical Formulation of Kinetics for Multistage Chemical Reactions and Numerical Solution to a Direct Problem

Nikita A. Lysenko[1] ✉, **Kamila F. Koledina**[1,2]
[1] Ufa State Petroleum Technological University, Ufa, Russian Federation
[2] Institute of Petrochemistry and Catalysis, UFRC RAS, Ufa, Russian Federation
✉ nikitka_lysenko_2016@mail,ru

Abstract
Introduction. The basis for research, analysis and mathematical optimization of any chemical process is an adequate mathematical model that takes into account the kinetics of the object. Kinetic analysis is a challenge in chemical technology, since it allows for optimizing synthesis processes and predicting their efficiency. Numerous chemical processes involve several stage reactions. For successful design and optimization, a mathematical model that describes each stage is needed. Creating such a model manually can be time-consuming and costly, since it requires processing a large amount of information. The modern level of automation makes it possible to accelerate the obtaining of a mathematical formulation of the kinetics of multistage reactions. In this case, working with data is greatly simplified, and the probability of making mistakes is reduced. The resulting mathematical model can be applied for further analysis and optimization of the process. The paper considers the industrial reaction of catalytic reforming of gasoline, which occupies an important place in the modern scheme of oil refining, since it is a source of high-octane components of commercial gasolines and individual aromatic hydrocarbons. This process is characterized by the participation of a large number (up to 300) of various hydrocarbons, a change in the number of moles, and non-isothermality in it. Mathematical modeling of such processes involves detailing the stages to the required level. The detailing of up to 173 stages is considered. In this setting, automation of the formation of a mathematical formulation of kinetics for catalytic reforming of gasoline has not been carried out before. Therefore, the presented work aimed at implementing effective numerical methods and algorithms for automating the building of a mathematical model taking into account kinetics, thermodynamics, and changes in the number of moles.
Materials and Methods. The mathematical formulation of the kinetics of multistage reactions was developed on the basis of the mass action law. The kinetic parameters values were taken from literary sources. The direct kinetics problem was solved using algorithms: the Gear method, the Runge-Kutta method of the 4th order, and the scipy.odeint() method of the Python language. The automation concept was implemented using the IDEF0 methodology. The software was written in the Python programming language.
Results. A new software was created to automate the process of forming a mathematical model, taking into account the kinetics, thermodynamics, and the volume of the reaction mixture. The program results were presented by the example of catalytic reforming of gasoline. The model implemented the possibility of taking into account the intermediate heating of the mixture in the reactor cascade. Numerical values of temperature changes corresponding to industrial data were obtained.
Discussion and Conclusion. The results obtained through modeling chemical transformations in the cascade of gasoline catalytic reforming reactors confirmed the exothermic nature of the reaction. The developed software product provides displaying changes in the concentrations of reactants, as well as temperature variations in the reactor, and it can be used in scientific research organizations for the analysis of multistage catalytic processes. The results of the reaction kinetics modeling will be used in the subsequent optimization of the process conditions in production.

Keywords: kinetic analysis, mathematical formulation, automation, differential equation system, direct problem, computational methods

Acknowledgements. The authors would like to thank the reviewers for valuable comments that contributed to the improvement of the article.

Funding information. The research was done within the framework of the leadership project "Development of a computer system for analyzing the kinetics of chemical processes and their multicriteria optimization", Ufa State Petroleum Technological University.

For citation. Lysenko NA, Koledina KF. Automation of the Formation of a Mathematical Formulation of Kinetics for Multistage Chemical Reactions and Numerical Solution to a Direct Problem. *Advanced Engineering Research (Rostov-on-Don)*. 2023;23(4):398–409. https://doi.org/10.23947/2687-1653-2023-23-4-398-409

Научная статья

Автоматизация формирования математического описания кинетики для многостадийных химических реакций и численное решение прямой задачи

Н.А. Лысенко[1] ✉, **К.Ф. Коледина**[1,2]

[1] Уфимский государственный нефтяной технический университет, г. Уфа, Российская Федерация

[2] Институт нефтехимии и катализа УФИЦ РАН, г. Уфа, Российская Федерация

✉ nikitka_lysenko_2016@mail.ru

Аннотация

Введение. Основой для исследования, анализа и математической оптимизации любого химического процесса является адекватная математическая модель, учитывающая кинетику объекта. Кинетический анализ в химической технологии является важной задачей, поскольку позволяет оптимизировать процессы синтеза и прогнозировать их эффективность. Многие химические процессы включают в себя несколько стадийных реакций. Для успешного проектирования и оптимизации необходима математическая модель, которая описывает каждую стадию. Создание такой модели вручную может быть трудоемким и затратным процессом, требующим обработки большого объема информации. Современный уровень автоматизации позволяет ускорить получение математического описания кинетики многостадийных реакций. В этом случае значительно упрощается работа с данными и уменьшается вероятность совершения ошибок. Полученная математическая модель может быть применена для последующего анализа и оптимизации процесса. В работе рассмотрена промышленная реакция каталитического риформинга бензина, занимающая важное место в современной схеме переработки нефти, поскольку является источником высокооктановых компонентов товарных бензинов и индивидуальных ароматических углеводородов. Данный процесс характеризуется участием в нем большого числа (до 300) различных углеводородов, изменением числа молей и неизотермичностью. Математическое моделирование таких процессов предполагает детализацию стадий до необходимого уровня. Рассмотрена детализация до 173 стадий. В такой постановке задачи автоматизация формирования математического описания кинетики для каталитического риформинга бензинов ранее не проводилась. Поэтому целью представленной работы явилась реализация эффективных численных методов и алгоритмов для автоматизации формирования математической модели с учётом кинетики, термодинамики и изменения числа молей.

Материалы и методы. Математическое описание кинетики многостадийных реакций разрабатывается на основе закона действующих масс. Значения кинетических параметров взяты из литературных источников. Решение прямой задачи кинетики проводилось с применением следующих алгоритмов: метод Гира, Рунге-Кутты 4 порядка и метод scipy.odeint() языка Python. Концепция автоматизации реализована с помощью методологии IDEF0. Программное обеспечение написано на языке программирования Python.

Результаты исследования. Создано новое программное обеспечение для автоматизации процесса формирования математической модели с учетом кинетики, термодинамики и учета объема реакционной смеси. Приведены результаты работы программы на примере каталитического риформинга бензина. Реализована возможность учета в модели промежуточного подогрева смеси в каскаде реакторов. Получены численные значения изменения температуры, соответствующие промышленным данным.

Обсуждение и заключение. Результаты, полученные при моделировании химических превращений в каскаде реакторов каталитического риформинга бензина, подтвердили экзотермический характер реакции. Разработанный программный продукт позволяет отобразить изменения концентраций веществ реакции, а также изменение температуры в реакторе и может быть использован в научных исследованиях организаций для анализа многостадийных каталитических процессов. Результаты моделирования кинетики реакции будут использоваться в последующей оптимизации условий проведения процесса на производстве.

Ключевые слова: кинетический анализ, математическое описание, автоматизация, система дифференциальных уравнений, прямая задача, методы численного решения

Благодарности. Авторы выражают признательность рецензентам за ценные замечания, способствовавшие повышению качества статьи.

Финансирование. Работа выполнена в рамках лидерского проекта «Разработка компьютерной системы анализа кинетики химических процессов и их многокритериальной оптимизации» Уфимского государственного нефтяного технического университета.

Для цитирования. Лысенко Н.А., Коледина К.Ф. Автоматизация формирования математического описания кинетики для многостадийных химических реакций и численное решение прямой задачи. *Advanced Engineering Research (Rostov-on-Don)*. 2023;23(4):398–409. https://doi.org/10.23947/2687-1653-2023-23-4-398-409

Introduction. Studies on the kinetics of multistage chemical processes is of theoretical and practical importance, since it allows for revealing the mechanism of reactions and carrying out control. At the same time, it becomes possible to accelerate target or slow down side chemical reactions. Kinetic analysis, being an important task of chemical engineering, contributes to the optimization of synthesis processes and the prediction of their effectiveness [1–3]. A great many chemical processes are multistage reactions. For their effective design and optimization, it is required to have a mathematical model describing all stages [4, 5]. Manual formation of such a model can be very time-consuming and costly, since it implies processing a large amount of information [6].

The object of the study is the industrial process of catalytic reforming of gasoline. The target product of the reaction — reformate — provides obtaining the bulk of commercial gasoline. The remaining components are products of isomerization, catalytic cracking, and alkylation. Most oil refineries in Russia and worldwide use catalytic reforming units [7, 8]. Catalytic reforming of gasoline makes it possible to obtain aromatic hydrocarbons (xylene, toluene, benzene), which can then be used in the petrochemical industry [9, 10]. However, for commercial gasoline, the presence of aromatic hydrocarbons in the product is limited by environmental criteria. Therefore, detailed complex kinetics, demonstrating the step-by-step formation of components, is able to operate the process conditions to control the yield of the product and limit the content of aromatic hydrocarbons. The process of catalytic reforming of gasoline is carried out in a reactor unit consisting of three consecutive reactors, between which furnaces are installed to heat the mixture. This is a necessity since the reaction is endothermic. In the mathematical formulation of the reactor unit, it is required to take into account the variation of temperature and volume of the reaction mixture along with changes in the concentrations of the components from the conditional contact time of the catalyst and the reaction mixture.

Automation of modeling of such complex processes makes it possible to significantly speed up obtaining a mathematical formulation of the kinetics of multistage reactions, reduce the probability of errors, and simplify the process of working with data [11]. In general, automation of the formation of a mathematical formulation for multistage chemical reactions is an important tool for effective process management in various industries, as well as for achieving more accurate and efficient implementation of chemical reactions in the laboratory.

Thus, the study aimed at developing a software product to help automate the formation of a mathematical formulation of multistage chemical reactions, taking into account the kinetics, thermodynamics and changes in the volume of the reaction mixture, as well as obtaining a numerical solution of the compiled mathematical model.

To achieve the research goal, the following tasks were solved in this work:

– development of a software module for the formation of a mathematical formulation of kinetics using the Python programming language;

– development of a software module for numerical solution to a direct problem according to a compiled mathematical formulation using the Python programming language;

– obtaining the results of the software product for the reaction of catalytic reforming of gasoline.

Materials and Methods. Mathematically, this process can be described by a system of ordinary nonlinear differential equations with initial data, which is a mathematical model. Considering that the catalytic reforming of gasoline is an exothermic reaction with a change in the volume of the reaction mixture, the model of multistage chemical kinetics can be considered in the following context:

$$\frac{dy_i}{d\tau} = \sum_{j=1}^{M} v_{ij} \times w_j, i = 1,...N; \quad (1)$$

$$\frac{dQ}{d\tau}=\sum_{i=1}^{N}\frac{dy_i}{d\tau};Q(0)=Q^0; \tag{2}$$

$$w_j=k_j\times\prod_{i=1}^{N}(\frac{y_i}{Q})^{|\alpha_{ij}|}-k_{-j}\times\prod_{i=1}^{N}(\frac{y_i}{Q})^{\beta_{ij}}. \tag{3}$$

$$k_j=k_j^0\times\exp\left(-\frac{E_{j^+}}{RT}\right);\ k_{-j}=k_{-j}^0\times\exp\left(-\frac{E_j^-}{RT}\right); \tag{4}$$

$$\frac{dT}{d\tau}=-\frac{\sum_{i=1}^{N}\frac{dy_i}{d\tau}\times\Delta H_i(T)}{\sum_{i=1}^{N}y_i\times C_{pi}(T)};\quad T(0)=T^0; \tag{5}$$

$$H_i(T)=\Delta H_i(298)+\int_{298}^{T}C_{pi}(T)dT; \tag{6}$$

$$C_{pi}(T)=a_i+b_iT+c_iT^2+d_iT^3; \tag{7}$$

with initial conditions at $\tau=0, y_i(0)=y_i^0$, $T=763K$, $Q=1.014;\tau\in[0,t^*]$ [11].

In this formula of reaction kinetics there are a number of variables and coefficients that determine the concentration of reagents, contact time and reaction rate. Specifically, Q and y_i (concentrations of reaction reagents) can be expressed in mol/l or in fractions, and variable τ, showing the conditional contact time of the reaction mixture with the catalyst, in kg×min/mol or kg of the catalyst. The formula also includes the following indicators: the number of stages M (173 stages) and the number of substances N (38 substances), as well as stoichiometric matrix ν_{ij}. α_{ij} — these are all negative elements of matrix ν_{ij} at the intersection of the i-th row and the j-th column, and β_{ij} — all positive elements of matrix ν_{ij} at the intersection of the i-th row and the j-th column. The rate of the j-th reaction stage w_j can be expressed in 1/min or in mol/(kg×min), and the rate constants of stages k_j, k_{-j} — in 1/min. In addition, the formula specifies pre-exponential factors k_j^0, k_{-j}^0, expressed in 1/min, the activation energies of the forward and reverse reactions E_j^+, E_j^-, expressed in kcal/mol, gas constant R and temperature T, measured in Kelvins. The period of reaction t* is determined by the time required to complete it in minutes, and the enthalpy of the formation of the i-th component $\Delta H_i(T)$ is measured in J/mol. The specific heat capacity $C_{pi}(T)$ of the i-th component, measured in J/(mol×K), can be expressed in terms of the coefficients of the temperature dependence of the heat capacity of this component, which are indicated by letters a_i, b_i, c_i, d_i [12]. i — serial number of the substance involved in the reaction.

When modeling chemical transformations of catalytic reforming of gasoline, it is required to take into account a large number of individual hydrocarbons. Therefore, in the article, group components are used in the model for the separation of types of hydrocarbons and the number of carbon atoms in the structure of the molecule: A_l — aromatic hydrocarbons; ACP_l — five-membered naphthenes; ACH_l — six-membered naphthenes; iP_l — paraffin isomers; nP_l — normal paraffins. Here, l — number of carbon atoms in the molecular structure. Table 1 shows the average coefficients of the temperature dependence of the heat capacity of the group components that are used in the calculations.

Table 1

Coefficients of temperature dependence of group components

l	Hydrocarbon group	a_i	b_i	c_i	d_i
1	nP_1	34.942	–0.03996	0.19184	–0.153
2	nP_2	28.146	0.043447	0.18946	–0.1908
3	nP_3	28.277	0.116	0.19597	–0.2327
4	nP_4	20.56	0.2815	–0.013143	–0.09457
5	IP_4	6.772	0.34147	–0.10271	–0.03685
6	nP_5	26.671	0.32324	0.04282	–0.1664
7	iP_5	–0.881	0.47498	–0.24797	0.06751
8	nP_6	25.924	0.41927	–0.012491	–0.1592
9	iP_6	–7.123	0.58327	–0.30338	0.06802
10	nP_7	26.984	0.50387	–0.04748	–0.1684
11	iP_7	19.245	0.55072	–0.14055	–0.08248
12	nP_8	29.053	0.58016	–0.057103	–0.1955
13	iP_8	–3.367	0.75824	–0.38216	0.05736
14	nP_9	29.687	0.66821	–0.096492	–0.2001
15	iP_9	68.581	0.44754	0.31908	–0.5118
16	nP_{10}	31.78	0.74489	–0.10945	–0.2267
17	iP_{10}	–46.17	1.108	–0.70316	0.1787
18	nP_{11}	125.21	0.31401	0.79137	–0.9141
19	iP_{11}	–8.791	1.0548	–0.5778	0.1192
20	ACH_6	13.783	0.20742	0.53682	–0.6301
21	ACH_7	4.296	0.42716	0.21058	–0.3999
22	ACH_8	–51.866	0.78827	–0.35255	–0.006855
23	ACH_9	–120.89	1.2728	–1.0794	0.4035
24	ACH_{10}	90.421	0.23264	0.94595	–1.057
25	ACH_{11}	–65.48	1.1809	–0.68379	0.1458
26	ACP_6	–9.939	0.42528	0.012521	–0.1886
27	ACP_7	–28.514	0.58607	–0.094379	–0.1644
28	ACP_8	–69.713	0.92602	–0.62526	0.2049
29	ACP_9	–116.73	1.3097	–1.2439	0.5292
30	ACP_{10}	–67.341	1.0922	–0.704	0.1906
31	ACP_{11}	–68.23	1.187	–0.7575	0.2018
32	A_6	–31.368	0.4746	–0.31137	0.08524
33	A_7	–24.097	0.52187	–0.29827	0.06122
34	A_8	–17.36	0.5647	–0.26293	0.01122
35	A_9	–10.933	0.64349	–0.27829	–0.01443
36	A_{10}	–24.187	0.79716	–0.48265	0.1341
37	A_{11}	–26.717	0.91044	–0.53876	0.1203
38	H_2	29.07	–0.0836	0.1064	0.5752

Equations (1), (3) and (4) describe changes in reagent concentrations in the process, and in system (2), molar fractions are used to describe changes in the molar flow rate of the mixture. In (5), the dependence of the reaction temperature change on the thermodynamic characteristics of substances is considered. In (6), (7), the dependence for calculating the enthalpy of formation of the i-th component and the specific heat capacity is given.

In this model, the direct problem (solving a system of differential equations) is both rigid and non-rigid. The Gear method used to solve the catalytic reforming model is based on backward differentiation [13–15]. To compare the results and identify the optimal method, an explicit one-step Runge-Kutta numerical integration fourth-order method and an explicit numerical integration method scipy.odeint() of the Python programming language were used.

The concept of automating the formation of a mathematical formulation of kinetics for multistage chemical reactions and a numerical solution method is illustrated using the IDEF0 methodology.

Figure 1 shows a contextual diagram of the process of automating the formation of a mathematical formulation of kinetics for multistage chemical reactions and solutions by numerical method.

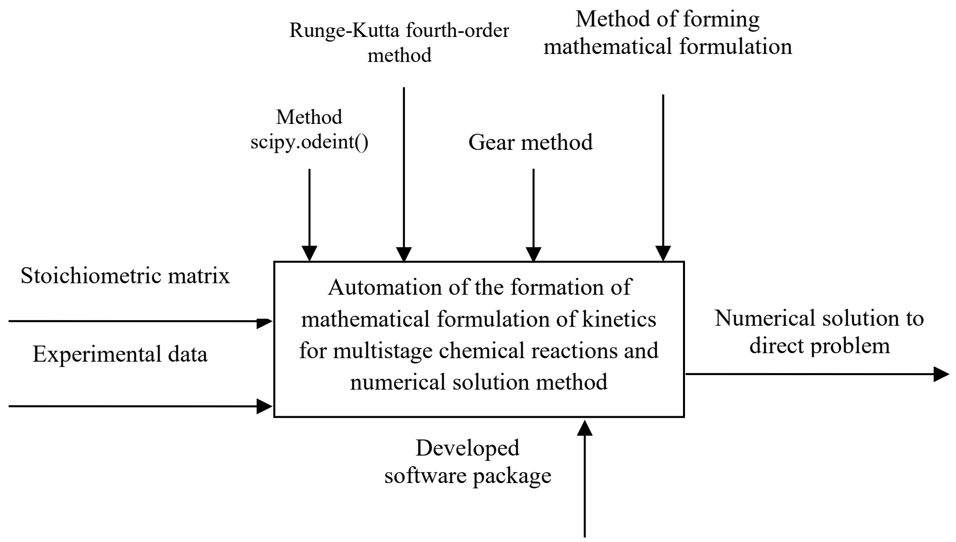

Fig. 1. Context diagram "Automation of the formation of mathematical formulation of kinetics for multistage chemical reactions and a numerical solution method"

The input parameters are the stoichiometric reaction matrix and experimental data. These include initial data on the concentration of substances, temperature, pre-exponential multiplier, activation energies. The result of solving the problem is a numerical solution to the direct problem. The controls are numerical methods for comparing the results, as well as the method of forming a mathematical description. The mechanism is the developed software package for automating the mathematical formulation of the kinetics of multistage reactions and solving a direct problem. Figure 2 shows the decomposition of the process of automating the formation of a mathematical formulation of kinetics for multistage chemical reactions and solutions by numerical method into stages:

– formation of mathematical formulation;

– direct problem solution.

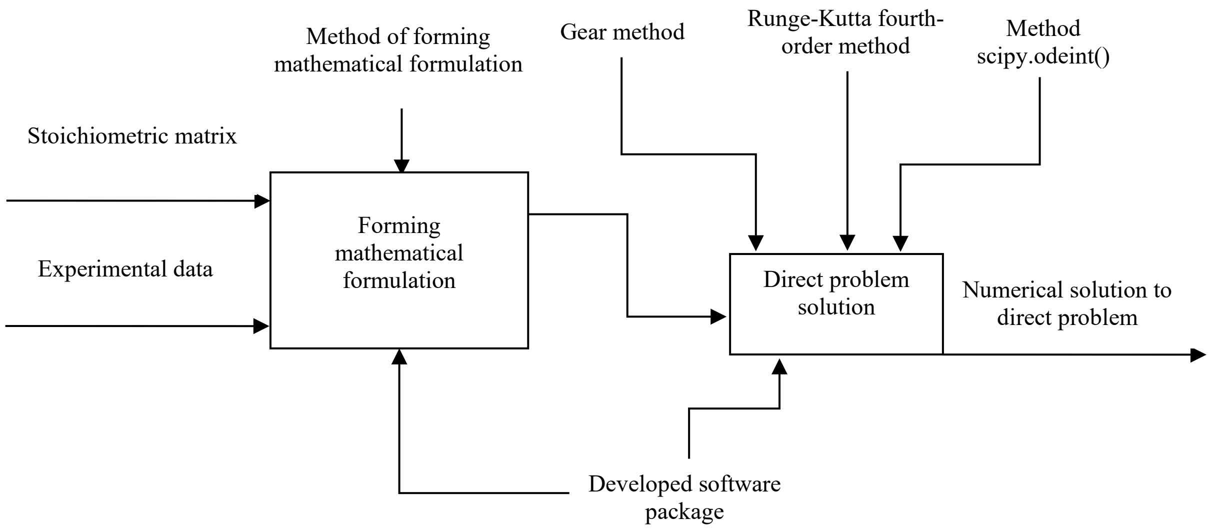

Fig. 2. Stages of the problem solution
"Automation of the formation of mathematical formulation of kinetics for multistage chemical reactions and a numerical solution method"

The developed software package capabilities are represented by the features described below.

With the help of the program, you can create a kinetic model of a multistage chemical reaction and present its solution by the previously described methods, using a given stoichiometric matrix. If the reaction is exothermic and there is a change in the volume of the reaction mixture, two complementary equations are added to the system of differential equations to describe these changes.

The mathematical model of catalytic reforming of gasoline is a system of differential equations (DES) of form (1)–(7), consisting of 40 differential equations with respect to the number of group components, temperature dependence, and the mole change equation.

The basic functionality of the program is:

– main application window with the output of the mathematical formulation according to the stoichiometric matrix entered by the user;

– window with visualization of the solution: for each numerical method (Python-odeint, fourth-order Runge-Kutta, Gear method), the operating time, an array of time *t* and the solution of a system of differential equations at each moment of time are displayed, which are graphs of changes in the concentration of substances, changes in the reaction temperature or the volume of the reaction mixture.

Research Results. The catalytic reforming reaction took place in three reactors, between which a heating furnace was located. The initial temperature of the first reactor was 766 K (493°C). For the first 9.6 conditional hours, the reaction proceeded in the first reactor, the temperature dropped. After that, heating took place in the furnace between the two reactors to 763 K (490°C), and the chemical process passed into the second reactor. In the second reactor, the process occurred in the time interval from 9.6 to 32.3 conventional hours, the temperature decreased. Before proceeding to reactor 3, the mixture was heated in the second intermediate furnace to 768 K (495°C) and flew in this reactor in the time interval from 32.3 to 60 conventional hours.

Figures 3–5 show the kinetic curves of the hydrocarbon groups involved in the reaction and obtained using the Gear method. The intermittent transitions on the graphs indicate that the mixture is moving from one reactor to another with intermediate heating.

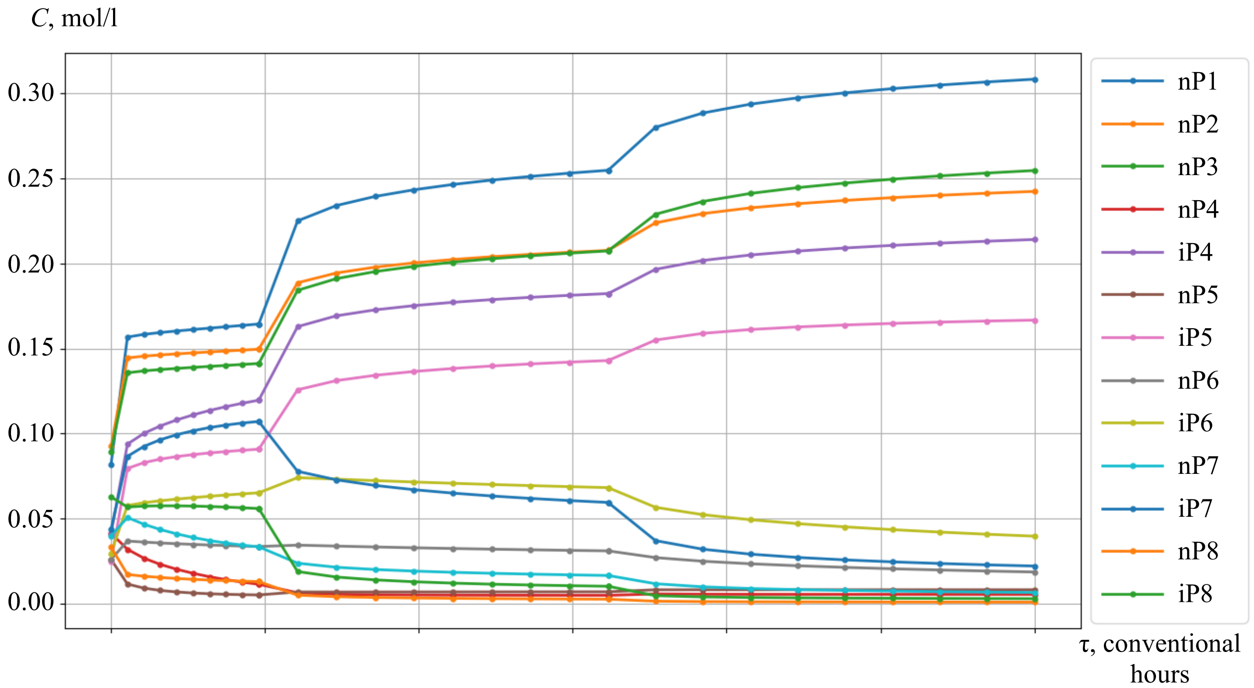

Fig. 3. Kinetic curves of catalytic reforming of gasoline

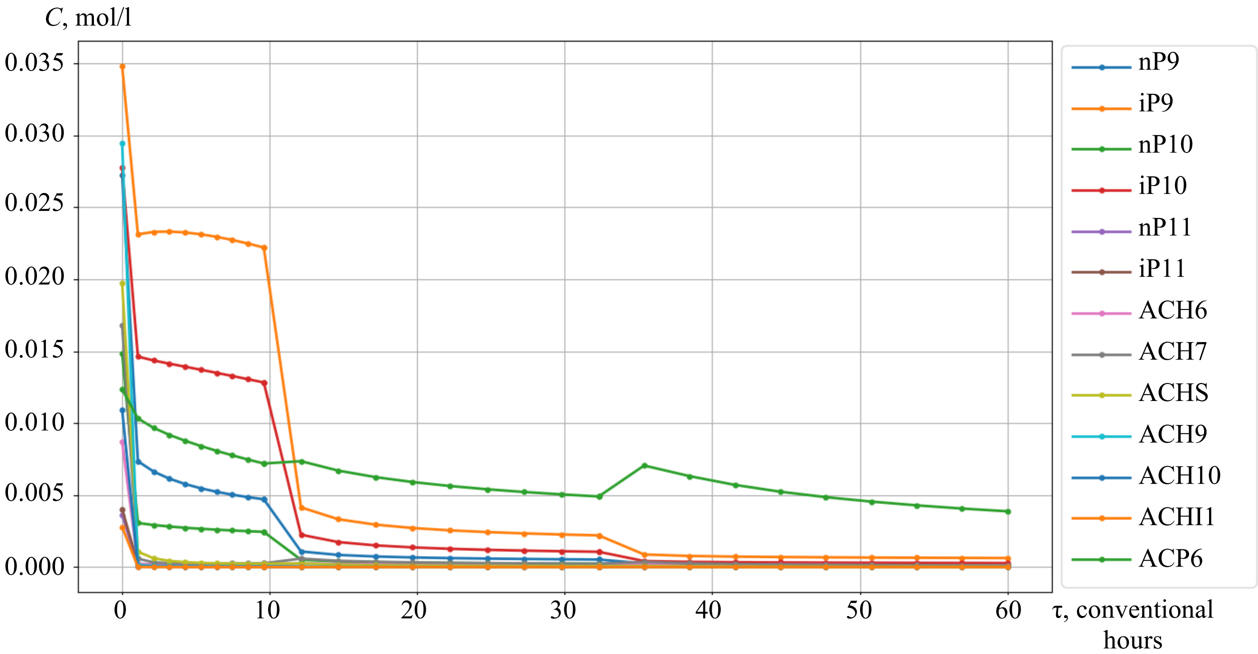

Fig. 4. Kinetic curves of catalytic reforming of gasoline

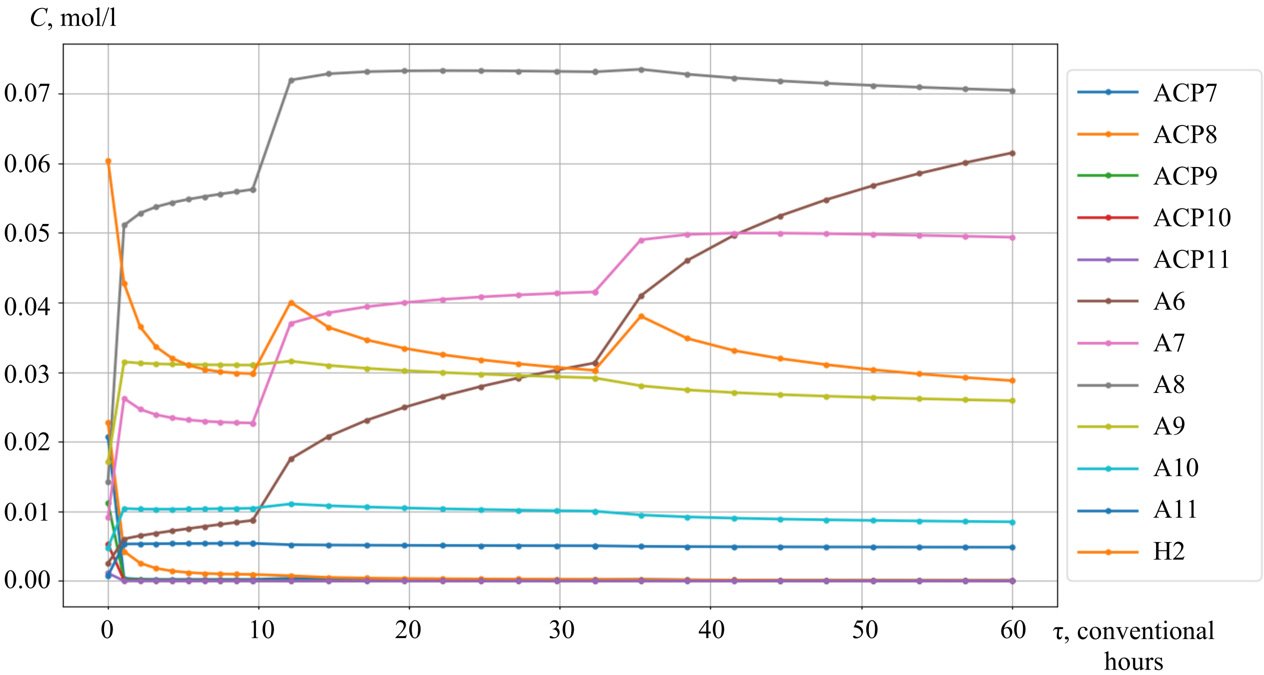

Fig. 5. Kinetic curves of catalytic reforming of gasoline

The curves of changes in the concentrations of the group components are given depending on the time of contact of the reaction mixture with the catalyst (Fig. 3–5). As an example, symbol nP1 stands for normal paraffin with one carbon atom, and symbol A9 — stands for aromatic hydrocarbon with nine carbon atoms. Figures 6 and 7 show, respectively, the curves of changes in temperature and volume of the reaction mixture of the catalytic reforming reaction of gasoline.

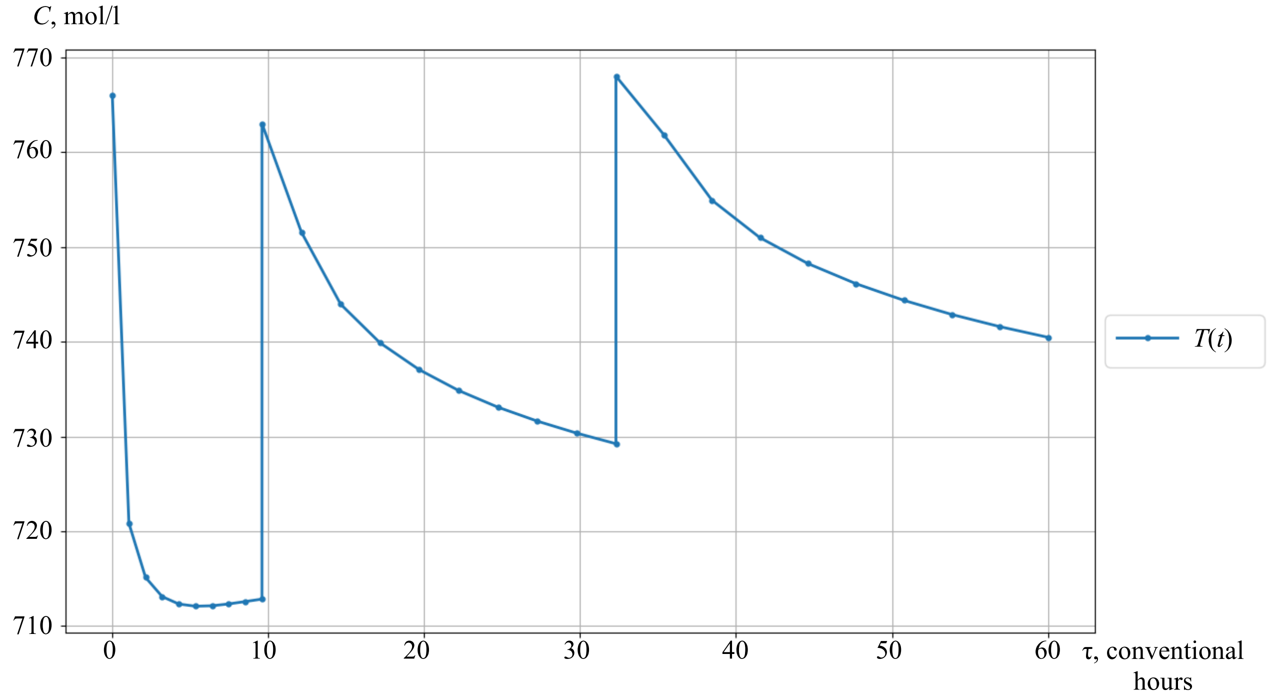

Fig. 6. Temperature curve

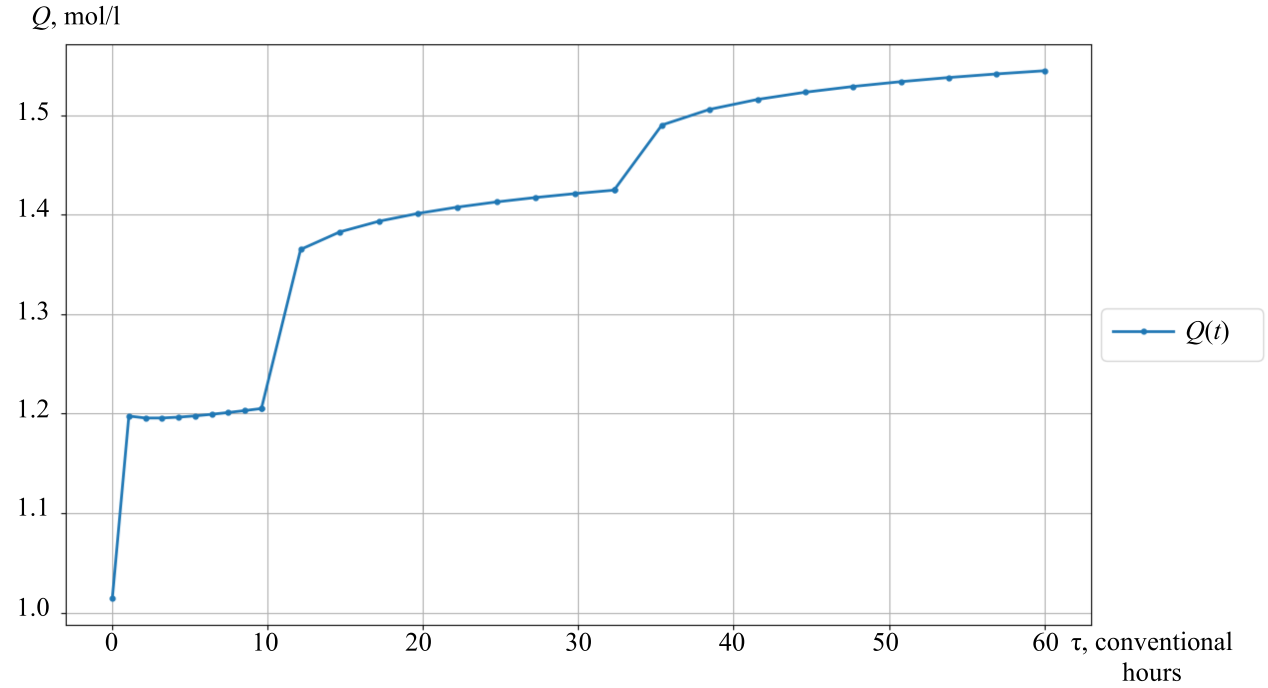

Fig. 7. Reaction mixture volume change curve

Discussion and Conclusion. In the presented work, a software module for the formation of a mathematical formulation of kinetics for complex multistage reactions has been developed. This makes it possible to analyze complex processes, including industrial, to consider various possible mechanisms in an acceptable time.

The developed software module for the numerical solution of a direct kinetic problem provides monitoring the dynamic change in the concentrations of components and the process temperatures in the case of its non-isothermality. In addition to the presented graphs of changes in component concentrations, measurements of the operating time of each of the three implemented methods were made. According to the scipy.odeint() method, the solution to the direct problem lasted 80.5 seconds; according to the Runge-Kutta fourth-order method — 111.8 seconds. The most optimal time, equal to 39.8 seconds, was shown by the Gear method. This confirms that Gear's method is optimized for working with rigid systems of differential equations.

The implemented approach was applied to modeling the industrial process of catalytic reforming of gasoline. Automation of the formation of a mathematical formulation of kinetics and the implementation of a numerical solution to a direct problem allowed us to develop a kinetic model of a detailed scheme of chemical transformations in an acceptable time, and obtain concentration and temperature profiles in the process reactors corresponding to industrial data.

References

1. Naryshkin DG. Computer Mathematics in the Course “Physical Chemistry”. *Modern Information Technologies and IT-Education.* 2012;(8):430–440. (In Russ.)

2. Qi Han, Xian-Tai Zhou, Xiao-Qi He, Hong-Bing Ji. Mechanism and Kinetics of the Aerobic Oxidation of Benzyl Alcohol to Benzaldehyde Catalyzed by Cobalt Porphyrin in a Membrane Microchannel Reactor. *Chemical Engineering Science*. 2021;245:116847. https://doi.org/10.1016/j.ces.2021.116847

3. Gheorghe Maria. A CCM-Based Modular and Hybrid Kinetic Model to Simulate the Tryptophan Synthesis in a Fed-Batch Bioreactor Using Modified *E. Coli* Cells. *Computers and Chemical Engineering*. 2021;153:107450. https://doi.org/10.1016/j.compchemeng.2021.107450

4. Fayzullin MR, Balaev AV. Computer-Aided System for Kinetic Studies of Complex Chemical Reactions. *Bulletin of BSU*. 2008;13(3-1):835–839.

5. Khamidullina ZA, Ismagilova AS, Spivak SI. Analysis Informativity of Kinetic Parameters of Complex Chemical Reactions. *Herald of TvSU. Series “Chemistry”*. 2020;39(1):70–80. https://doi.org/10.26456/vtchem2020.1.9

6. Koledina KF, Gubaydullin IM, Koledin SN. Mathematical Modeling and Computational Aspects of Multi-Criteria Optimization of the Conditions of a Laboratory Catalytic Reaction. *Numerical Analysis and Applications*. 2022;15:104–111. http://doi.org/10.1134/S1995423922020033

7. Zainullin RZ, Koledina KF, Akhmetov AF, Gubaidullin IM. Kinetics of the Catalytic Reforming of Gasoline. *Kinetics and Catalysis.* 2017;58(3):279–289. https://doi.org/10.1134/S0023158417030132

8. Zainullin RZ, Koledina KF, Akhmetov AF, Gubaidullin IM. Possible Ways of Upgrading Reactor Unit of Catalytic Reforming Based on Kinetic Model. *Electronic Scientific Journal of Oil and Gas Business.* 2018;(6):78–97.

9. Brasseur GP, Jacob DJ. *Modeling of Atmospheric Chemistry*. Cambridge: Cambridge University Press; 2017. 606 p. https://doi.org/10.1017/9781316544754

10. Gubaydullin I, Koledina K, Sayfullina L. Mathematical Modeling of Induction Period of the Olefins Hydroalumination Reaction by Diisobutylaluminiumchloride Catalyzed with Cp_2ZrCl_2. *Engineering Journal*. 2014;18(1):13–24. https://doi.org/10.4186/ej.2014.18.1.13

11. Meshalkin VP, Dovi VG, Soboleva IV. Method and Algorithm for Bayesian Estimation of Kinetic Parameters of Chemical Processes with Fluctuating Independent Variables. *Theoretical Foundations of Chemical Engineering.* 2009;43(6):861–868. http://doi.org/10.1134/S0040579509060037

12. Safiullina LF, Koledina KF, Gubaydullin IM, Zaynullin RZ. Study of a Mathematical Model of Gasoline Catalytic Reforming by Sensitivity Analysis Methods. *Numerical Methods and Programming*. 2020;21(4):440–451. https://doi.org/10.26089/NumMet.v21r435 (In Russ.)

13. Murphy JA. Physical Organic Chemistry. *Beilstein Journal of Organic Chemistry*. 2010;(6):1025. https://doi.org/10.3762/bjoc.6.116

14. Zaynullin RZ, Koledina KF, Gubaydullin IM, Akhmetov AF, Koledin SN. Kinetic Model of Catalytic Gasoline Reforming with Consideration for Changes in the Reaction Volume and Thermodynamic Parameters. *Kinetics and Catalysis*. 2020;61:613–622. https://doi.org/10.1134/S002315842004014X

15. Safiullina LF, Gubaydullin IM, Uzyanbaev RM, Musina AE. Computational Aspects of Simplification of Mathematical Models of Chemical Reaction Systems. *Journal of Physics: Conference Series*. 2019;1368:042022. http://doi.org/10.1088/1742-6596/1368/4/042022

Received 07.10.2023
Revised 02.11.2023
Accepted 15.11.2023

About the Authors:

Nikita A. Lysenko, undergraduate student of the Information Technology and Applied Mathematics Department, Ufa State Petroleum Technological University (1, Kosmonavtov St., Ufa, 450064, RF), SPIN-code: 5938-7991, ORCID, ResearcherID, nikitka_lysenko_2016@mail.ru

Kamila F. Koledina, Dr.Sci. (Phys.-Math.), Professor of the Information Technology and Applied Mathematics Department, Ufa State Petroleum Technological University (1, Kosmonavtov St., Ufa, 450064, RF), Senior Researcher, Laboratory of Mathematical Chemistry, Institute of Petrochemistry and Catalysis, UFRC RAS (141, pr. Oktyabrya, Ufa, 450075, RF), SPIN-code: 2449-0255, ORCID, ResearcherID, ScopusID, koledinakamila@mail.ru

Claimed contributorship:
NA Lysenko: software development, text preparation, formulation of conclusions.
KF Koledina: academic advising, provision of initial data, correction of conclusions, revision of the text of the article.

Conflict of interest statement: the authors do not have any conflict of interest.

All authors have read and approved the final manuscript.

Поступила в редакцию 07.10.2023
Поступила после рецензирования 02.11.2023
Принята к публикации 16.11.2023

Об авторах:

Никита Андреевич Лысенко, магистрант кафедры информационные технологии и прикладная математика Уфимского государственного нефтяного технического университета, (450064, РФ, г. Уфа, ул. Космонавтов, 1), SPIN-код: 5938-7991, ORCID, ResearcherID, nikitka_lysenko_2016@mail.ru

Камила Феликсовна Коледина, доктор физико-математических наук, профессор кафедры информационные технологии и прикладная математика Уфимского государственного нефтяного технического университета, (450064, РФ, г. Уфа, ул. Космонавтов, 1), старший научный сотрудник лаборатории математической химии Института нефтехимии и катализа УФИЦ РАН (450075, РФ, г. Уфа, проспект Октября, 141), SPIN-код: 2449-0255, ORCID, ResearcherID, ScopusID, koledinakamila@mail.ru

Заявленный вклад авторов:

Н.А. Лысенко — разработка программного обеспечения, подготовка текста, формулировка выводов.

К.Ф. Коледина — научное руководство, предоставление исходных данных, корректировка выводов, доработка текста статьи.

Конфликт интересов: авторы заявляют об отсутствии конфликта интересов.

Все авторы прочитали и одобрили окончательный вариант рукописи.

INFORMATION TECHNOLOGY, COMPUTER SCIENCE AND MANAGEMENT

UDC 004.58

https://doi.org/10.23947/2687-1653-2023-23-4-410-421

Original article

EDN: QPFEMG

Optimal 2D Placement of Virtual Objects in Physical Space for Augmente Applications

Marianna V. Alpatova ✉, **Yuri V. Rudyak**

Moscow Polytechnic University, Moscow, Russian Federation

✉ m.v.alpatova@yandex.ru

Abstract

Introduction. Research and applied works on the placement of virtual objects in real space most often focus on issues of interactivity, integration of reality and virtuality, physical properties of virtual elements. However, the task of simultaneously free and optimal placement of objects, taking into account their size and the surrounding comfort zone, has not been sufficiently worked out. In the literature, you can find a description of a similar task — about packing in a rectangular container. In our case, the goal is not limited to the greatest possible dense placement. Two conditions should be taken into account: rigid dimensions of the objects (it is forbidden to violate them) and additional areas — comfort zones (it is undesirable to occupy them). The work aims at creating and implementing such a 2D algorithm for placing objects in physical space, which takes into account the above limitations.

Materials and Methods. Using a set of numerical methods, the authors applied the previously created 1D algorithm for the placement of objects. Calculations were based on a system of linear equations. In the one-dimensional case, the optimal placement of virtual objects was reduced to a task that did not depend on the type of comfort function. The elements of such a system were the dimensions of objects, the distances between them, as well as the distances to the edge of the embedding area, a comfort zone. The proposed 2D algorithm for optimal placement of virtual objects was implemented in the form of a program code in C# using the well-known *Unity* game engine. The solution was tested on gadgets in peak load mode for 5, 10, 15, 20, 25, 35, 40, 45, and 50 objects. 1.8 thousand devices were used for experiments. About 77 thousand events were analyzed. To exclude unrepresentative values, each calculation was repeated 10 times, and a *z*-score was performed for each value. Abnormal events (more than 3 and less than -3) were excluded.

Results. In this paper, a 2D placement algorithm that implements filling a rectangular area with virtual objects has been created. Each of the objects had a size and another characteristic — a comfort zone. The authors compiled a flowchart for the implementation of this algorithm in a given two-dimensional left-hand coordinate system. It was shown, in particular, at what stage objects were sorted by length, when their batches were formed, and arrangements were made along two axes. The first axis was horizontal, the second was directed forward from the user (this is the depth vector, or frontal measurement). The 1D-placement algorithm for the generated row provided optimal positioning the objects along *X*-axis based on the calculated comfort coefficient K. Calculations were made and schemes were drawn up to obtain certain comfort indicators. For each object of the first string, the displacement along *Z*-axis from the edge of the plane was determined so that the comfort in front was equal to the comfort along *X*. Starting from the 2nd row, to calculate the displacement, the presence of potential neighbors who were a row higher and had common areas along *X* with the object being processed, was checked. Each element of the string was set along *Z*-axis so that its comfort from above was the maximum of the one-sided horizontal comfort in this and the previous strings. The principle of calculating *Z* coordinate for a string object was presented in the form of a flowchart. The initial data for the implementation of this algorithm were 7 objects with 14 different sizes and 28 comfort zones. After the software implementation, the operation of the described 2D algorithm was tested in practice — in an augmented reality mobile application. Analytical data of user sessions was recorded. The average execution time was calculated. The hypothesis of quadratic dependence that arose during the work was tested on a personal computer. For this purpose, a similar experiment was conducted for a range of [10-10,000] objects. The hypothesis was confirmed. The algorithm can be assigned a complexity of $O(n^2)$.

To compare the calculation speed, 10 of the most popular models of user devices were utilized. The results were presented in the form of a diagram. The minimum registered execution time was 0.093 ms, the maximum — 0.146 ms. Calculations showed high efficiency of the two-dimensional algorithm. Additionally, the placement schemes for different numbers and parameters of objects were visualized.

Discussion and Conclusion. The proposed algorithm of two-dimensional placement enables the user to work with a set of virtual objects with different sizes and comfort zones. Sufficiently high performance and stability are shown. On average, the algorithm is implemented in fractions of a millisecond, even with large batches of objects. Possible future focus areas:

– expansion of the approach for building 3D models and algorithms;

– inclusion of objects in the rotation algorithm for greater flexibility of their location and better use of space.

The research results can be of interest to engineers and interface designers. In the future, it is required to study the user experience and the possibilities of including additional restrictions on positioning.

Keywords: virtual objects in physical space, virtual objects in augmented reality, comfortable placement of virtual objects

Acknowledgements. The authors appreciate the editorial team of the journal and the reviewer for their competent expertise and valuable recommendations for improving the article.

Funding information. The research was done with the financial support from RFFI within the framework of scientific project No. 21-510-07004.

For citation. Alpatova MV, Rudyak YuV. Optimal 2D Placement of Virtual Objects in Physical Space for Augmented Reality Applications. *Advanced Engineering Research (Rostov-on-Don).* 2023;23(4):410–421. https://doi.org/10.23947/2687-1653-2023-23-4-410-421

Научная статья

Оптимальная 2D-расстановка виртуальных объектов в физическом пространстве для приложений дополненной реальности

М.В. Алпатова ✉**, Ю.В. Рудяк**
Московский политехнический университет, г. Москва, Российская Федерация
✉ m.v.alpatova@yandex.ru

Аннотация

Введение. Научные и прикладные работы о размещении виртуальных объектов в реальном пространстве чаще всего фокусируются на вопросах интерактивности, интеграции реальности и виртуальности, физических свойствах виртуальных элементов. Однако недостаточно проработана задача одновременно свободного и оптимального размещения объектов с учетом их размеров и окружающей зоны комфортности вокруг них. В литературе можно найти описание схожей задачи — об упаковке в прямоугольный контейнер. В нашем случае цель не ограничивается максимально плотным размещением. Следует учесть два условия: жесткие размеры объектов (их запрещено нарушать) и дополнительные области — зоны комфортности (их нежелательно занимать). Цель работы — создание и реализация такого 2D-алгоритма размещения объектов в физическом пространстве, который будет учитывать обозначенные выше ограничения.

Материалы и методы. Используя аппарат численных методов, авторы задействовали созданный ранее 1D-алгоритм размещения объектов. Расчеты основываются на системе линейных уравнений. В одномерном случае оптимальное размещение виртуальных объектов сводится к задаче, не зависящей от вида функции комфортности. Элементы такой системы — размеры объектов, дистанции между ними, а также расстояния до края области встраивания, зоны комфортности. Предлагаемый 2D-алгоритм оптимальной расстановки виртуальных объектов реализовали в виде программного кода на языке C# с использованием известного игрового движка *Unity*. Решение тестировали на гаджетах в режиме пиковой нагрузки для 5, 10, 15, 20, 25, 35, 40, 45 и 50 объектов. Для опытов задействовали 1,8 тыс. устройств. Проанализировали около 77 тыс. событий. Чтобы исключить нерепрезентативные значения, каждый расчет повторяли 10 раз, и для каждого значения провели z-оценку. Аномальные (больше 3 и меньше –3) исключили.

Результаты исследования. В работе создан алгоритм 2D-расстановки, который реализует заполнение прямоугольной области виртуальными объектами. У каждого из них есть размер и еще одна характеристика — зона комфортности. Авторы составили блок-схему реализации данного алгоритма в заданной двумерной левосторонней системе координат. Показано, в частности, на каком этапе объекты сортируются по длине, когда формируются их партии и выполняются расстановки по двум осям. Первая — горизонтальная, вторая направлена вперед от пользователя (это вектор глубины, или фронтальное измерение). Алгоритм 1D-размещения для сформированного ряда позволяет оптимально расположить объекты вдоль оси *X* на основе рассчитанного коэффициента комфортности K. Выполнены расчеты и составлены схемы с целью достичь определенных показателей комфортности. Для каждого объекта первой линии смещение по оси *Z* от края плоскости определяется так, чтобы комфортность спереди равнялась комфортности по *X*. Начиная со 2-го ряда для вычисления отступа проверяется наличие потенциальных соседей, которые находятся на ряд выше и имеют общие участки по *X* с обрабатываемым объектом. Каждый элемент строки устанавливается по оси *Z* так, чтобы его комфортность сверху была максимальной из односторонних горизонтальных комфортностей в данной и предыдущей строках. Принцип расчета координаты *Z* для объекта строки представлен в виде блок-схемы. Исходными данными для реализации этого алгоритма были 7 объектов с 14 разными размерами и 28 зонами комфортности. После программной реализации работу описанного 2D-алгоритма проверили на практике — в мобильном приложении дополненной реальности. Записали аналитические данные пользовательских сессий. Рассчитали среднее время выполнения. Возникшую в ходе работы гипотезу о квадратичной зависимости проверили на персональном компьютере. С этой целью провели аналогичный эксперимент для диапазона [10–10000] объектов. Гипотеза подтвердилась. Алгоритму можно присвоить сложность O(n^2). Для сравнения скорости вычисления задействовали 10 самых популярных моделей пользовательских устройств. Результаты представили в виде диаграммы. Минимальное зарегистрированное время выполнения — 0,093 мс, максимальное — 0,146 мс. Расчеты показали высокую эффективность двумерного алгоритма. Дополнительно визуализировали схемы расстановки для разного количества и параметров объектов.

Обсуждение и заключение. Предлагаемый алгоритм двумерного размещения позволяет работать с набором виртуальных объектов с разными размерами и зонами комфортности. Показаны достаточно высокие производительность и стабильность. В среднем алгоритм реализуется за доли миллисекунды даже при больших партиях объектов. Возможные будущие направления работы:

– расширение подхода для построения 3D моделей и алгоритмов;

– включение в алгоритм вращения объектов для большей гибкости их расположения и лучшего использования пространства.

Итоги работы могут представлять интерес для инженеров и дизайнеров интерфейсов. В перспективе следует изучить пользовательский опыт и возможности включения дополнительных ограничений на позиционирование.

Ключевые слова: виртуальные объекты в физическом пространстве, виртуальные объекты в дополненной реальности, комфортное размещение виртуальных объектов

Благодарности. Авторы выражают признательность редакционной команде журнала и рецензенту за компетентную экспертизу и ценные рекомендации по улучшению статьи.

Финансирование. Исследование проводилось при финансовой поддержке РФФИ в рамках научного проекта № 21–510–07004.

Для цитирования. Алпатова М.В., Рудяк Ю.В. Оптимальная 2D-расстановка виртуальных объектов в физическом пространстве для приложений дополненной реальности. *Advanced Engineering Research (Rostov-on-Don).* 2023;23(4):410–421. https://doi.org/10.23947/2687-1653-2023-23-4-410-421

Introduction. A well-known task of augmented reality (AR) applications is the placement of virtual objects in real physical space. A number of studies [1–3] focus on interactivity, the merging of real and virtual spheres. The issues of physical properties of virtual objects are also studied.

The task of such placement of objects, which would be free and optimal at the same time, taking into account not only the geometry of objects, but also comfort zones around them, has not been sufficiently worked out. In [6], the external similarity of this problem and the well-known problem of packing into a rectangular container is noted [5]. However, there is a significant difference. In the case under study, it is not enough to provide the greatest possible dense packaging. When placing virtual objects, it is required to take into account not only their rigid dimensions, which cannot be violated, but also additional areas — comfort zones. It is undesirable to occupy them. These additional areas provide getting closer to the object and performing some actions with it.

Materials and Methods. Earlier [4], the authors defined what a comfortable placement of virtual objects was, and introduced the concept of comfort function $k(x)$. It increases monotonically from 0 to 1 at $0 \le x \le 1$ and is equal to 1 at $x > 1$, where $x = X/D$, X — distance from the edge of the object to the nearest obstacle, D — size of the comfort zone. For each measurement, the object has two one–way comfort zones $D–$ and $D+$. Comfort on each side is calculated separately.

It is shown in [6] that the problem of one-dimensional placement of n virtual objects in a free region of space with length L is reduced to a system of linear equations that do not depend on the type of comfort function k(x):

$$\begin{cases} \dfrac{X_-^{(1)}}{D_-^{(1)}} = \dfrac{X_-^{(2)}}{\tilde{D}_+^{(1)}}, \\ \dfrac{X_-^{(i)}}{\tilde{D}_-^{(i)}} = \dfrac{X_-^{(i+1)}}{\tilde{D}_+^{(i)}}, \\ \dfrac{X_-^{(n)}}{\tilde{D}_-^{(n)}} = \dfrac{L - \sum\limits_{i=1}^{n}\left(X_-^{(i)} + l^{(i)}\right)}{\tilde{D}_+^{(n)}}. \end{cases} \tag{1}$$

Here, $X_-^{(1)}$ — distance of the first object from the left edge of the embedding area; $X_-^{(i)}$, $i = 2,3,...,n$ — distance between objects with numbers i and $(i-1)$; $D_-^{(i)}$ and $D_+^{(i)}$ — left and right comfort zones, respectively; $l^{(i)}$ — object size; $\tilde{D}_+^{(i)} = \tilde{D}_-^{(i+1)} = D_+^{(i)} + D_-^{(i+1)}$, $i = 1,2,\ldots,(n-1)$.

Matrix of system (1) is strongly sparse; therefore, it is possible to avoid using not the fastest universal methods, it is easy enough to find a solution. As an example, in the first $(n-1)$ equalities, it is possible in each i-th equation, to express $X_-^{(i+1)}$ by $X_-^{(i)}$, then, substitute this into the last equation and get a linear equation with respect to $X_-^{(1)}$.

After that, values $X_-^{(2)}, X_-^{(3)}, ..., X_-^{(n)}$ are sequentially determined from the first equation to the $(n-1)$-th. The authors implemented this 1D algorithm for placing objects using numerical methods. It showed high speed and efficiency. This 1D algorithm became the basis for the scientific research described in the presented paper. The authors proposed a 2D algorithm for optimal placement of virtual objects It was implemented in the form of C# programming code using the *Unity* game engine, which is widely utilized to create augmented reality mobile applications [8]. During the experiment, an algorithm was run on the user's device operating in peak load mode to 5, 10, 15, 20, 25, 35, 40, 45, and 50 objects. The time spent on calculations was measured (in milliseconds). Each calculation was repeated 10 times to avoid abnormal values. In total, 1.8 thousand devices participated in the experiment, about 77 thousand events with the results were collected from them and analyzed.

Filtering anomalies using z-score allowed the authors to identify values that can be defined as outliers [9]. The data was standardized, and a z-score was calculated for each value. Those with a z-score greater than 3 or less than –3 were considered abnormal. They were excluded and focused on typical and representative data.

Research Results. Thus, on X, Z plane there is a rectangular area with width L_x and length L_z. It should be filled with a certain number of virtual objects. Each object, in addition to its size $l_x^{(i)}$ and $l_z^{(i)}$ (where i — number of the object), is also characterized by comfort zones $D_{x-}^{(i)}, D_{x+}^{(i)}, D_{z-}^{(i)}, D_{z+}^{(i)}$. Figure 1 shows a block diagram of the described algorithm.

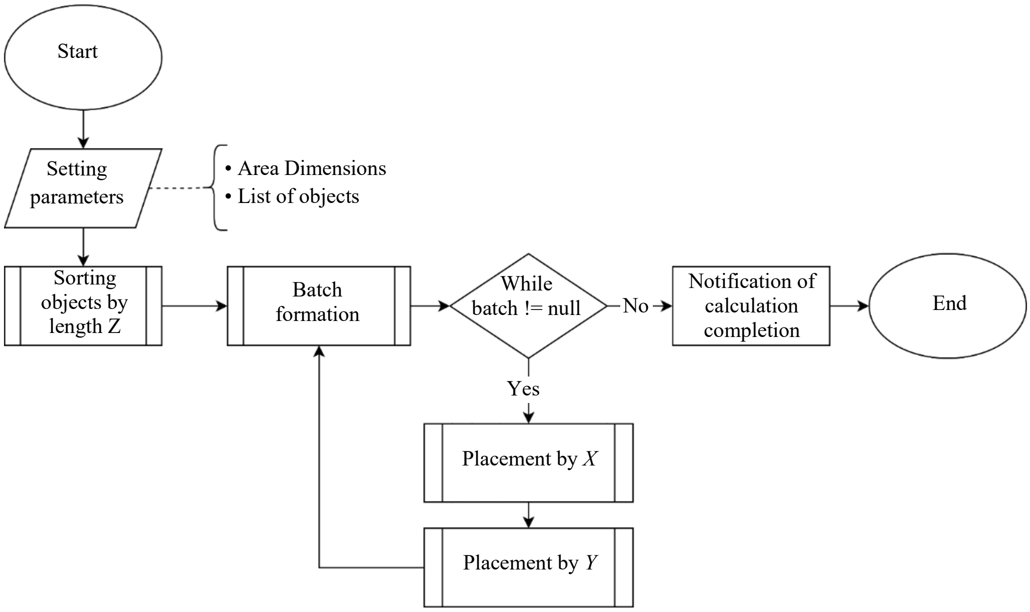

Fig. 1. Top-level 2D placement algorithm

In this work, a left-sided coordinate system is used: *X*-axis denotes the horizontal placement vector, *Z*-axis is directed forward from the user and is the depth vector, or frontal measurement [7]. Objects are placed in a horizontal plane (e.g., on the floor, countertop, etc.), therefore, the vertical *Y*-axis is not considered, and all illustrations assume a top view of the resulting composition.

In the lower left corner of each virtual object, a pivot is denoted. It determines the final coordinates of the object placement. Next, the set of objects is sorted in descending order by $l_z^{(i)} + D_{z-}^{(i)} + D_{z+}^{(i)}$ — overall length of the objects, taking into account the comfort zones located in front and behind in accordance with the coordinate axis under consideration. After sorting, objects that occupy more space in depth are located farther away from the user (or higher — for the scheme presented in the horizontal projection). A block diagram of the formation of a batch of objects is shown in Figure 2.

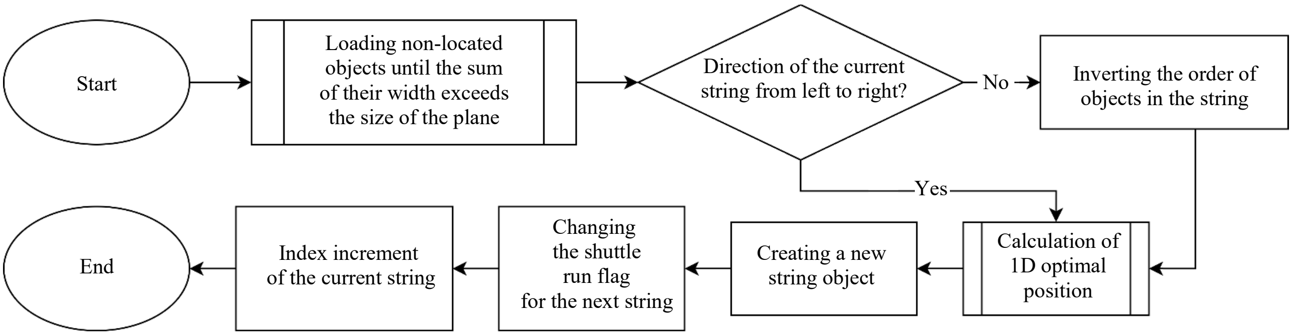

Fig. 2. Algorithm for forming a batch of objects

Then separate strings, or batches, are formed from the ordered set of objects. Each string includes the minimum number of objects, the sum of the width of which, together with the comfort zones, exceeds the width of the filled region L_x. If, when adding the next object, the calculated occupied width exceeds the horizontal size of the available space inside the rectangle, the batch is considered completed. Thus, each batch can be placed as a line within the region. Rows alternate from left to right and from right to left to mix large and small objects. This can be called a "shuttle run" (Fig. 3).

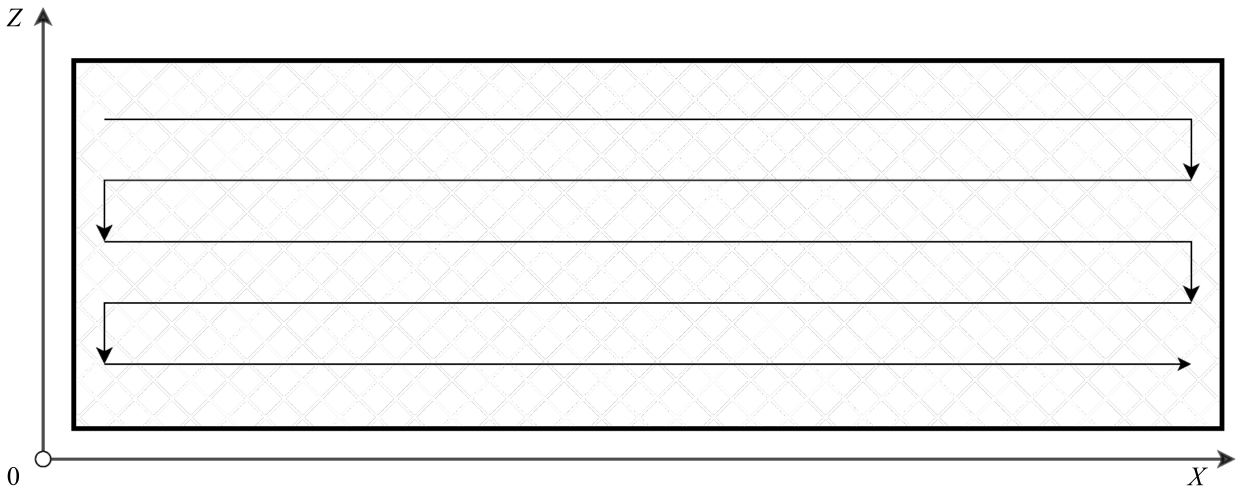

Fig. 3. Scheme of the "shuttle run" on the coordinate plane

For the formed row, 1D-placement algorithm is used, which provides for the optimal placement of a number of objects along *X*-axis based on the calculated comfort coefficient *K*, which is the same for all objects in the row. For each object of the first string, Z-axis offset from the edge of the plane is determined in such a way that the comfort in front is equal to the comfort along *X*:

$$\frac{Z_+^{(1)}}{D_{z+}^{(1)}} = \frac{X_-^{(1)}}{D_{x-}^{(1)}}, \frac{Z_+^{(i)}}{D_{z+}^{(i)}} = \frac{X_-^{(i)}}{\tilde{D}_{x-}^{(i)}},\ i = 2,3,...,n. \tag{2}$$

Starting from the 2nd row, to calculate Z_+ indent, the presence of potential neighbors from above from the overlying row that have common sections with the current object being processed along *X* coordinate is checked. At the same time, each object of the placed row is installed along *Z*-axis in such a way that its comfort from above is the maximum of the one-sided horizontal comfort in this row and the previous rows. The algorithm for calculating *Z* coordinates is shown in Figure 4.

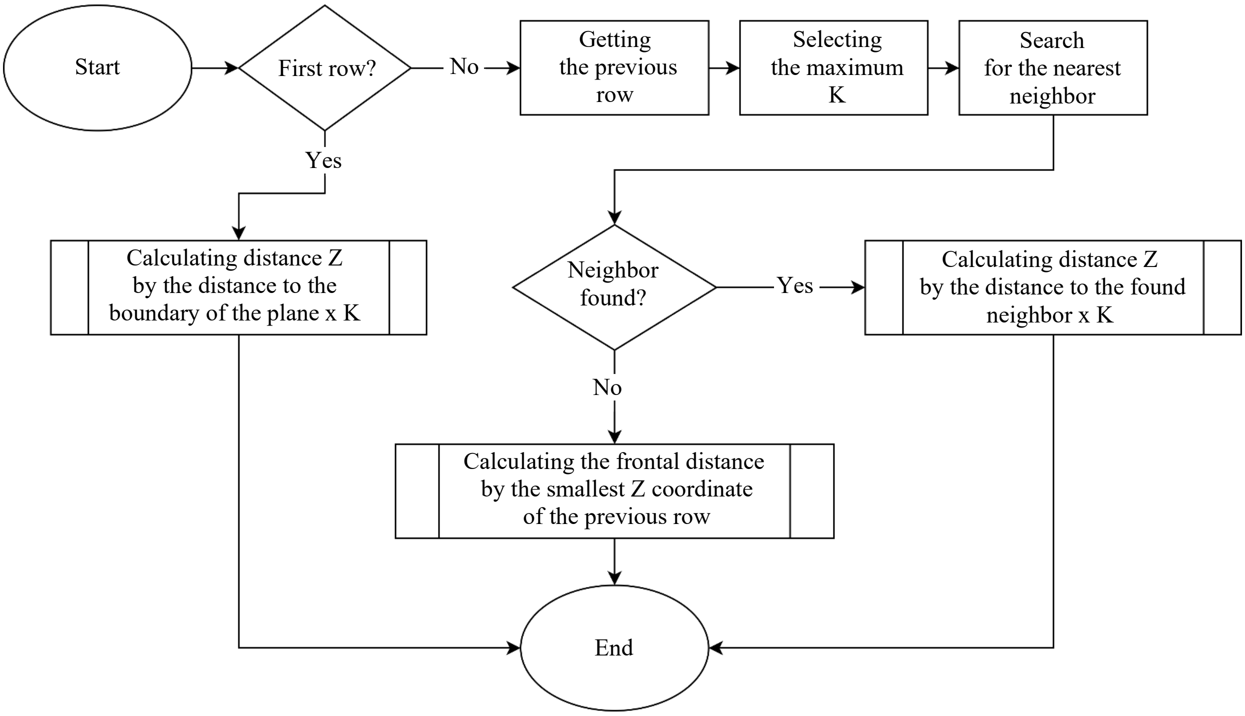

Fig. 4. Principle of calculating Z coordinate for the string object

It can be seen from the flowchart that the indent is calculated similarly for all three possible scenarios:

– indent from the edge of the plane to install the object;

– indent from the neighbor from above;

– in the absence of a neighbor in the previous string, the object closest from all previous strings along *Z* is taken.

New batches are formed until all objects are assigned a row, or until the physical space runs out.

The initial data for the described algorithm are systematized in Table 1. Objects are sorted by their vertical dimensions.

Table 1

Source data for the example of the operation of the described algorithm

Object number	Size	Comfort zone
1	(7; 4)	(4; 3; 3; 5)
2	(10; 4)	(4; 3; 5; 3)
3	(5; 4)	(2; 3; 5,25; 2,25)
4	(12; 4)	(2,8; 3,3; 3,8; 4,65)
5	(5; 4)	(2,5; 4; 1,75; 5,8)
6	(18; 4)	(3,2; 2,4; 5; 2,25)
7	(11; 4)	(2,1; 2,45; 2; 14,2)

Table 1 corresponds to Figure 5, which demonstrates the placement of objects.

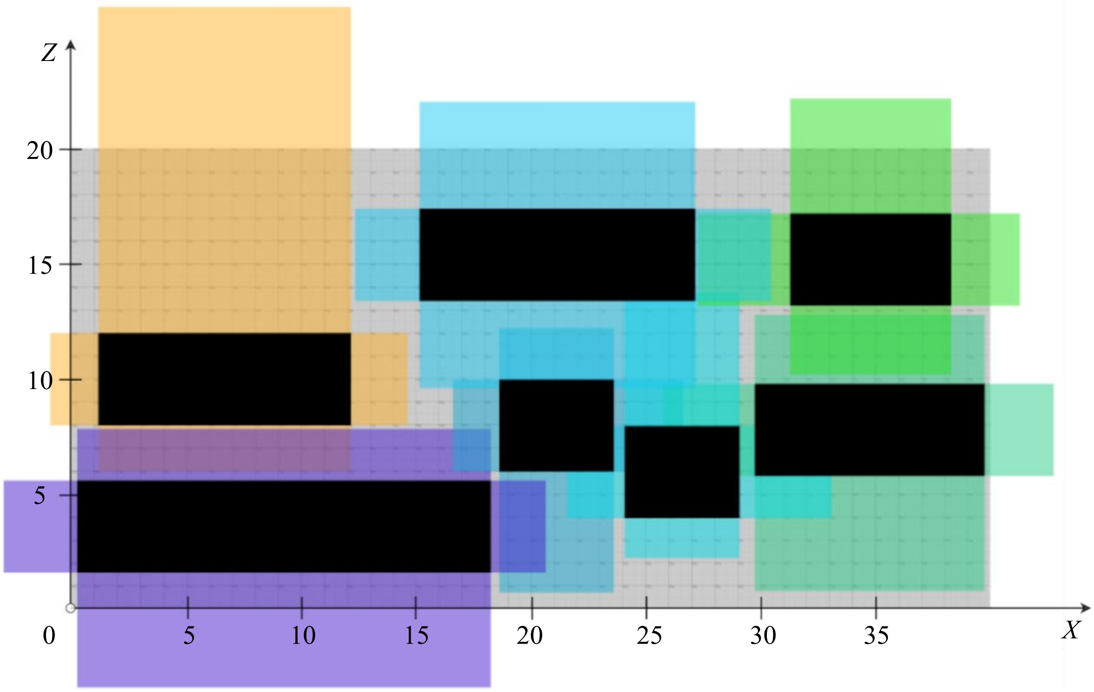

Fig. 5. Layout of the objects for the example under consideration. Top view

A gray rectangle is a free area on which objects are placed. Black areas are objects in their overall dimensions. Colored areas, with overlays, are preset comfort zones for each object. As noted above, comfort zones of objects may partially overlap and go beyond the free space, but the approach used allows for a balance so that the comfort of various objects is equally reduced.

Recall that this model includes the concept of comfort function $k(x)$. The resulting system of equations (1) does not depend on it, and hence the optimal placement of objects. But the values of one-sided comfort of objects are determined both by their placement and by the type of function $k(x)$. Here are two examples:

– in the case of linear function $k(x)$, one-sided comforts of objects in the upper row of Figure 5 are equal to 0.6;

– for dependence $\sqrt{1-(x-1)^2}$ — value 0.9.

After the software execution of the described 2D algorithm, it was implemented into an augmented reality mobile application, and the analytical data of user sessions was recorded. The authors grouped information for each unique device model, for each number of objects placed in the range [10]. The average execution time was calculated (Fig. 6).

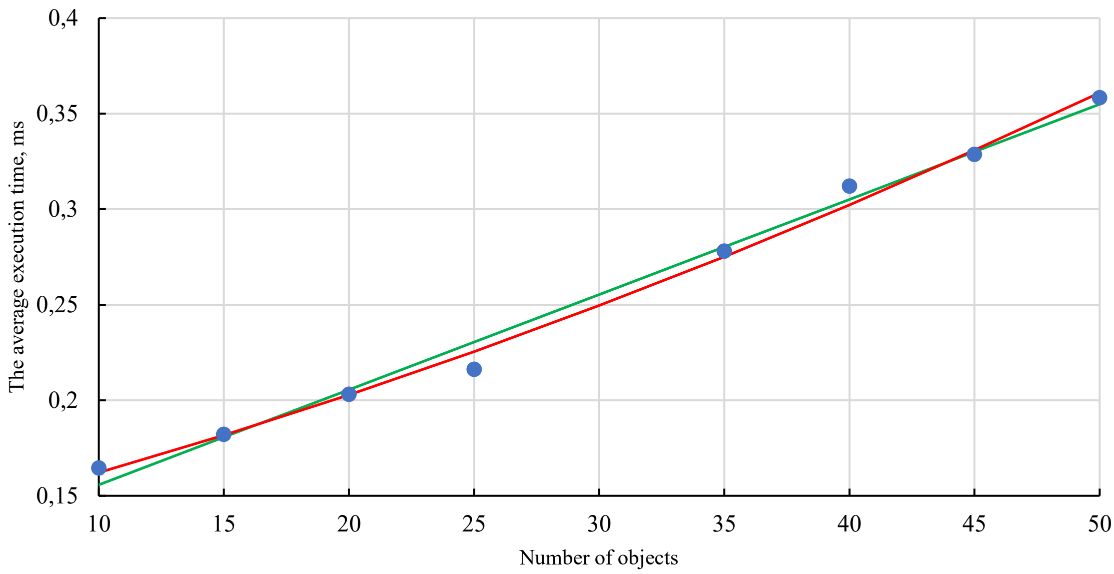

Fig. 6. Algorithm execution time on custom devices: ● — real data; ——— a = 0,00498, b = 0,10593 — linear approximation; ——— a = 0,00003, b = 0,00317, c = 0,12743 — quadratic approximation

Within the specified range, it is impossible to immediately determine the exact complexity of the algorithm calculation. As can be seen from Figure 6, the data are close to linear and quadratic approximations. Using the residual sum of squares method, a quantitative estimate of both approximations was calculated and values of 0.00035 and 0.00021 were obtained, respectively [10].

To confirm the hypothesis of quadratic dependence, a similar experiment was launched on a personal computer for a range of [10-10,000] objects. Figure 7 confirms the hypothesis; therefore, the algorithm can be assigned complexity O(n^2). However, the situation with 10,000 objects is rather theoretical, and in practice, the user is unlikely to work with more than 1–2 dozen objects in augmented reality.

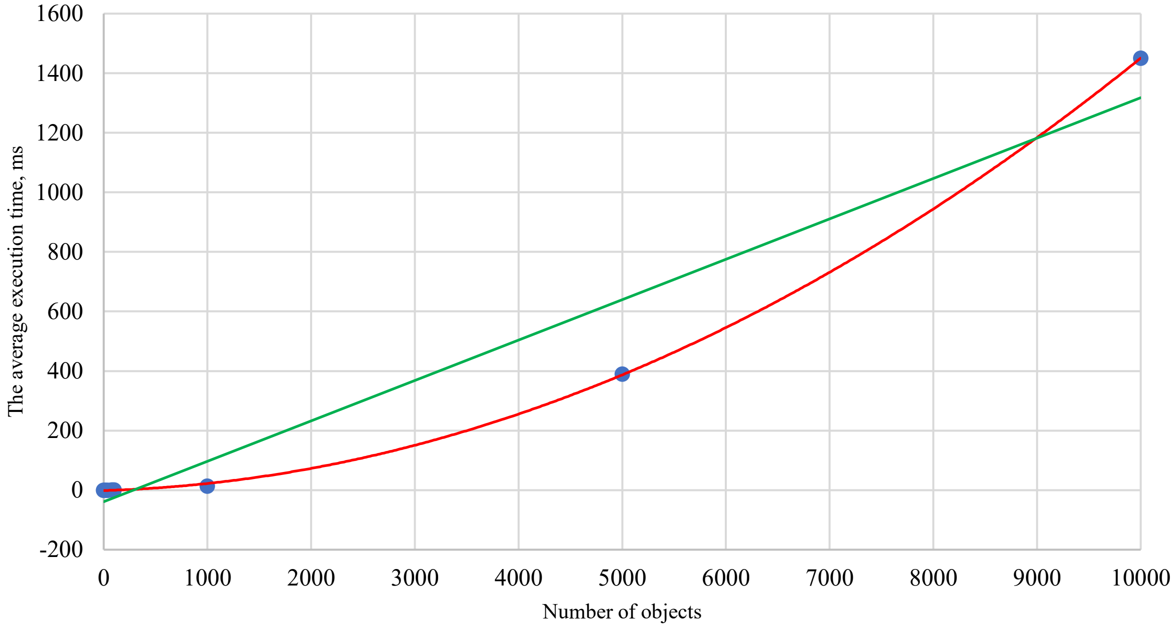

Fig. 7. Algorithm execution time for a large number of objects: ● — actual data; —— a = 0,1365, b = –45,455 — linear approximation; —— a = 0,00001, b = 0,0103, c = –1,6178 — quadratic approximation

The execution time on different user devices was compared, 10 most popular models were selected, and a diagram based on the calculations results was built (Fig. 8).

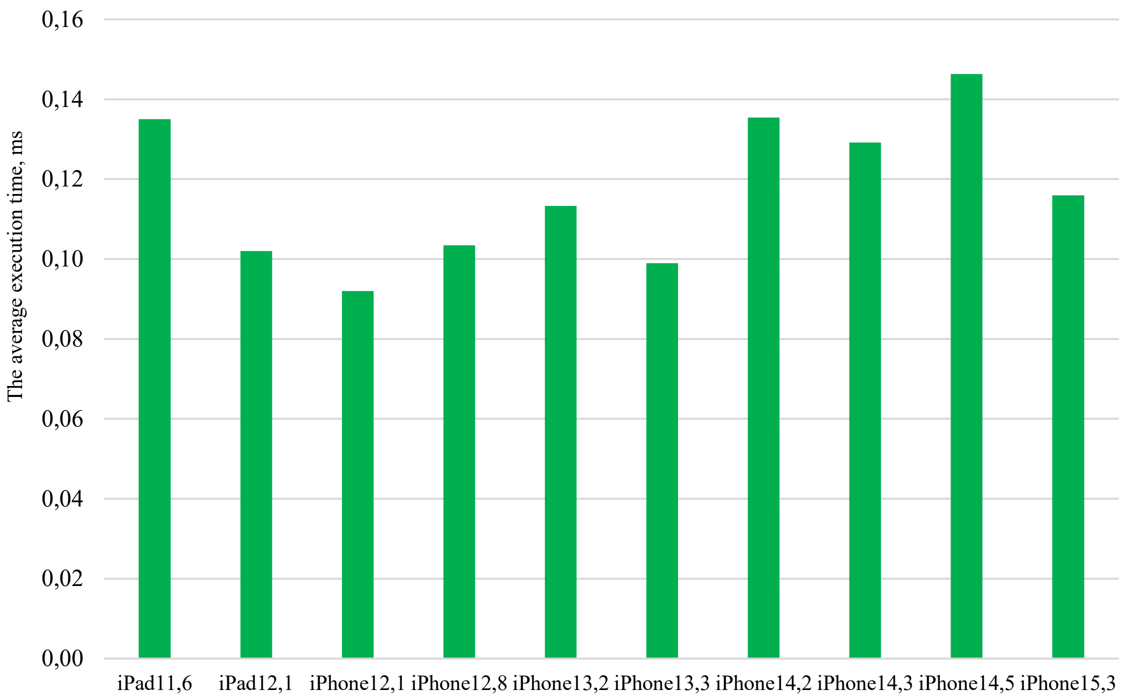

Fig. 8. Comparison of computing speed on different devices for 10 objects

The minimum registered execution time was 0.093 ms, the maximum — 0.146 ms. For this sample, the correlation between the device model and the execution time was only 0.177. This is a pretty low value.

Calculations have shown the high efficiency of the two-dimensional algorithm. This is due to the splitting of the entire set of objects into separate strings and the use of a fast one-dimensional algorithm in each string, described at the beginning of the article. This algorithm provides solving the problem with less resources and time.

Figure 9 shows additional visualizations of placement schemes for different numbers of objects and their parameters.

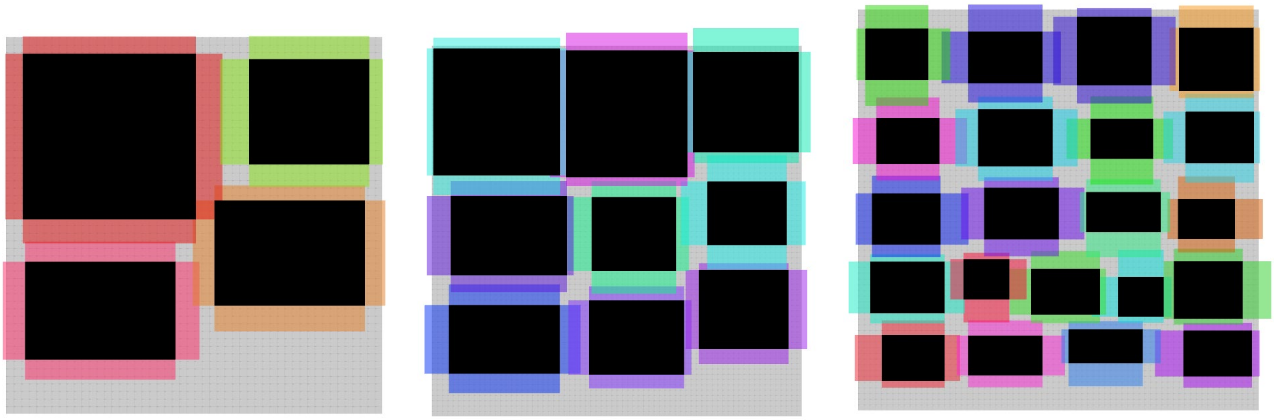

a) *b*) *c*)

Fig. 9. Examples of placing different numbers of objects:
a — 4 objects; *b* — 9 objects; *c* — 21 objects

Thus, the proposed algorithm of two-dimensional placement provides working with a set of virtual objects. Each of them is characterized by certain sizes and comfort zones. The algorithm is designed to optimally position such objects in a rectangular physical space that recreates the user's environment.

Discussion and Conclusion. For the previously described one-dimensional problem, an effective algorithm for optimal placement of virtual objects is proposed and implemented in the program code. A model of optimal placement was constructed for the two-dimensional case. Based on it, an effective algorithm has been developed, implemented in the program code.

The performance of the algorithm, which was measured by the execution time, was analyzed. It was found that there was no significant correlation between the execution time and the device model. The average time was fractions of a millisecond even for large batches of objects. This indicated a relatively stable performance of the algorithm under various conditions. However, the possible influence of other untested factors cannot be excluded. Further research is needed to fully characterize performance dependences.

The authors outline several areas of future work to improve the performance and adaptability of the algorithm. This is, firstly, the improvement of the solution, which will allow using the full size of objects, when possible, without intersections of comfort zones. Their sizes will be reduced only if absolutely necessary. This should provide for optimal use of space and further improve the interactive user experience.

Secondly, the inclusion of rotation of elements in the algorithm will increase flexibility in their arrangement and make it possible to use space better. In addition, this will allow the algorithm to take into account more different objects, thereby expanding its practical application.

Note that in an augmented reality application, placing three or more objects by the user is a rather time-consuming task. It requires considerable time, and significantly complicates the work.

The proposed technology for placing objects in 2D allows the optimal positioning of virtual content to improve the user experience in augmented reality. Automated location calculation reduces manual work and makes it possible to focus on valid interaction with AR.

Scientific research in this direction involves seamless integration of virtual and physical spaces. The results can be applied in practice by developers of augmented reality glasses who face the problem of rapid intelligent positioning of objects depending on user preferences and context. Moreover, the results of the work may be of interest to:

– engineers working on smart home systems;

– interface designers, for whom it is important to effectively and harmoniously combine controls and information on the screen.

The introduction of fuzzy logic allows developers to adapt the solution to specific tasks and use cases. In future research, it is advisable to study and apply user experience, include additional restrictions on the positioning of objects.

References

1. Yahya Ghazwani, Shamus Smith. Interaction in Augmented Reality. In: *Proc. 4th International Conference on Virtual and Augmented Reality Simulations*. New York, NY: Association for Computing Machinery; 2020. P. 39–44. https://doi.org/10.1145/3385378.3385384

2. Müller J, Butscher S, Feyer SP, Reiterer H. Studying Collaborative Object Positioning in Distributed Augmented Realities. In: *Proc. 16th Int. Conf. on Mobile and Ubiquitous Multimedia*. New York, NY: Association for Computing Machinery; 2017. P. 123–132. https://doi.org/10.1145/3152832.3152856

3. Regenbrecht HT, Wagner MT. Interaction in a Collaborative Augmented Reality Environment. In: *CHI '02 Extended Abstracts on Human Factors in Computing Systems*. New York, NY: Association for Computing Machinery; 2002. P. 504–505. https://doi.org/10.1145/506443.506451

4. Alpatova MV, Glazkov AV, Rudyak YuV. Mathematical Model of Rational Location of Augmented Reality Objects in User's Environment. In: *Proc Int. Sci. Conf. "Smart Nations: Global Trends In The Digital Economy"*. Cham: Springer; 2022. P. 248–254. https://doi.org/10.1007/978-3-030-94873-3_30

5. Gimadi EKh, Zalyubovskii VV. Bin Packing: Asymptotically Exact Approach. *Russian Mathematics. (Iz. VUZ)*. 1997;(12(427)):25–33. URL: https://kpfu.ru/portal/docs/F1486686603/03_12.PDF (accessed: 20.09.2023). (In Russ.).

6. Alpatova MV, Rudyak YuV. Placement of Multiple Virtual Objects in Physical Space in Augmented Reality Applications. *Advanced Engineering Research*. 2023;23(2):203–211. https://doi.org/10.23947/2687-1653-2023-23-2-203-211

7. Karev GB. Directionality in Right, Mixed and Left Handers. *Cortex*. 1999;35(3):423–31. https://doi.org/10.1016/S0010-9452%2808%2970810-4

8. Sung Lae Kim, Hae Jung Suk, Jeong Hwa Kang, Jun Mo Jung, Laine TH, Westlin J. Using Unity 3D to Facilitate Mobile Augmented Reality Game Development. In: *Proc. IEEE World Forum on Internet of Things* (*WF-IoT*). New York City: IEEE; 2014. P. 21–26. https://doi.org/10.1109/WF-IoT.2014.6803110

9. Warner RA. Using Z Scores for the Display and Analysis of Data. In book: *Optimizing the Display and Interpretation of Data*. Amsterdam: Elsevier; 2016. P. 7–51. https://doi.org/10.1016/B978-0-12-804513-8.00002-X

10. Wolfe DA. Ranked Set Sampling: Its Relevance and Impact on Statistical Inference. *ISRN Probability and Statistics*. 2012;2012:568385. https://doi.org/10.5402/2012/568385

Received 23.10.2023
Revised 14.11.2023
Accepted 22.11.2023

About the Authors:

Marianna V. Alpatova, Senior Lecturer of the Computer Science and Information Technology Department, Moscow Polytechnic University (38, Bolshaya Semyonovskaya St., Moscow, 107023, RF) SPIN-code: 1458-7868, ScopusID, ORCID, m.v.alpatova@yandex.ru

Yuri V. Rudyak, Dr.Sci. (Phys.-Math.), Professor of the Computer Science and Information Technology Department, Moscow Polytechnic University (38, Bolshaya Semyonovskaya St., Moscow, 107023, RF), SPIN-code: 4283-0952, ScopusID, ORCID, rudyak@mail.ru

Claimed contributorship:

MV Alpatova: basic concept formulation, setting of research objectives and tasks, text preparation, formulation of conclusions.

YuV Rudyak: academic advising, computational analysis, revision of the text, correction of the conclusions.

Conflict of interest statement: the authors do not have any conflict of interest.

All authors have read and approved the final manuscript.

Поступила в редакцию 23.10.2023
Поступила после рецензирования 20.11.2023
Принята к публикации 27.11.2023

Об авторах:

Марианна Валерьевна Алпатова, старший преподаватель кафедры информатики и информационных технологий Московского политехнического университета (107023, г. Москва, ул. Большая Семеновская, 38) SPIN-код: 1458-7868, ScopusID, ORCID, m.v.alpatova@yandex.ru

Юрий Владимирович Рудяк, доктор физико-математических наук, профессор кафедры информатики и информационных технологий Московского политехнического университета (107023, г. Москва, ул. Большая Семеновская, 38), SPIN-код: 4283-0952, ScopusID, ORCID, rudyak@mail.ru

Заявленный вклад соавторов

М.В. Алпатова — формирование основной концепции, постановка целей и задач исследования, подготовка текста, формулирование выводов.

Ю.В. Рудяк — научное руководство, расчеты, доработка текста, корректировка выводов.

Конфликт интересов: авторы заявляют об отсутствии конфликта интересов.

Все авторы прочитали и одобрили окончательный вариант рукописи.

INFORMATION TECHNOLOGY, COMPUTER SCIENCE AND MANAGEMENT

UDC 004.94/ 519.6
https://doi.org/10.23947/2687-1653-2023-23-4-422-432

Original article

EDN: QPFEMG

Web Application for Mathematical Modeling of Unsteady Oil Flow in Porous Medium

Aynur A. Mazitov
Institute of Petrochemistry and Catalysis, Ufa Federal Research Centre, RAS, Ufa, Russian Federation
✉ mazitov.ainur13@gmail.com

Abstract

Introduction. The analysis and interpretation of hydrodynamic research data are based on theoretical models and computational algorithms. Despite the demand for this topic, numerous issues related to unsteady fluid flows in oil reservoirs still require solutions. Therefore, mathematical setting of problems related to the account of unsteady fluid flow, the development of effective numerical methods and algorithms, their solution using modern web technologies are pressing. This study is aimed at developing a web application for mathematical modeling of the process of fluid filtration in single- porosity reservoirs when conducting a hydrodynamic study at a production well.

Materials and Methods. To solve the problem, the methods of continuum mechanics and computational mathematics were applied. A model of oil flow in a single-porosity reservoir was presented. Python and JavaScript programming languages were used in the development of the application. The calculation results were stored in a relational database implemented using PostgreSQL tools.

Results. A new web application has been developed for modeling the oil filtration process in single- porosity reservoirs. It is applicable for studying fluid dynamic processes and can be used to predict flowrates, production and calculation of optimal well operation modes.

Discussion and Conclusion. The developed web application provides for building pressure and temperature fields in the reservoir near a flowing and shut-in production well and at various distances from it. This information makes it possible to urgently assess the duration of hydrodynamic studies, as well as to regulate the operation of wells. The application can be deployed in an existing network infrastructure and use all the functionality by connecting to a remote server. It is optimized for use on various platforms and has broad prospects for further development.

Keywords: web application, mathematical model, hydrodynamic studies, database, pressure, temperature

Acknowledgements. The author would like to thank Yu.O. Bobreneva, the consultant of the scientific project, for valuable comments and constant support in the implementation of the project.

Funding information. The research was supported by the Russian Foundation for Basic Research, grant No. 20–37–90080 “Mathematical Modeling of Unsteady Multiphase Flow of in Porous Environment”.

For citation. Mazitov AA. Web Application for Mathematical Modeling of Unsteady Oil Flow in Porous Medium. *Advanced Engineering Research (Rostov-on-Don).* 2023;23(4):422–432. https://doi.org/10.23947/2687-1653-2023-23-4-422-432

Научная статья

Web-приложение для математического моделирования нестационарного течения нефти в пористой среде

А.А. Мазитов

Институт нефтехимии и катализа Уфимского федерального центра Российской академии наук,
г. Уфа, Российская Федерация

✉ mazitov.ainur13@gmail.com

Аннотация

Введение. Основу для анализа и интерпретации данных гидродинамических исследований составляют теоретические модели и вычислительные алгоритмы. Но, несмотря на востребованность данной тематики, многие вопросы, связанные с нестационарными течениями жидкостей в нефтяных пластах, все еще требуют решений. Поэтому математические постановки задач, связанных с учетом нестационарного течения жидкости, разработка эффективных численных методов и алгоритмов, их решение с применением современных web-технологий являются актуальными. Цель данной работы — разработка web-приложения для математического моделирования процесса фильтрации жидкости в однопоровых коллекторах при проведении гидродинамического исследования на добывающей скважине.

Материалы и методы. Для решения поставленной задачи применены методы механики сплошной среды и вычислительной математики. Представлена модель течения нефти в однопоровом коллекторе. При разработке приложения использованы языки программирования Python и JavaScript. Результаты расчетов хранятся в реляционной базе данных, реализованной средствами PostgreSQL.

Результаты исследования. Разработано новое web-приложение для моделирования процесса фильтрации нефти в однопоровых коллекторах, которое применимо для изучения флюидодинамических процессов и может быть использовано для прогноза дебитов, добычи и расчета оптимальных режимов работы скважин.

Обсуждение и заключение. Разработанное web-приложение позволяет строить поля давления и температуры в пласте около работающей и остановленной добывающей скважины и на различных расстояниях от нее. Данная информация дает возможность оперативно оценивать длительность гидродинамических исследований, а также регулировать работу скважин. Приложение может быть развернуто в существующей сетевой инфраструктуре, пользоваться всем функционалом, подключаясь к удаленному серверу. Оно оптимизировано для использования на различных платформах и имеет широкие перспективы дальнейшего развития.

Ключевые слова: web-приложение, математическая модель, гидродинамические исследования, база данных, давление, температура

Благодарности. Автор выражает благодарность консультанту научного проекта Ю.О. Бобренёвой за ценные замечания и постоянную поддержку при выполнении проекта.

Финансирование. Работа выполнена при финансовой поддержке Российского фонда фундаментальных исследований, грант № 20–37–90080 «Математическое моделирование нестационарного течения многофазного потока в пористой среде».

Для цитирования: Мазитов А.А. Web-приложение для математического моделирования нестационарного течения нефти в пористой среде. *Advanced Engineering Research (Rostov-on-Don).* 2023;23(4):422–432. https://doi.org/10.23947/2687-1653-2023-23-4-422-432

Introduction. The Russian Federation is one of the leading countries in the world in terms of oil production. Every year, over 500 million tons of oil are produced in the country's fields, the vast majority of which is exported in crude form to the countries of the Asia-Pacific region, Europe and the near abroad. The oil industrial growth in our country has an impact on other industries and spheres of activity; therefore, the solution to tasks for the effective development and exploitation of oil fields has been and remains promising. The basis of modern scientific technologies of oil development is a comprehensive study of the properties of productive reservoirs, the substances contained in them, and the complex processes occurring during fluid flow.

The base target in oil production is to increase the rate of drainage from the productive reservoir and maintain reservoir pressure. The planning of work on the effective development and optimal operation of an oil well is of complex character, associated with the hydrodynamic processes occurring during the fluid flow in the "well — formation" system [1]. Hydrodynamic well testing (WT) is used to study the productive properties of reservoirs and fluids. WT means provide for the reservoir data collection using bottomhole or wellhead instruments, as well as the postprocessing of measurements and interpretation of the data obtained (productivity, filtration properties of fluids, type of collector, etc.) [2].

When studying reservoirs through WT, theoretical models based on classical equations and laws are used, as well as computational algorithms for modeling fluid filtration processes. However, despite the demand for this topic, a number of issues related to the mathematical and computational aspects of modeling nonstationary flows in reservoirs require further development [3, 4].

There are a number of domestic ("Avton", "Gidrozond") and foreign (OLGA, LedaFlow, FlowVision, MAST, Saphir NL) programs for the analysis and interpretation of WT results [5–7]. With all the advantages they have, there are some disadvantages, such as the inability to perform a full range of calculations, viewing and changing the parameters of the original models. All the presented software products are desktop, commercial, difficult to operate, many have an overloaded interface. Under the conditions when it is required to carry out calculations promptly or in real time, large commercial simulators are ineffective. Therefore, to perform similar work, it is proposed to use a web application that has many advantages.

Unlike desktop applications, web applications are independent of the operating system and computing power of personal computers. The program code of a web application is written once for a specific platform where it will be deployed. Web applications attract attention because of their simple implementation, ease of use, and high performance. Their basic characteristics are accessibility, reliability, security, scalability, flexibility, cross-platform character. To work with a web application from a user's personal computer, it is necessary to be on the same network with the server on which it is deployed. Such a network can be a local enterprise network or a global Internet network, if we are talking about websites. Compared to desktop applications, web applications have one drawback — response time, depending on the distance of the personal computer from the server.

The operating logic of a web application differs from a desktop application, which launches and executes code on the user's computer. Therefore, desktop applications are distinguished by a more advanced and responsive user interface and allow for implementing more complex domain logic. However, with the development of web technologies, this advantage is leveled every year, and web applications are increasingly capable of implementing complex user scenarios. Thus, web applications become more competitive in terms of the implementation of production tasks.

In this regard, the mathematical formulation of problems taking into account the unsteady fluid flow in all its elements (formation, stack pipes, flow channels), the development of effective numerical methods and algorithms, their subsequent solutions using modern web development technologies are important today. The use of the obtained numerical algorithms makes it possible to quantitatively describe the behavior of pressure and temperature in oil wells. The algorithm and web application will provide users, experts in the field of analysis and interpretation of hydrodynamic studies, with a convenient and easily adaptable tool for calculating complex processes occurring under the development of porous reservoirs.

Materials and Methods. A production well is considered, on which a hydrodynamic study is carried out by the build-up test. The well operates a terrigenous reservoir, which belongs to the single-porosity reservoirs. The formation is unconfined, there is no impact of neighboring wells. The fluid flow in the formation is horizontal, there are no crossflows between the layers. The well operates in a steady state with a constant bottomhole pressure. Constant pressure and temperature are maintained at the boundary of the contour. To conduct the investigation, the measuring device is lowered to the depth of the upper perforation holes. The calculation of pressure and temperature dynamics is carried out in the spatial one-dimensional case.

In numerical modeling, it is important to take into account all the parameters of the reservoir and fluid to achieve the most qualitative description of the oil mass transfer process in a single-porosity reservoir. Let us consider a mathematical model describing the process of oil filtration in a single-porosity reservoir. The piezoconductivity and thermal response equations serve as the basis for the model. The mathematical model in radial coordinates is a partial differential system:

$$\begin{gathered} \varphi c_t \frac{\partial P}{\partial t} = \frac{1}{r}\frac{\partial}{\partial r}\left(\frac{k}{\mu} r \frac{\partial P}{\partial r}\right), \\ c\rho \frac{\partial T}{\partial t} = \frac{1}{r}\frac{\partial}{\partial r}\left(\lambda \frac{\partial T}{\partial r}\right) - c\rho u\left(\frac{\partial T}{\partial t} + \varepsilon \frac{\partial P}{\partial r}\right) + \eta\varphi c\rho \frac{\partial P}{\partial t}, \end{gathered} \tag{1}$$

where φ — formation porosity; c_t — formation compressibility (1/Pa); k — formation permeability (m^2); μ — fluid viscosity (Pa·s); P — formation pressure (Pa); r — distance to the well wall (m); t — time (s); c — oil heat capacity (J/kg·K); ρ — oil density (kg/m^3); T — formation temperature (K); λ — thermal conductivity of the porous medium (W/m^3·K); u — rate of convective heat transfer in a porous medium (m/s); ε — Joule-Thomson coefficient (K/Pa); η — adiabatic expansion coefficient (K/Pa).

The first equation describes the process of pressure change in the reservoir, the second — the process of heat transfer of fluid.

The rate of convective heat transfer in a porous medium is determined by the expression:

$$u = -\frac{k}{\mu}\frac{\partial P}{\partial r}. \tag{2}$$

System of equations (1) is given in the space-time interval:

$$\begin{gathered} r_w \le r \le R, \\ 0 \le t \le t_\kappa, \end{gathered} \tag{3}$$

where r_w — well radius; R — distance to the boundary of the contour of the investigation (m); t_κ — time of the investigation (s).

Based on the above conditions for the well and the considered area for system (1), the initial and boundary conditions are set as follows:

$$\begin{gathered} t = 0 : P = P_0, T = T_0, r_w \le r \le R, \\ r = r_w : P = P_0, T = T_0, t > 0, \\ r = R : \frac{\partial P}{\partial r} = 0, \frac{\partial T}{\partial r} = 0, t > 0. \end{gathered} \tag{4}$$

After determining the initial and boundary conditions, a model of the oil filtration process in a single–porosity reservoir (1)–(4), was obtained, characterizing the redistribution of pressure and temperature in the formation.

The initial stage of solving the system is to bring it to a discrete form. The finite difference method is used for this purpose [8]. A uniform space-time grid is being constructed:

$$\begin{gathered} \overline{G_h} = \left\{ r_i = r_w + (i-1)h, i = 1, 2, ..., N, h = \frac{R - r_w}{N-1} \right\}, \\ \overline{G_t} = \left\{ t_n = n\tau, n = 0, 1, ..., M, \tau = \frac{t_\kappa}{M} \right\}, \end{gathered} \tag{5}$$

where h — grid spacing; τ — grid time step; N — number of nodes in space; M — number of nodes by time.

After replacing the differential expressions with difference analogues, a system of equations is obtained:

$$\varphi c_t \frac{P_i^{n+1}-P_i^n}{\tau}=\frac{k}{\mu}\frac{1}{r_i}\frac{r_{i+\frac{1}{2}}P_{i+1}^{n+1}-\left(r_{i+\frac{1}{2}}+r_{i-\frac{1}{2}}\right)P_i^{n+1}+r_{i-\frac{1}{2}}P_{i-1}^{n+1}}{h^2},$$
$$c\rho\frac{T_i^{n+1}-T_i^n}{\tau}=\frac{\lambda}{r_i}\frac{T_{i+1}^{n+1}-2T_i^{n+1}+T_{i-1}^{n+1}}{h^2}-c\rho u_i\left(\frac{T_i^{n+1}-T_i^n}{\tau}+\varepsilon\frac{P_{i+1}^{n+1}-P_i^{n+1}}{h}\right)+ \tag{6}$$
$$\eta\varphi c\rho\frac{P_i^{n+1}-P_i^n}{\tau},i=2,...,N-1,n\geq 0.$$

System (6) is a system of linear equations (SLE), which is reduced to a three-point equation of the general form:

$$A_i y_{i+1}^{n+1}-B_i y_i^{n+1}+C_i y_{i-1}^{n+1}=F_i, i=1,...,N,n\geq 0. \tag{7}$$

The coefficients are equal to:

$$A_i^P=\frac{k}{\mu h^2}\frac{r_{i+\frac{1}{2}}}{r_i},B_i^P=\left(\frac{k}{\mu h^2}\frac{r_{i+\frac{1}{2}}+r_{i-\frac{1}{2}}}{r_i}+\frac{\varphi c_t}{\tau}\right),C_i^P=\frac{k}{\mu h^2}\frac{r_{i-\frac{1}{2}}}{r_i},F_i^P=-\frac{\varphi c_t}{\tau}P_i^n,$$
$$A_i^T=\frac{\lambda}{h^2 r_i},B_i^T=\left(\frac{2\lambda}{h^2 r_i}+\frac{c\rho u_i}{\tau}+\frac{c\rho}{\tau}\right),C_i^T=\frac{\lambda}{h^2 r_i}, \tag{8}$$
$$F_i^T=-\frac{c\rho}{\tau}\left(u_i+1\right)T_i^n+c\rho u_i\varepsilon\frac{P_{i+1}^{n+1}-P_i^{n+1}}{h}-\eta\varphi c\rho\frac{P_i^{n+1}-P_i^n}{\tau}.$$

System (7) is solved by the scalar sweep method [9, 10]. The problem is non-stationary; therefore, the method is used to determine the spatial distribution of formation pressure and temperature at each time layer [11, 12]. The problem is solved sequentially, at the first stage, the equation for pressure is solved, at the second — for temperature.

A web application has been developed to automate the solution to the problem. In general, its structure is shown in Figure 1. It identifies five basic components: input information flows, output information flows, information processing methods, hardware, database [13, 14].

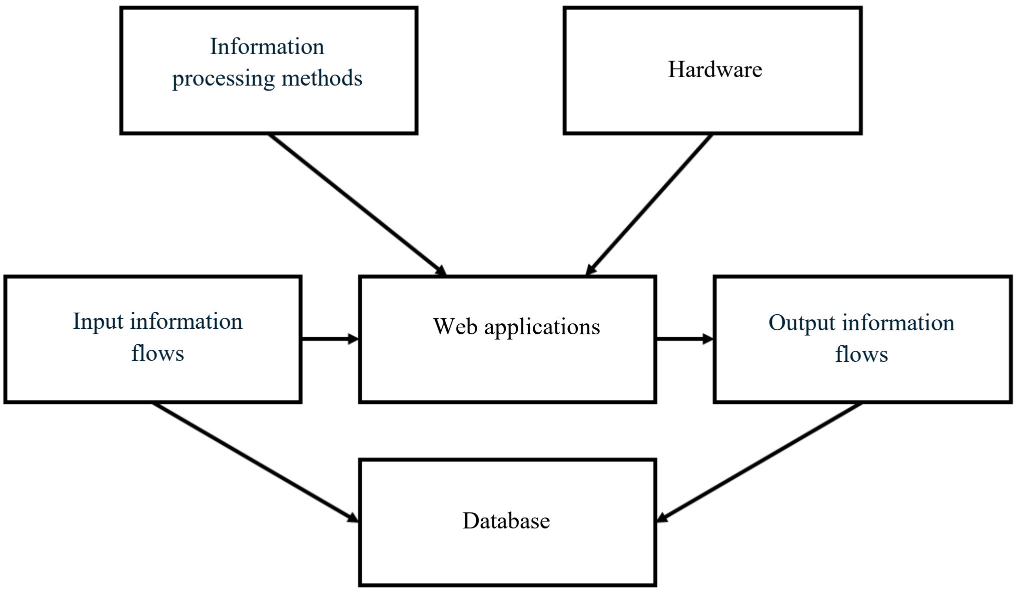

Fig.1. General application structure

The input information flows are data on the model parameters, and the output data are graphs reflecting the temporal or spatial dependences of bottomhole pressure and temperature. Information processing methods are understood as numerical methods and methods of interpretation of hydrodynamic studies. The hardware is the server on which the application is hosted, and the user's personal computer. A database is used to store input parameters and calculation results.

The final type of the software depends on the means selected for its development. Development tools are paradigms and programming languages, environments and technologies for development. The selection of tools affects the way of the task implementation, the criteria for software quality, the presentation of data, and the type of graphical user interface. To develop the application, Python using the Flask microframework was chosen as the programming language for the server side, and JavaScript with Vue.js — for the client side [15, 16]. PostgreSQL was used as a DBMS for database design and development [17].

Research Results. The developed software is a cross-platform client-server web application. Data storage and calculations take place on a web server with which the user interacts through a browser (all modern Internet browsers are supported). The client part can be used on a wide range of platforms (PCs, laptops, smartphones) and operating systems (Windows, MacOS, Android, iOS).

A large part of the web application main window is occupied by a tool for plotting temperature and pressure. The graphs are constructed after the calculation is performed by selecting the appropriate menu item. It is also possible to plot graphs based on previously performed calculations. For this purpose, the required calculation is selected on the left side of the window. Graphs are based on spatial and temporal coordinates. To change the chart view, select the corresponding items in the upper part of the window.

All calculations performed are stored in the developed flowcalcdb relational database, whose structure is shown in Figure 2.

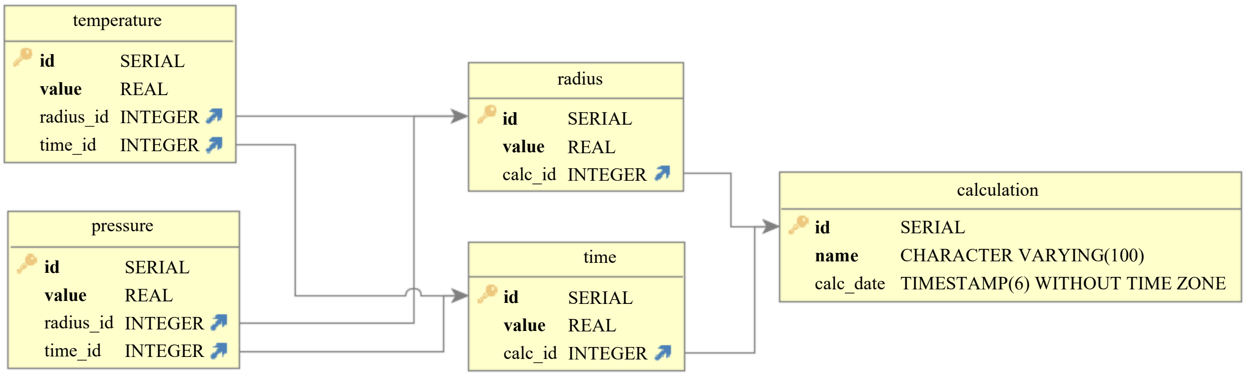

Fig. 2. Structure of the flowcalcdb database

In total, the database contains five tables, which are in the third normal form [18]. All tables have primary keys. The primary table, calculation, stores the name of the calculation and the date of its creation. Two tables dependent on it, radius and time, store information on space-time coordinates. The temperature and pressure tables store the temperature and pressure values, respectively.

A number of computational experiments have been carried out in the developed application to evaluate the result of its work. The values from Table 1 are used for modeling.

Table 1

Initial and boundary conditions, calculation parameters

Parameter	Value	Measurement unit
Well radius, r_w	0.102	m
Radius of investigation, R	100	m
Time of investigation, t	24	h
Initial pressure, P_0	25	MPa
Final pressure, Pк	30	MPa
Permeability, k	1e-14	m^2
Porosity	0.2	
Oil viscosity, μ	1.10e-3	Pa·s
Oil compressibility	1.58e-9	1/Pa
Heat capacity, c_ρ	1.4	$MJ/m^3 \cdot K$
Thermal conductivity, λ	0.6	W/m·K
Joule-Thomson coefficient, ε	3.94e-7	K/Pa
Adiabatic expansion coefficient, η	3.15e-7	K/Pa
Initial temperature, T_0	363.15	K
Number of points by time, N	1,000	
Number of points by space, M	1,000	

Using the data from Table 1, graphs of the pressure and temperature distribution over space are plotted, shown respectively in Figures 3 and 4.

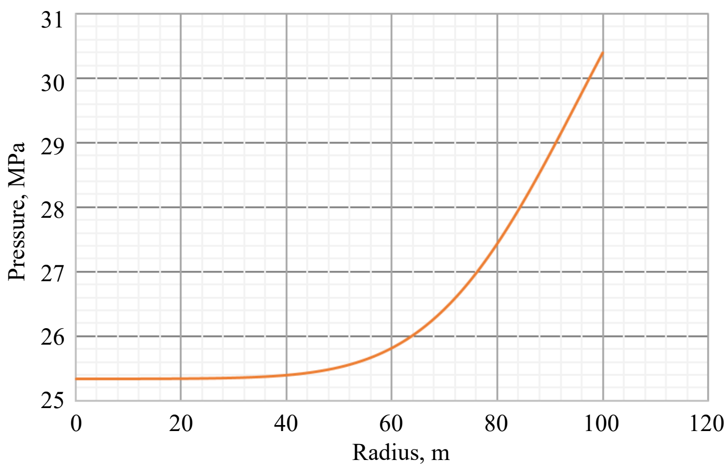

Fig. 3. Distribution of pressure over space at a finite point in time

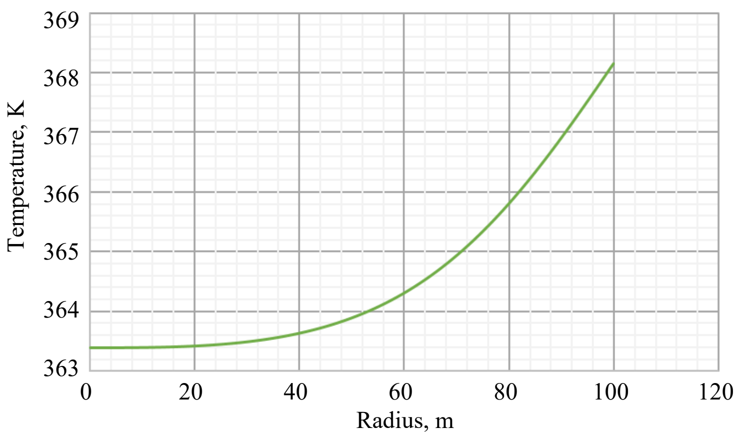

Fig. 4. Distribution of temperature over space at a finite point in time

As follows from the data in Figures 3 and 4, after stopping the well for hydrodynamic examination, pressure and temperature are restored, and the farther away from the walls of the well, the greater the recovery value. Figures 5 and 6 show exactly how pressure and temperature are distributed at different points in time (6, 12, 24 hours) after the well is stopped. This information is useful for experts in the analysis and interpretation of hydrodynamic studies, as it provides for the assessment of the dynamics of pressure and temperature and decision making on continuing or stopping the investigation, as well as carrying out additional measures.

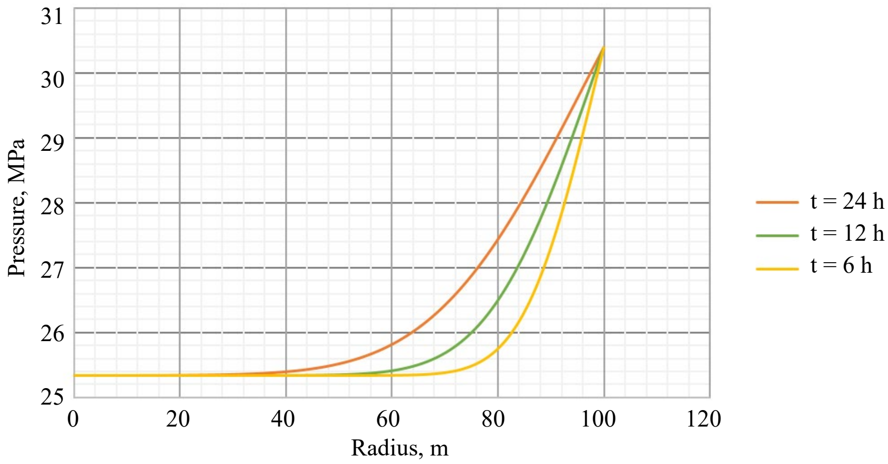

Fig. 5. Distribution of pressure across space at different points in time

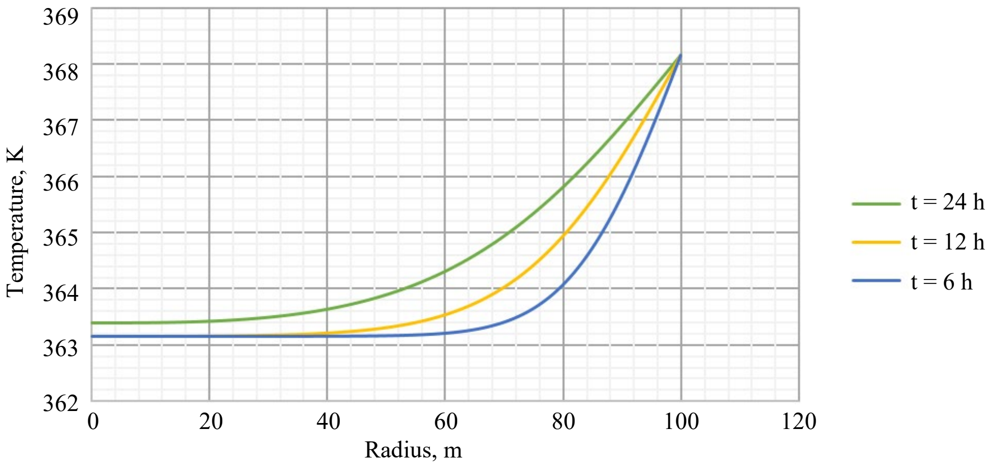

Fig. 6. Distribution of temperature across space at different points in time

Based on the calculations performed, it was found that the permeability of the formation had the greatest impact on the behavior of pressure and temperature. Figures 7 and 8 show graphs of pressure and temperature dynamics depending on different permeability values near the walls of the well (low-permeability reservoir — 1 mD, medium-tight reservoir — 10 mD, high-permeability reservoir — 100 mD (1D = 10^{-12}m^2)). As can be seen in the graphs, the rate of pressure and temperature recovery grows with increasing reservoir permeability. Figure 7 shows a graph for real field data (reservoir permeability is 80 mD).

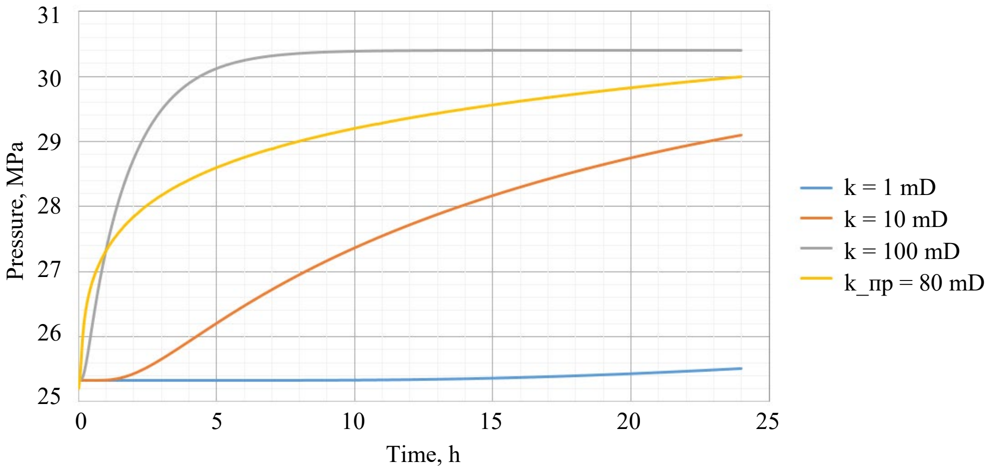

Fig. 7. Pressure dynamics for different permeabilities

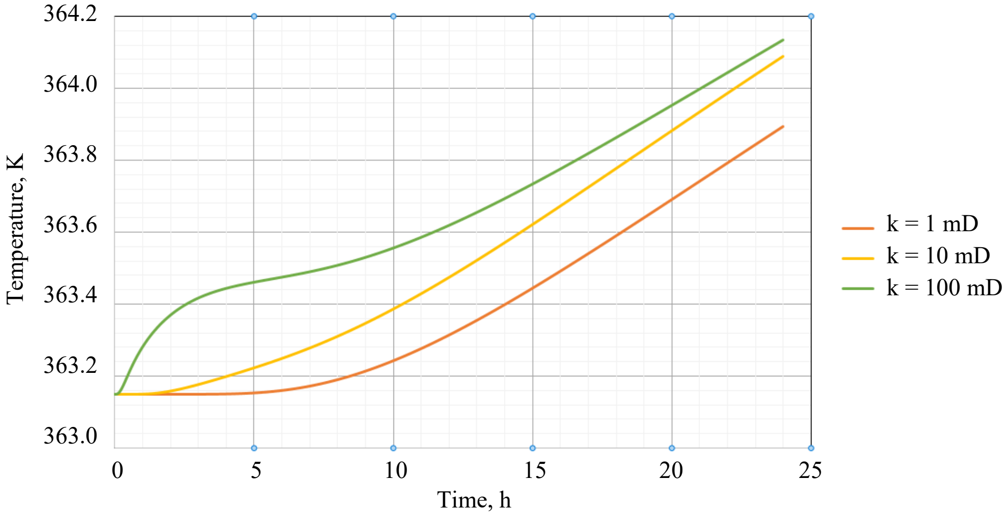

Fig. 8. Temperature dynamics for different permeabilities

Based on the pressure dynamics, it is possible to determine the time of the investigation (Fig. 7). As an example, for a high-permeability reservoir, it makes no sense to conduct an investigation for more than ~6 hours, since after this time the pressure practically does not change, and an idle well is ineffective, since production losses are occurring.

Discussion and Conclusion. The developed web application can be used for the analysis and interpretation of hydrodynamic research data. The web application provides a user-friendly interface and reduces support costs. It can be deployed in an existing network infrastructure or connected to a remote server to provide full functionality. The application allows us to qualitatively and quantitatively assess the behavior of pressure and temperature in single-porosity reservoirs. Storing the calculation results in a database makes it possible to perform an analysis using the results of a variety of studies. On its basis, a summary report can be compiled, and recommendations for further use of the well or field as a whole can be formulated. The models used are stable and convergent. Graphs are built using a written web application, and therefore, it can be used in production.

The application has broad development prospects, specifically, it is possible to implement other models of fluid flow, or provide for the presence of several phases. Also, at the time of writing this work, the issue of abandoning foreign commercial products in favor of domestic simulators has become acute. Therefore, the development of such products is promising.

References

1. Hussein A. *Essentials of Flow Assurance Solids in Oil and Gas Operations: Understanding Fundamentals, Characterization, Prediction, Environmental Safety, and Management,* 1st ed. Houston, TX: Gulf Professional Publishing; 2022. 1122 p.

2. Kamartdinov MR, Kulagina TE, Mangazeev PV, Pankov MV. *Hydrodynamic Studies of Wells*. Moscow: YUKOS; 2003. 810 p. (In Russ.)

3. Bobreneva YuO, Mazitov AA, Gubaydullin IM. Researching the Mechanisms of Fluid Flow in the Fracture-Porous Reservoir Based on Mathematical Modeling. *Computational Mathematics and Information Technologies*. 2018;2(2):133–143.

4. Bobreneva YuO, Mazitov AA, Gubaydullin IM. Mathematical Modelling of Fluid Flow Processes in the Fracture-Porous Reservoir. *Journal of Physics: Conference Series*. 2019;1096:012187. https://doi.org/10.1088/1742-6596/1096/1/012187

5. Lisakov SA, Sypin EV, Zyryanova MN, Pavlov AN, Galenko YuA. Modeling the Process of Unsteady Combustion of a Methane-Air Mixture in Coal Mines. *Industrial Safety*. 2018;(1):40–53. URL: https://tesis.com.ru/infocenter/downloads/flowvision/fv_bti-secna.pdf (accessed: 18.09.2023). (In Russ.)

6. Zhluktov SV, Aksenov AA, Kharchenko SA, Moskalev IV, Sushko GB, Shishaeva AS. Modeling of Separated Flows in CFD Software FlowVision-HPC. *Numerical Methods and Programming*. 2010;11(1):234–245. URL: https://num-meth.ru/index.php/journal/article/view/395/402 (accessed: 18.09.2023). (In Russ.)

7. Konovalov DA, Shmatov DP, Drozdov IG, Dahin SV. Simulation of Heat and Mass Transfer in Porous Elements of Thermal Protection Systems Using Software FlowVision. *Bulletin of Voronezh State Technical University*. 2011;7(4):143–147.

8. Mazitov AA, Bobreneva YuO, Gubaydullin IM, Poveshchenko YuA. Mathematical Modeling of a Multiphase Flow in a Single-Pore Reservoir. *Preprints of the Keldysh Institute of Applied Mathematics*. 2022;62:1–14. https://doi.org/10.20948/prepr-2022-62

9. Fedorov AA, Bykov AN. The Method of Two-Level Parallelization for Solving Tridiagonal Systems on Hybrid Computers with Multicore Coprocessors. In: *Proc. Int. Sci. Conf. Parallel Computational Technologies*. Chelyabinsk: SUSU Publishing Center; 2016. P. 334–346.

10. Bykov AN, Erofeev AM, Sizov EA, Fedorov AA. A Parallel Sweep Method for Hybrid Supercomputers. *Numerical Methods and Programming*. 2013;14(2):43–47.

11. Bobreneva YuO, Rahimly PI, Poveshchenko YuA, Podryga VO, Enikeeva LV. On One Method of Numerical Modeling of Piezoconductive Processes of a Two-Phase Fluid System in a Fractured-Porous Reservoir. *Journal of Physics: Conference Series.* 2021;2131:022001. https://doi.org/10.1088/1742-6596/2131/2/022001

12. Bobreneva YuO, Mazitov AA, Gubaydullin IM. Mathematical Modeling of Fluid Flow Processes in the Fractured-Porous Reservoir. In: *Proc. V Int. Conf. and the Youth School "Information Technologies and Nanotechnologies"*. Samara: Novaya tekhnika; 2018. P. 1775–1780. (In Russ.)

13. Gubaydullin IM, Koledina KF, Safin RR. Automated System for Structural and Parametric Identification of Kinetic Models of Chemical Reactions Involving Organometallic Compounds Based on the Kinetic Research Database. *Control Systems and Information Technologies*. 2014;58(4):10–16. (In Russ.)

14. Gubaydullin IM, Koledina KF, Spivak SI. Structural and Parametric Identification of Kinetic Models of Chemical Reactions Involving Organometallic Compounds Based on an Information and Computational Analytical System. *Chemical Industry Developments*. 2014;11:18–27. (In Russ.)

15. Grinberg M. *Flask Web Development,* 2nd ed. Sebastopol, CA: O'Reilly Media, Inc.; 2018. 312 p.

16. Au-Yeung J. *Vue.js 3 By Example: Blueprints to Learn Vue Web Development, Full-Stack Development, and Cross-Platform Development Quickly*. Birmingham, UK: Packt Publishing; 2021. 320 p.

17. Riggs S, Ciolli G. *PostgreSQL 14 Administration Cookbook.* Birmingham, UK: Packt Publishing; 2022. 608 p.

18. DeBarros A. *Practical SQL, 2nd Edition: A Beginner's Guide to Storytelling with Data.* San Francisco, CA: No Starch Press; 2022. 464 p.

Received 02.10.2023
Revised 31.10.2023
Accepted 10.11.2023

About the Author:

Aynur A. Mazitov, Intern researcher, Laboratory of Mathematical Chemistry, Institute of Petrochemistry and Catalysis, Ufa Federal Research Centre of the Russian Academy of Sciences (141, pr. Oktyabrya, Ufa, 450075, RF), SPIN-код: 3903-2281, ORCID, mazitov.ainur13@gmail.com

Conflict of interest statement: the author does not have any conflict of interest.

The author has read and approved the final manuscript.

Поступила в редакцию 02.10.2023
Поступила после рецензирования 31.10.2023
Принята к публикации 10.11.2023

Об авторе:

Айнур Асгатович Мазитов, стажер-исследователь лаборатории математической химии института нефтехимии и катализа Уфимского федерального исследовательского центра Российской академии наук (450075, РФ, Уфа, пр. Октября, 141), SPIN-код: 3903-2281, ORCID, mazitov.ainur13@gmail.com

Конфликт интересов: автор заявляет об отсутствии конфликта интересов.

Автор прочитал и одобрил окончательный вариант рукописи.

INFORMATION TECHNOLOGY, COMPUTER SCIENCE AND MANAGEMENT

Check for updates

UDC 004.85
https://doi.org/10.23947/2687-1653-2023-23-4-433-450

Original article

EDN: RKAOTZ

Modeling of Ultrasonic Flaw Detection Processes in the Task of Searching and Visualizing Internal Defects in Assemblies and Structures

Boris V. Sobol[1] ✉, **Arkadiy N. Soloviev**[2], **Pavel V. Vasiliev**[1] **Alexandr A. Lyapin**[1]
[1] Don State Technical University, Rostov-on-Don, Russian Federation
[2] Crimean Engineering and Pedagogical University named after Fevzi Yakubov, Simferopol, Russian Federation
✉ b.sobol@mail.ru

Abstract
Introduction. Inverse problems are a specific type of tasks where the consequences of phenomena are studied to identify their causes. They are widely used in scientific studies, specifically, those dealing with large amounts of experimental data. In the presented paper, inverse problems in mechanical engineering and structural diagnostics are considered. These areas require precise methods to identify internal defects in various materials, which can be critical to ensure the safety and efficiency of technical structures. Despite the many flaw detection methods available, there is a need for innovative developments that can provide higher accuracy and efficiency. This study integrates different scientific methods and technologies. It opens up new perspectives in nondestructive testing for the detection of internal defects in various materials and structures. Its objective is to develop and implement nondestructive testing methods based on a neural network device to improve the accuracy of defect identification, as well as to build a neural network model and evaluate its effectiveness for the refinement of ultrasonic visualization of internal defects in solid materials. In this regard, the task to be solved is to create a reliable tool for accurate visualization of sizes, shapes, location and orientation of internal defects in various materials.
Materials and Methods. The technique of determining the geometric parameters of defects in materials through nondestructive testing is used. The approach combining modeling of ultrasonic wave propagation in acoustic medium and artificial neural network technologies is applied. This approach identifies nonlinear relationships between the geometry of defects and the amplitude-frequency and amplitude-time data obtained during signal analysis. Artificial neural networks are a model that can be trained on examples, which provides for an effective solution to problems that are difficult to express in traditional forms. The study uses the finite difference method in the time domain. It is applied to identify and visualize internal defects in materials using ultrasonic nondestructive testing and convolutional generative neural networks.
Results. A convolutional neural network has been developed to visualize internal defects using ultrasonic nondestructive testing techniques. This neural network successfully determines the size of defects, their location, shape and orientation with high accuracy and reliability.
Discussion and Conclusion. The authors highlight the key influence of defect size on the accuracy of ultrasonic imaging in various scenarios. The validation of the model for three different cases of defects with different mechanical parameters has shown that for successful visualization of defects, the wavelength of the ultrasonic pulse must be ten times smaller than the size of the defect. When analyzing the impact of defect size on the accuracy of the neural network, it is found that the visualization error increases for defects of smaller size. It has also been found that the relative speed of sound in materials has a greater effect on the accuracy of the method than the relative density of the material. Based on the results obtained by the authors, it can be argued that the developed methods and technical solutions are of great importance for future research in the field of flaw detection. They have significant potential for scientific and practical applications.

Keywords: ultrasonic nondestructive testing, defects, ultrasonic response, convolutional neural networks

Acknowledgements. The authors would like to thank the Editorial board and the reviewers for their attentive attitude to the article and for the specified comments that improved the quality of the article.

For citation. Sobol BV, Soloviev AN, Vasiliev PV, Lyapin AA. Modeling of Ultrasonic Flaw Detection Processes in the Task of Searching and Visualizing Internal Defects in Assemblies and Structures. *Advanced Engineering Research (Rostov-on-Don)*. 2023;23(4):433–450. https://doi.org/10.23947/2687-1653-2023-23-4-433-450

Научная статья

Моделирование процессов ультразвуковой дефектоскопии в задаче поиска и визуализации внутренних дефектов в узлах агрегатов и конструкций

Б.В. Соболь[1] ✉, **А.Н. Соловьев**[2], **П.В. Васильев**[1], **А.А. Ляпин**[1]

[1] Донской государственный технический университет, г. Ростов-на-Дону, Российская Федерация,

[2] Крымский инженерно-педагогический университет имени Февзи Якубова, г. Симферополь, Российская Федерация

✉ b.sobol@mail.ru

Аннотация

Введение. Обратные задачи представляют собой специфический тип задач, где изучаются последствия явлений с целью определения их причин. Они широко используются в научных исследованиях, особенно тех, что имеют дело с большими объемами экспериментальных данных. В представленном исследовании рассмотрены обратные задачи в машиностроении и диагностике конструкций. Эти области требуют точных методов для выявления в различных материалах внутренних дефектов, которые могут иметь критические значения для обеспечения безопасности и эффективности использования технических конструкций. Несмотря на множество имеющихся методов дефектоскопии существует потребность в инновационных разработках, способных обеспечить ее более высокую точность и эффективность. В данном исследовании объединены различные научные методы и технологии, оно открывает новые перспективы в неразрушающем контроле для обнаружения внутренних дефектов в различных материалах и структурах. Его цель — развитие и внедрение методов неразрушающего контроля на основе нейросетевого аппарата для повышения точности идентификации дефектов, а также разработка нейросетевой модели и оценка ее эффективности для усовершенствования процесса ультразвуковой визуализации внутренних дефектов в твердых материалах. В связи с этим задача, которую предстоит решить для достижения поставленной цели, заключается в создании надежного инструмента для точной визуализации размеров, форм, местоположения и ориентации внутренних дефектов в различных материалах.

Материалы и методы. Применяется методика определения геометрических параметров дефектов в материалах с использованием неразрушающего контроля. Также используется метод, объединяющий моделирование распространения ультразвуковых волн в акустической среде и технологии искусственных нейронных сетей. Он выявляет нелинейные связи между геометрическими характеристиками дефектов и амплитудно-частотными и амплитудно-временными данными, полученными при анализе сигналов. Искусственные нейронные сети представляют собой модель, которая может обучаться на примерах, что позволяет эффективно решать задачи, которые сложно выразить в традиционных формах. В исследовании используется метод конечных разностей во временной области. Он применяется для идентификации и визуализации внутренних дефектов в материалах с использованием ультразвукового неразрушающего контроля и сверточных генеративных нейронных сетей.

Результаты исследования. Разработана сверточная нейронная сеть для визуализации внутренних дефектов с использованием техник ультразвукового неразрушающего контроля. Эта нейронная сеть успешно определяет размер дефектов, их местоположение, форму и ориентацию с высокой точностью и надежностью.

Обсуждение и заключение. Авторы подчеркивают ключевое влияние размера дефекта на точность ультразвуковой визуализации в различных сценариях. Проведенная валидация модели для трех различных случаев дефектов с разными механическими параметрами показала, что для успешной визуализации дефектов длина волны ультразвукового импульса должна быть в десятки раз меньше размера дефекта. При анализе влияния

размера дефектов на точность работы нейронной сети выявлено, что ошибка визуализации увеличивается для дефектов меньшего размера.
Установлено также, что относительная скорость звука в материалах оказывает большее влияние на точность метода, чем относительная плотность материала. На основании полученных авторами результатов можно утверждать, что разработанные методики и технические решения имеют большое значение для будущих исследований в области дефектоскопии, обладают весомым потенциалом для научных и практических сфер применения.

Ключевые слова: ультразвуковой неразрушающий контроль, дефекты, ультразвуковой отклик, сверточные нейронные сети

Благодарности. Авторы выражают благодарность редакции и рецензентам за внимательное отношение к статье и указанные замечания, которые позволили повысить ее качество.

Для цитирования. Соболь Б.В., Соловьев А.Н., Васильев П.В., Ляпин А.А. Моделирование процессов ультразвуковой дефектоскопии в задаче поиска и визуализации внутренних дефектов в узлах агрегатов и конструкций. *Advanced Engineering Research (Rostov-on-Don)*. 2023;23(4):433–450. https://doi.org/10.23947/2687-1653-2023-23-4-433-450

Introduction. Inverse problems in the framework of research are those tasks in which the consequences of certain phenomena or processes are analyzed to formulate hypotheses and conclusions about their causality. Inverse problems are found in various areas of research, especially, in cases where there are large amounts of experimental data that allow for identifying the characteristics and features of the process that have given rise to these data. Thus, inverse problems provide scientists with the opportunity to determine the parameters of processes that are not available for direct observation.

Currently, there is a standard technique for solving inverse problems, which is based on the analysis of the system's response to certain input actions. Modern approaches to solving inverse problems divide them into different categories, which facilitates their formalization and adaptation depending on the specific situation.

The technique of solving inverse problems for the diagnosis of mechanical systems is widely used in mechanical engineering. The study of the dynamic response of such systems, including the analysis of transient characteristics, provides for obtaining detailed and accurate information about the state of the system, which, in turn, makes it possible to determine its performance and quality.

In the field of diagnostics of structures and products, there is a growing need to assess the current state of technical systems to identify and eliminate potential hazards that can cause production losses or accidents. Such assessments can only be given by highly qualified experts in reengineering.

Taking into account these aspects, the task was set to develop and further evaluate the possibilities of using a neural network model to solve applied problems of ultrasonic imaging of internal defects in solids for various materials.

There are a large number of scientific papers on this topic. Thus, in [1], the authors focused their attention on the analysis of composite materials containing defects. The presence of defects in such composites can significantly affect their performance characteristics; therefore, it is of particular interest to researchers. To search for defects, each of the studied objects is subjected to ultrasonic scanning, during which vibrations are recorded and their characteristics are determined. The next stage of the analysis is the classification of the obtained characteristics using artificial neural networks. This method provides obtaining an image of the defect area with high accuracy. Such visualization reflects both the nature and extent of the defect in the material under study. It is important to note that this technique provides a clear identification of the damage zone, and the resulting image corresponds to visual observations.

Paper [2] presents the acoustic emission method in the context of the assessment of composite materials, which is a promising area of research. Special attention is paid to the identification of acoustic signals associated with the micro-structure of fibers under conditions of high noise levels and using film sensors. Multilayer composites based on reinforced glass fiber, made by various methods, were prepared for research. The experiments included loading composite samples under static conditions, while a PVDF film was installed on their surface. The acoustic signals were carefully recorded and then classified using an artificial neural network. The results of this study indicate the possibility of successfully classifying various destruction mechanisms in composite materials using neural networks.

Study [3] analyzed the collapse incidents that occurred during excavations in rock layers at the Wudongde hydroelectric power plant in China. Its authors presented an improved artificial neural network (ANN) model for predicting the probability and depth of such collapses. However, it should be said that a single parameter is not capable of providing absolute accuracy in predicting the depth of collapses. In this study, an integrated method of intelligent forecasting based on the use of artificial neural networks was proposed. Analytical and statistical studies were carried out for its development, which allowed for determining six key input parameters: coating depth, ratio of main and minor stresses, geological strength index, excavation method, support strength, and rock orientation.

The ANN model was trained using data collected during excavations at the Wudongde hydroelectric power plant, among them there were 45 samples for training and 6 test samples for verification. A genetic algorithm was used to optimize the parameters of the ANN, such as structural characteristics and initial weights. After completing the learning stage, the trained neural network was successfully applied to predict the depth of collapses at several excavation sites. The results of the forecasts showed high compliance with the data obtained during observations at these sites.

Article [4] presents an innovative method for detecting defects in frame structures. It differs significantly from the others and consists of two stages. The first stage focuses on the exact localization of the defect in the bar. To do this, an analysis of the frequencies and waveforms associated with the object under study is used. The results of the analysis of oscillation patterns play a crucial role in solving the problem of the first stage. At the second stage, after successful localization of the defect, an analytical or finite element model of the structure is created, taking into account the identified defects. Using this model, the degree of damage to the frame structure is assessed. The application of this method is illustrated by the example of calculating the defect parameters in an elastic cantilever bar. This calculation is based on experimental observations obtained in a finite element complex. The presented algorithm provides a new tool for more accurate and effective identification of defects in frame structures, which is of great importance for research activities and engineering practice. The results of the modeling carried out within the framework of this study indicate a decrease in the precipitation prediction error. This indicates an improvement in functional approximation and, consequently, excellent learning characteristics of this method, compared to traditional neural networks with sigmoid or other activation functions.

Study [5] proposes an innovative method for diagnosing defects in a manual transmission based on the analysis of vibration signals obtained during experimental tests. The main focus is on the early detection of anomalies in the operation of gears. For effective analysis of vibration signals, data processing focused on the time-frequency domain is used. One of the key methods is the use of continuous wavelet transform, which makes it possible to extract statistically significant characteristics from the signals. To optimize the signal processing, a method of distinguishing features is being introduced, which helps to determine the most important parameters, which, in turn, reduces the computational load and speeds up the analysis process. Genetic algorithms are used to select optimal input features and further reduce the computational complexity of the study. This intelligent approach contributes to improving the efficiency of the data analysis process. The next important step in the research is to evaluate the effectiveness of the proposed method. Advanced technologies of neural back propagation networks were used for this purpose. The attained results and the performance of the classifiers were carefully evaluated on a variety of vibration signals obtained through experimental tests under various operating conditions of mechanical gearboxes.

Studies on nondestructive testing systems and the search for defects in solids often affect the field of modeling the corresponding processes [6]. The primary focus is on solving inverse geometric problems closely related to the theory of elasticity, for their further application in the analysis of a flat rectangular area. The task is to restore the characteristics of circular cavities and cracks.

To effectively solve inverse problems, researchers rely on the obtained information about the first four natural resonant frequencies. These parameters represent an additional dataset that significantly enriches information about the system. The technique used to solve inverse problems is based on minimizing the residual functional. The principle of this technique is to minimize the discrepancy between the measured input data and the values obtained as a result of numerical solution to direct problems. In this case, the parameters of defects in the solid are preset.

Thus, research in the field of nondestructive testing of defects in solids is focused on the development and application of mathematical methods and modeling, which makes it possible to accurately identify and analyze defects hidden inside the material. These studies are applied in the field of safety and quality control of technical systems. The authors explore the possibilities of using neural network technologies in solving inverse problems of mechanics, including the problem of two-dimensional visualization of internal defects. These methods are widely used in medicine, civil engineering, non-destructive testing and other fields.

In [7], a system was proposed for detecting cracks in metal structures and determining their depth based on the analysis of two-dimensional images. The major objective of this work was to create an affordable and convenient control system, a more cost-effective alternative to expensive measuring devices. Within the framework of this study, a specific learning strategy was developed, and several neural network architectures were considered, contributing to a more accurate detection of cracks and assessment of their depth.

The neural network training process included providing the network with characteristics of two-dimensional crack profiles, as well as data on the maximum depth of the crack measured using a laser microscope. This made it possible to create a model that was able to accurately determine the depth of defects in the material. It should be noted that the average error in the operation of this neural network was only about 18% on test samples. This result exceeded critically the results of previous studies, which were based on a variety of learning strategies and analysis techniques. Thus, this study has significantly improved the quality of determining the depth of cracks in metal structures. Its value resides in the development of new learning strategies and a tool for more accurate assessment of the depth of cracks.

Study [8] emphasizes the importance of labeled data containing images with defects. One of the latest proposals in this field is the presented deep transfer learning model designed to extract the characteristic signs of internal defects in X-ray images obtained as a result of inspection of aviation composite materials. This model is a tool for automatic analysis of such images. This tool provides optimizing the defect detection process and increasing the efficiency of nondestructive testing.

In the course of the study, the proposed model efficiency was checked on the problem of detecting defects-inclusions in X-ray images. An analysis of the experimental results has shown that this model is capable of achieving high accuracy (96% according to F1 metric). Such encouraging results indicate the potential of this approach and its ability to produce satisfactory results in defect identification tasks. This opens up new horizons in the field of nondestructive testing and makes it possible to more effectively provide the safety and reliability of composite materials in the aviation industry.

Paper [9] shows a method that offers reconstruction and visualization of internal anomalies in the form of three-dimensional representations. This approach uses an economically and temporarily advantageous technique known as pulsed thermography. In this context, an innovative method is presented that is able to quickly and accurately assess both the depth and thickness of internal anomalies using a one-way inspection. The practicability and efficiency of this method have been successfully demonstrated through studying composite and steel samples containing semi-closed air gaps. The study results confirmed that with the proposed method, the error in estimating the total volume of three-dimensional anomalies is only 10% for composite samples. Thus, this innovative method provides new opportunities for nondestructive testing and visualization of internal defects in various materials and samples, while providing high accuracy and cost-effectiveness.

In [10], the fundamental factors causing failures in the operation of solid rocket engines are considered. One of the key aspects that have a critical impact on the integrity of the engines is the peeling phenomenon at the interface between propellant, insulation and protective layer. Modern methods of diagnostics and assessment of the structural integrity of rocket engines, as a rule, are limited to visual inspection and analysis of their components. This approach has its limitations and requires improvement. In this context, an innovative algorithm is presented, designed to identify surface skin defects that can disrupt the connection between solid fuel and rocket engine insulation. To optimize the operation of the neural network, a number of tests were conducted in which various network parameters were changed. These studies allow for achieving the classification accuracy of 99.08% for the class of serviceable elements, 90.66% — for the class of foreign objects, and 99.48% — for the class associated with defects. The results obtained indicate the high efficiency of the proposed method and its potential for use for the diagnostics of solid-fuel rocket engines.

The research conducted and published by the author in article [11] was aimed at exploring the potential of deep learning methods in the context of electromagnetic inversion. The principle of this approach is to use deep neural networks based on a convolutional architecture to analyze and process data obtained within the framework of this task. An important aspect of this research is learning using extensive sets of synthetic data obtained through three-dimensional modeling. Deep neural networks here are trained on a variety of synthetic data representing information about the distribution of electromagnetic fields inside objects and environments. These data provide valuable information about their properties and compositions, which makes the electromagnetic inversion method more accurate and effective. The efficiency of the proposed method has been successfully demonstrated on various models that are of high practical importance. As an example, when monitoring the electromagnetic field in the area of carbon dioxide accumulation located underground, the inversion method allows for analyzing and controlling this field using a source on the surface.

Previously, the authors of the presented study have already considered tasks combining modern methods of deep machine learning and well-established classical approaches to defect identification [12–14]. In the current work, the emphasis is on a neural network model that effectively performs two-dimensional acoustic visualization of internal anomalies. This project takes the field of nondestructive ultrasonic testing to a new level providing an opportunity to conduct system analysis using numerical experiments.

The objective of the presented research is to develop and evaluate the efficiency of a neural network model for improving ultrasonic visualization of internal defects in solid materials. To identify nonlinear relationships between geometry of defects and ultrasonic control signals, the authors propose to use a technique based on solving the inverse problem of solid mechanics and using artificial neural networks. The basic task in this case is to create a reliable tool for accurate visualization of the sizes, shapes, location and orientation of internal defects in various materials. Numerical experiments approximate the process of ultrasonic probing of samples in which internal defects with various geometric shapes and mechanical characteristics are present. These experiments serve as the initial data for training a neural network and then checking it for proper functioning and accuracy. Thus, it can be argued that this study covers a wide range of scientific methods and technologies, including the development of neural networks, modeling of ultrasonic waves, and analysis of acoustic data.

Materials and Methods. In this work, feed-forward neural networks (FFNN) and convolutional neural networks (CNN) are used. Analytical software is used to determine the most rational network architecture. ANN are trained by the algorithm RProp (stable back propagation) and Adam (adaptive moment estimation method).

RProp algorithm is based on the gradient descent method. In contrast to the standard error back-propagation algorithm, RProp uses only the signs of partial productions to adjust the weight coefficients. The algorithm uses epoch-based learning, and the correction of weights occurs after processing the entire volume of the training sample. The weight values are updated as follows:

$$\Delta_{ij}^{(t)}=\begin{Bmatrix}\eta^{+}\Delta_{ij}^{(t)},\dfrac{\partial E^{(t)}}{\partial\omega_{ij}}\dfrac{\partial E^{(t-1)}}{\partial\omega_{ij}}>0\\ \eta^{-}\Delta_{ij}^{(t)},\dfrac{\partial E^{(t)}}{\partial\omega_{ij}}\dfrac{\partial E^{(t-1)}}{\partial\omega_{ij}}<0\end{Bmatrix},\ \Delta\omega_{ij}^{(t)}=\begin{Bmatrix}-\Delta_{ij}^{(t)},\dfrac{\partial E^{(t)}}{\partial\omega_{ij}}>0\\ +\Delta_{ij}^{(t)},\dfrac{\partial E^{(t)}}{\partial\omega_{ij}}<0\\ 0,\dfrac{\partial E^{(t)}}{\partial\omega_{ij}}=0\end{Bmatrix},\ 0<\eta^{-}<1<\eta^{+},$$

after which the weights are adjusted: $\omega_{ij}^{(t+1)}=\omega_{ij}^{(t)}+\Delta\omega_{ij}^{(t)}$.

Adam uses grouped averages of both gradients and second moments of gradients. If parameters $w^{(t)}$ are set, and loss function $\mathcal{L}^{(t)}$, where t reflects the index of the current iteration, the recalculation of the parameter by the algorithm is specified as follows:

$$m_{\omega}^{(t+1)}\leftarrow\beta_1 m_{\omega}^{(t)}+(1-\beta_1)\nabla_{\omega}\mathcal{L}^{(t)}$$

$$v_{\omega}^{(t+1)}\leftarrow\beta_2 v_{\omega}^{(t)}+(1-\beta_2)\left(\nabla_{\omega}\mathcal{L}^{(t)}\right)^2,$$

$$\hat{m}_\omega = \frac{m_\omega^{(t+1)}}{1-\beta_1^{(t+1)}},\ \hat{v}_\omega = \frac{v_\omega^{(t+1)}}{1-\beta_2^{(t+1)}}, \omega^{(t+1)} \leftarrow \omega^{(t)} - \eta\frac{\hat{m}_\omega}{\sqrt{\hat{v}_\omega}+\varepsilon}$$

where ε is a small additive used to prevent division by 0, and β_1 and β_2 are the forgetting factors for gradients and second moments of gradients, respectively, η —basic learning rate. Squaring and square root are calculated elementwise.

Images processed by a convolutional ANN can be represented as a size tensor:

$$\dim(I) = \left(\hat{h}, \hat{\omega}, d\right),$$

where *h*ˆ and *w*ˆ — dimensions of a 2D image, *d* — number of image channels. Convolution core *K* has the following dimensions:

$$\dim(K) = (f, f, d),$$

where *f* — square convolution filter side.

The convolution operation can be defined as follows. The object of the convolution is two-dimensional image *I*. Convolution core *K* has dimensions *h* × *w*. The result of the convolution is:

$$(I * K)_{xy} = \sum_{i=1}^{h}\sum_{j=1}^{\omega} K_{ij} \times I_{x+i-1, y+j-1}.$$

A convolutional layer is built on this operator, which consists of a certain set of kernels $\vec{K}$, their corresponding displacements $\vec{b}$:

$$conv(I, K)_{xy} = \sigma\left(b + \sum_{i=1}^{h}\sum_{j+1}^{\omega}\sum_{k=1}^{d} K_{ijk} \times I_{x+i-1, y+j-1}\right),$$

where *d* — index of the image channel; *b* — displacement component; σ — activation function of the convolutional layer.

The trained parameters of this layer are filter *K* and displacement *b*.

There are several regularization techniques in machine learning. To prevent over-training of complex ANN models with a large number of parameters, Tikhonov regularization method (*ridge regression*, or *L2*), also called *weight decay* in machine learning, is used. Regularization coefficient is λ, which controls the minimization of the norm relative to the minimization of losses on the training dataset. Thus, for each weight *w,* the summand is added to objective function: $\frac{\lambda}{2}\|\vec{\omega}\|^2 = \frac{\lambda}{2}\sum_{i=1}^{W}\omega_i^2$. Within the applied *Keras* framework, regularization is used for each convolutional layer of the ANN model.

The initial initialization of the weights is carried out by *Xavier* method. During the initial setting of the weight values, a probability distribution is applied, both uniform and normal with variance $Var(W) = 2/(n_{in} + n_{out})$, where n_{in} and n_{out} — numbers of neurons in the previous and subsequent layers, respectively.

The variance of the output values of a linear neuron (without displacements) has the form:

$$V_{ar}\left(\sum_{i=1}^{n_{in}}\omega_i x_i\right) = \sum_{i=1}^{n_{in}} V_{ar}(W)V_{ar}(X) = n_{in}V_{ar}(W)V_{ar}(W)V_{ar}(X).$$

It is assumed that the weights and input values are uncorrelated and have zero expectation. From this, the variance of the probability distribution is obtained, on whose basis the primary initialization of the weights takes place, and which ensures that the variance of the input data is preserved after passing through the layer.

In this paper, the batch normalization layers (*Ioffe* and *Szegedy*) are actively applied in most of the developed ANN models using *Keras* framework. The method normalizes the input data in such a way that their expectation is zero, and the variance is one. In this case, normalization is performed on each layer for each data batch β:

$$\mathrm{B}x_1,\ldots,x_m,\mu_\mathrm{B} = \frac{1}{m}\sum_{i=1}^{m}x_i, \sigma_B^2 = \frac{1}{m}\sum_{i=1}^{m}(x_i - \mu_B)^2.$$

Based on these characteristics, the activation function is transformed:

$$\hat{x}_i = \frac{x_i - \mu_B}{\sqrt{\sigma_B^2 + \varepsilon}}, \varepsilon > 0, y_i = \gamma \hat{x}_i + \beta,$$

where β and γ — parameters that can be optimized using the gradient descent method based on the training set.

Dropout layers are used in ANN models in the task of identifying defects on the road surface, which serve to prevent over-training. When using this regularization tool, the mutual adaptation of neurons at the learning stage of the ANN is prevented. This method blocks (disables) neurons during learning with probability *p*. Given that $h(x) = xW + b$ — linear projection of input d_i — мерного вектора *x* на d_h — dimensional vector *x* onto $a(h)$ — an activation function, the application of *Dropout* to this projection at the training stage can be represented as modified activation function

$$f(h) = D \odot a(h),$$

where $D = (X_1, ..., X_{dh})$ — d_h-dimensional vector of random variables X_i, distributed according to Bernoulli's law. X_i has the following probability distribution:

$$f(k, p) = \begin{cases} p, \ k = 1 \\ 1 - p, \ k = 0 \end{cases},$$

where *k* — all possible output values.

The application of *Dropout* to the *i*-th neuron looks like this:

$$O_i = X_i a\left(\sum_{k=1}^{d_i} \omega_k x_k + b\right) = \begin{cases} a\left(\sum_{k=1}^{d_i} \omega_k + b\right), X_i = 1 \\ 0, \quad X_i = 0 \end{cases},$$

where $P(Xi = 0) = p$.

The neural networks described in this paper belong to direct propagation networks. The input information is compiled from data of numerical experiments and, passing through the network, generates output values that are estimated by the metric. Based on these data, the internal values of the weights of the neural network are adjusted. An iterative approach is used, which ensures that a satisfactory level of accuracy of the neural network is obtained.

Defect identification technique. In this paper, we consider a technique for determining the geometric parameters of defects based on data obtained during influencing the object under study. This task is included in the nondestructive testing of properties and parameters of objects oriented to the inverse problem of solid mechanics. To solve this problem, a systematic approach is used with the key role of artificial neural networks. The principle of this approach is to identify nonlinear relationships between various geometric characteristics of defects, such as their size, depth, angle of rotation and type, and the data obtained during the analysis.

Such data can be the amplitude-frequency and amplitude-time characteristics of the signals received in response to the action. This method makes it possible to effectively identify and evaluate the parameters of defects and provides accurate and reliable monitoring of the condition of objects. Artificial neural networks are a computational model used in machine learning, computer science, and other research disciplines. It is based on a large set of connected simple units called artificial neurons, similar to axons in the biological brain. Connections between neurons transmit an activation signal of varying magnitude. If the combined incoming signals are strong enough, the neuron is activated, and the signal travels to other neurons associated with it. Such systems can be trained using pre-prepared examples, rather than explicitly programmed. This method provides a significant advantage in areas where solutions and functions are difficult to express in traditional forms. Neural networks, as well as other machine learning methods, are used to solve various problems that are difficult to resolve through traditional programming based on such rules as computer vision and speech recognition. ANN are most commonly used to model complex connections between inputs and outputs to find patterns in experimental or other data (data mining) [15, 16].

A systematic approach to the identification problem under consideration involves dividing the technical task into a number of subtasks, which are solved using existing tools and approaches. The combination of these tasks forms a whole system that addresses production problems comprehensively.

An innovative method for identifying and visualizing internal defects using ultrasonic nondestructive testing (UNDT) and convolutional generative neural network architecture is proposed. The UNDT signal registered on the surface of the control object is passed through a trained neural network. As a result of processing by the network, a high-quality image is generated, which is a heatmap showing the internal defect of the object. To illustrate the efficiency of the proposed method and its prospects in industrial applications, a metal steel strip is selected as the object of research. Defects are assumed to be present inside this strip, which can simulate both cavities and rigid inclusions. The possibility of absence of defects is also taken into account. It should be noted that the characteristics of defects, such as shape, size and orientation, can vary significantly, which presents additional complexity for the visualization task. The procedure of this approach consists in conducting a series of numerical experiments on whose results a deep neural network is trained. To form a training dataset, a systematic change of mechanical parameters, geometric characteristics, as well as the position of internal defects is performed. Special attention is paid to modeling the process of propagation of an acoustic ultrasonic wave inside a material.

This innovative approach to the identification and visualization of internal defects provides an opportunity for more accurate and effective quality control of materials and products in various industries. Its application can contribute to improving the reliability and safety of end products, which is an important aspect in the modern industry. Based on the collected data, the optimal structure of the neural network model is built and trained. As a result, the neural network model can reconstruct the shape, size and position of the defect from the raw ultrasonic signal captured on the surface of the strip. Figure 1 shows a block diagram of the study.

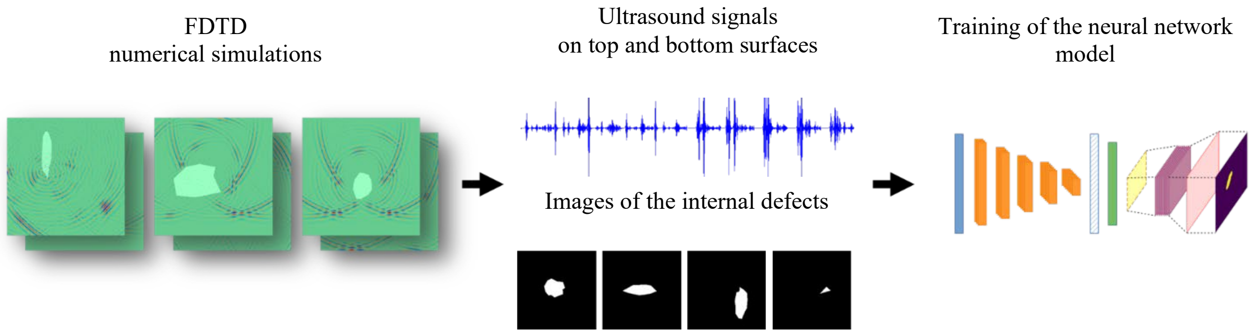

Fig. 1. Scheme for conducting a series of numerical experiments using the finite difference method (FDTD) in the time domain. A fragment of a strip in the defect area and the propagation of an ultrasonic wave (on the left). Construction of a dataset consisting of ultrasonic signals and corresponding binary images of the defect (in the center).
Architecture building and neural model training (on the right).

Method of finite differences in the time domain. It was proposed by Kane Yee [17]. Solving differential equations in the context of modeling media with dispersed and nonlinear properties identifies a unique class of methods — grid methods. These methods have found wide application in a variety of fields, ranging from geophysical tasks to tasks in the optical range.

One of the efficient techniques of studying physical phenomena in various media is the finite difference method in the time domain. It is a valuable tool in solving acoustic problems. It can also be successfully applied in elastic media.

The basic equation of this acoustic model in a flat formulation is:

$$\frac{\partial p}{\partial t}=-k\left(\frac{\partial v_x}{\partial x}+\frac{\partial v_y}{\partial y}\right)\frac{\partial v_x}{\partial t}=-\frac{1}{\rho}\frac{\partial p}{\partial x},\frac{\partial v_y}{\partial t}=-\frac{1}{\rho}\frac{\partial p}{\partial y}.$$

The speed and acoustic pressure of the particles of the simulated object are sampled in the spatial grid. It is possible to analyze the propagation of the sound field over a certain time interval by sequential calculating the values of these parameters. This method offers an opportunity to study various physical processes and phenomena, providing valuable data on the behavior of an environment with diverse characteristics.

Although the finite difference method in the time domain was originally developed to solve acoustic problems, it has a wide range of applications in other fields of physics. In particular, it finds its application in modeling the propagation of sound in various media, such as air or liquid. This versatility of the method makes it an integral part of scientific and engineering research in the field of physics and acoustics.

To verify the efficiency of the selected technique, a reference model was developed in the COMSOL calculation package designed to analyze the propagation of an acoustic ultrasonic wave. Two main numerical methods were used in this study: the finite element method (FEM) and the finite difference method (FDTD). The model is a square-shaped structure made of steel, with an inner hole.

Significant distinctions in the shape of the received signals are explained by different methods of specifying the source of ultrasonic vibrations. In the case of the finite element method, the source points are located on the circumference of the inner hole, while in the finite difference method in the time domain, the source is represented by a point located at the node of the grid.

However, it should be noted that the limited dimensions of the computational grid do not allow modeling the propagation of acoustic waves outside this area. To account for this fact, special boundary conditions are applied, such as absorbing Moore layers or PML (Perfectly Matched Layers). These boundary conditions significantly reduce the reflection of acoustic waves from the boundary of the computational domain, which makes it possible to simulate the passage of an ultrasonic wave into the structure with a high degree of accuracy.

Nondestructive testing model. A steel strip containing a defect is used as a model of nondestructive testing. Its size is 100x15 mm. The absorbing layers are installed on the left and right borders of the strip. The upper and lower parts of the bar are connected to the areas to which the mechanical parameters of the air are set. The defects are represented as convex polygons. The variety of internal defects is specified by changing the number of sides of the polygon, their length, and the distance between the vertices and the center of the defect. The physical parameters of defects vary relative to the thickness of the strip. The position of the defect varies from 0.3 to 0.7, the length of the sides is from 0.1 to 0.5. The input area of the sensor pulse is located on the upper surface of the strip. Vibrations are read on both the upper and lower surfaces. Thus, echo and shadow methods of nondestructive ultrasonic testing are modeled.

In this study, the input signal represented as a fixed set of discrete values depending on the time of the experiment is analyzed. The experimental time is strictly determined taking into account the requirement that the probing pulse, released on the initiating side and directed to the opposite surface of the tested beam, had sufficient time for the traveled distance and return to the source point.

It should be noted that the frequency of the probing pulse used is 10 MHz, which provides high resolution of the experimental system. This makes it possible to study the properties of the bar and its structural characteristics more precisely, based on the analysis of the reflected signal.

Figure 2 shows the scheme of the conducted numerical experiment. The defect is located inside the steel strip. The source of the ultrasonic signal is indicated in red; the signal reading points are indicated in green. The signal is also read at the points of its emission.

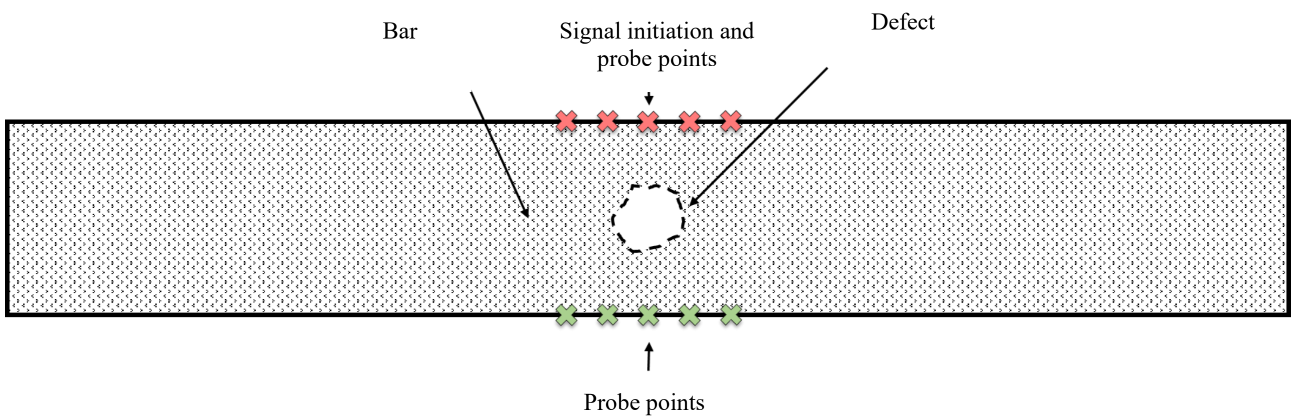

Fig. 2. Numerical experiment scheme

Figure 3 shows the vibrations of ultrasonic signals received at the specified points on the upper surface of the strip (right) and on the lower surface of the strip (left). This simulates the location of sensors on opposite surfaces of the control object. The given model assumes that sensors can move along the strip in search of a defect synchronously.

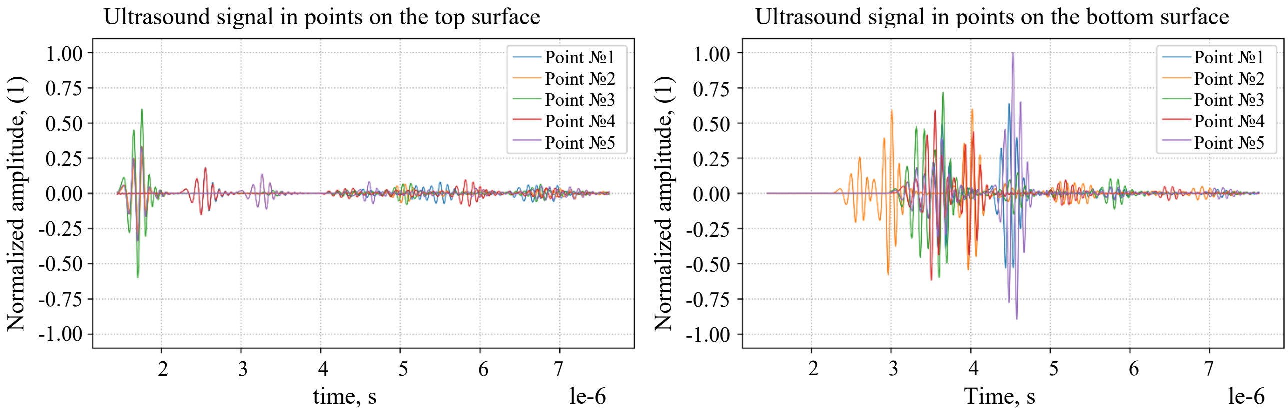

Fig. 3. Ultrasonic signals on the upper and lower surfaces of the strip
obtained as a result of numerical simulation

Neural network model. Convolutional neural networks (CNN) are a special neural network tool for processing discrete data (two-dimensional images, one-dimensional signals) [18]. Currently, it is one of the fastest growing and most promising deep learning tools [19–21].

Convolutional neural networks are effectively used in various fields, including video analysis and time series processing. They provide processing time series as one-dimensional arrays of data and highlighting important features in them using the convolution operation.

To visualize defects in control objects, the model architecture is used, including layers of one-dimensional convolution (Conv1D) and down-sampling layers (MaxPooling), to extract features from ultrasonic signals. The data is then transferred to a fully connected layer for analysis in the context of the defect visualization task. The second part of the network generates images showing the characteristics of defects.

To create the final image of the defect, data from a fully connected layer is processed and fed to a two-dimensional layer. Then, using the trained convolutional layers (Conv2D Transpose), the final image is formed.

Figure 4 shows the architecture of a convolutional neural network with an indication of the size of the input data and the number of convolutional filters for each layer.

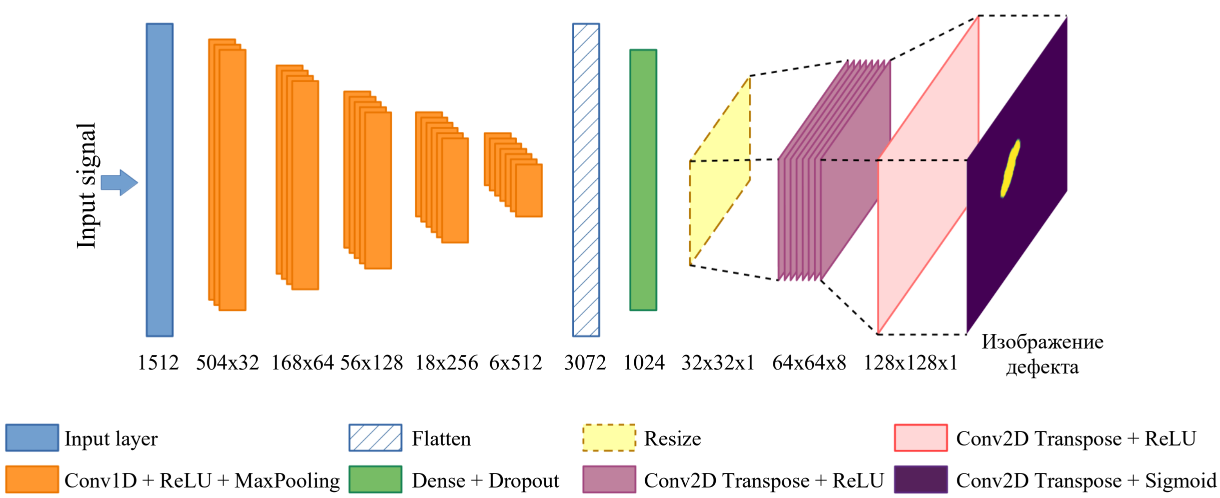

Fig. 4. Convolutional neural network model structure

Model training and validation. Three cases were considered within the framework of a set of numerical experiments. In case *A*, the defect modeled the cavity, and the parameters of the defect material corresponded to the parameters of the air. In case *B*, the defect simulated a rigid inclusion, and the defect parameters had the parameters of a material that was more rigid than steel. In this case, it was tungsten carbide. In case *C*, the mechanical parameters of defects varied, which corresponded to the parameters of gases, liquids, and solid materials.

For cases *A* and *B*, a total of 50,000 problems were solved for various geometric parameters of the defect. Of these, 35,000 copies were used for training, 10,000 — for testing, and 5,000 — for certification. In case *C*, 60,000 tasks were solved with the same percentage of test and validation samples.

In the process of evaluating the performance of the model, the key metrics are the minimum learning error and the reduction of the gap between learning and testing error. The efficiency of the machine learning model is analyzed using various regularization methods, such as Tikhonov regularization, also known as L2 regularization. The initialization of weights, carried out, e.g., by the Xavier method, is a significant stage in the training of neural networks.

One of the tools used to reduce the internal covariance shift and stabilize neural network learning is the batch normalization method. To increase the stability and generalization ability of the model, various regularization techniques are used, such as early stop and Dropout.

It should be noted that data augmentation is not used in this research work due to the extensive amount of training information. There is also no balancing of the dataset, which, however, has its advantages due to the normal distribution of defects in size.

It should be emphasized that neural network training is an optimization task, where selection of the appropriate loss function plays a crucial role. As an example, in computer vision and semantic segmentation tasks, the Jaccard similarity coefficient may turn out to be of great relevance. In this paper, the application of the Jaccard similarity coefficient in the context of the problem of object detection and segmentation is considered, which provides obtaining more accurate and stable results in image analysis:

$$IoU = \frac{|A \cap B|}{|A \cup B|} = \frac{|A \cap B|}{|A| + |B| - |A \cap B|}.$$

In this context, the loss function is expressed as the inverse of the Jaccard similarity coefficient (1–IoU) and is a metric that evaluates the difference between two instances. The Jaccard metric is known in the data analysis and machine learning as an indicator of the intersection and similarity of sets.

To evaluate the efficiency of a neural network model in the validation process, this metric is used as one of the criteria. It allows for determining the degree of correspondence between the output of the model and the reference data, which is important for analyzing and improving the operation of neural networks in information processing tasks:

$$F1 = \frac{2 \times IoU}{IoU + 1}.$$

In this study, one of the most common optimization algorithms, called Adam, is applied. Some of the most recognized and widely used libraries, TensorFlow and Keras, are utilized to solve the tasks of machine learning and neural network training. These software products currently act as standard tools for creating and training neural models and include advanced technologies in this field.

To achieve high accuracy of the models, training was conducted over 30 epochs in each of the three cases considered: *A, B* and *C*.

The neural network approach for solving inverse problems has already shown itself to good advantage [22–24]. With the deepening in the field of machine learning and the subsequent development of new techniques, cutting-edge tools for data analysis and solving traditional problems in mechanics and flaw detection are opening up. One of the significant scientific achievements in this field is a convolutional neural network created specifically to solve the problem of visualization of internal defects using ultrasonic nondestructive testing methods. A notable feature of this model is its relatively small volume, amounting to 37.2 mln parameters. This fact characterizes high efficiency of the learning process and expands the scope of its application in a variety of related fields. To simulate the propagation of ultrasonic waves more effectively, the finite difference method in the time domain is selected in this study. This choice of method has critically increased the speed of calculations compared to previous approaches used in earlier studies.

Research Results. In this paper, three states of the internal defect were considered. In case *A*, the defect simulated a cavity, while the parameters of the medium in the defect area corresponded to the parameters of the air. In case *B*, the defect modeled a rigid inclusion, while the medium parameters had parameters of a more rigid material than the strip material. In this case, it was tungsten carbide. In case *C*, the mechanical parameters of the defect were varied, which corresponded to the parameters of gases, liquids, and solids.

The results of this study, presented in Figure 5, demonstrate the efficiency of neural networks in analyzing and restoring information about defects. The visualized fragments of the strip in the defect area are displayed on the graph. The real defect is indicated by a solid black line, whereas the shape and position of the defect, predicted by the neural network, are represented by a dotted red line. The analysis of the drawing allows us to argue that the neural network model is able to restore the size of the defect, accurately determine its location, partially reproduce its shape, and even establish orientation. These results validate the potential of neural networks in solving image processing and analysis problems using high accuracy and reliability.

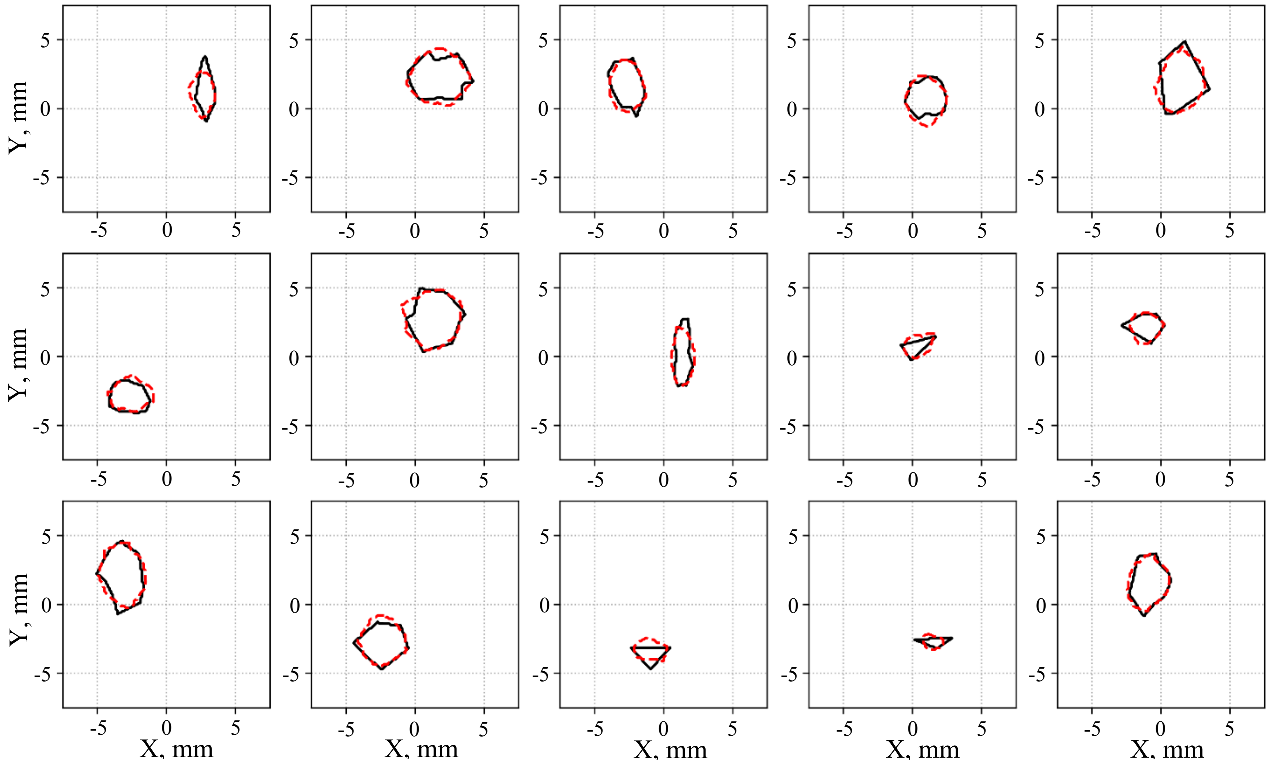

Fig. 5. Defect visualization results. Real defect is highlighted in black.
Neural network prediction is highlighted in red.

Validation was performed for each of the cases. Metric F1 was used to evaluate the overall efficiency of the model. In general, the accuracy of the proposed method was at a high level. Average value F1 for the entire validation set was 92% for case *A*, 90% — for case *B*, and 85% — for case *C*.

Figure 6 shows the dependence of visualization accuracy of the defect on its size. The defect size is the maximum distance between the vertices of the polygon simulating the defect. The data obtained show that for successful visualization of defects, the wavelength of the ultrasonic pulse must be ten times smaller than the size of the defect. The figure also shows the effect of an unbalanced data set on the neural network accuracy. For defects of the largest size, the visualization error increases.

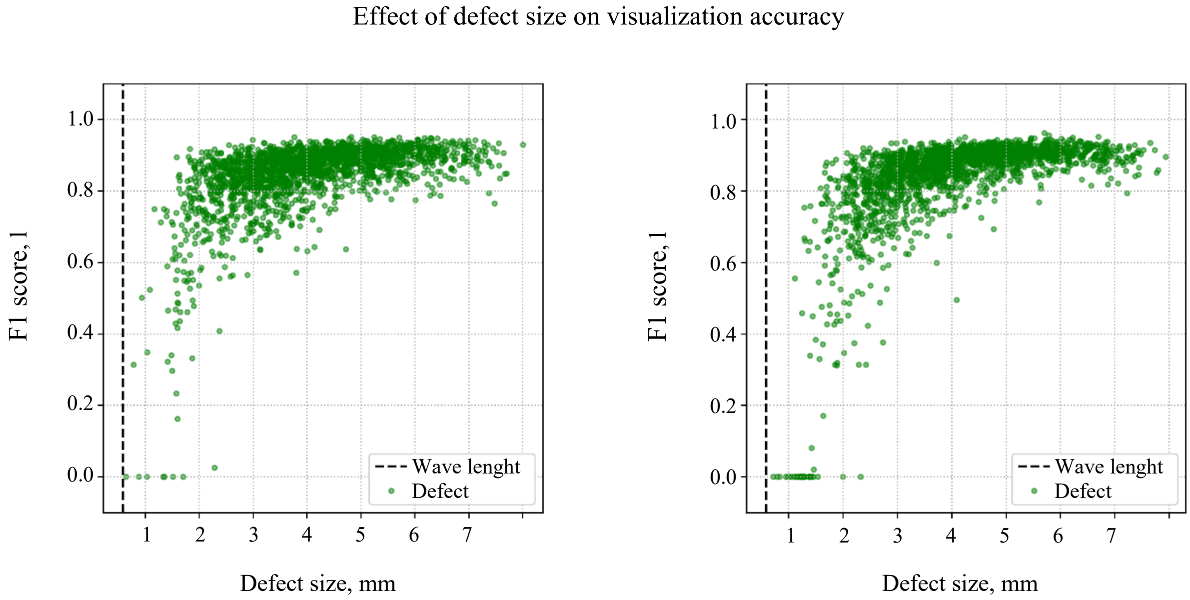

Fig. 6. Dependence of visualization accuracy of defects on their size for cases *A* (left) and *B* (right). Black dashed line shows the wavelength of the probing ultrasonic pulse

The authors also analyzed the effect of the mechanical parameters of the defect on their visualization accuracy. For each neural network from cases *A*, *B,* and *C*, validation was performed on a dataset with different mechanical parameters of defects. This study shows how well-trained neural network models are able to visualize various types of defects, including defects that are absent in the training sets. For ease of perception, the parameters of the material density and the speed of sound in the materials are presented as relative:

$$\rho_{relative} = \frac{\rho_{steel} - \rho_{defect}}{\rho_{steel}}, C_{relative} = \frac{C_{steel} - C_{defect}}{C_{steel}}.$$

Figure 7 shows how accurately neural network models *A*, *B*, and *C* visualize defects for a wide range of parameters. In the case where the neural network is trained only on dataset *A*, when the defect models a cavity, acceptable accuracy is achieved only for defects with $C_{relative} > 0,7$. In case *B*, when the defect simulates a hard inclusion, the accuracy of the neural network operation deteriorates significantly when value C_{defect} от заданного в эксперименте. deviates from the one specified in the experiment. In case *C*, when the neural network is trained on a dataset with different defect parameters, the results of the work are stable over the entire range of parameter changes. The exception is defects with value $C_{relative} \to 0$. In these cases, the sound speeds in the strip material and the defect material are very close to each other. It can also be concluded that the accuracy of the proposed method is more influenced by a change in parameter *C*, than ρ. Thus, the limits of the application of various neural network models for the identification of defects with different mechanical parameters are demonstrated.

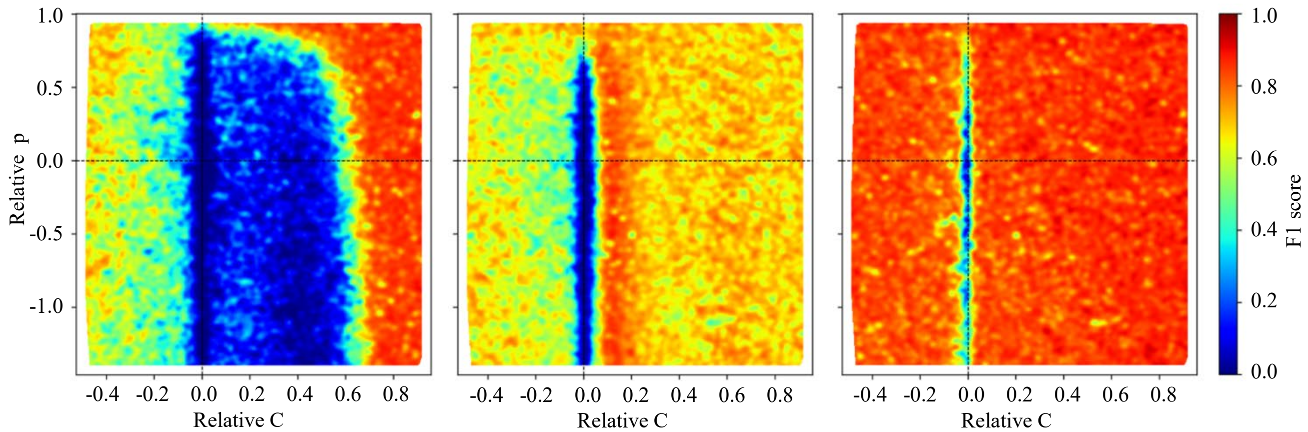

Fig. 7. Effect of defect parameters on the accuracy of neural networks.
Neural network *A* on the left, neural network *B* in the center, neural network *C* on the right.

Thus, it can be concluded that the neural network model developed by the authors represents a breakthrough in the field of nondestructive control, providing effective tools for the visualization of internal defects and creating new prospects for application in industry and scientific research [24–25].

Discussion and Conclusion. The results obtained present a new perspective on the field of nondestructive testing and its potential in detecting internal defects in various materials and structures. In the presented study, an innovative method based on the use of convolutional neural networks is proposed for the express diagnosis of defects in the structure of materials. A key aspect of this research is the demonstrated potential efficiency of the use of convolutional neural networks to improve the quality of ultrasound imaging. The authors have developed a model designed for nondestructive testing, and generated appropriate datasets used to train artificial neural networks. This convolutional neural network model is able to accurately determine not only the shape, but also the position and orientation of internal defects in a solid material. The experimental data obtained demonstrate the informative value of the ultrasonic signal, as well as its ability to accurately convey real characteristics of internal defects.

The authors analyzed several types of defects, each of which was given special attention. In the first case, the defect was classified as *A* and modeled as a cavity, in the second case — as *B* and represented a rigid inclusion, in the third — as *C*, with different mechanical parameters of the defect. In all scenarios of the study, a critical effect of the defect size on the ultrasound imaging accuracy was identified. In addition, the results obtained clearly confirm that the selection of the frequency of the probing signal is of crucial importance and should be optimized so that the wavelength is significantly smaller than the size of internal defects.

After conducting a system validation of convolutional neural networks in the context of each of the above-mentioned types of defects (*A*, *B,* and *C*), a range of values of the mechanical parameters of the defect was established for different mechanical characteristics of the defects, within which the proposed method did not provide sufficiently high-quality visualization.

In conclusion, it should be noted that the methods and technical solutions developed in the course of this study are of great importance for further research in the field of flaw detection and solving inverse problems in a wide context of scientific and practical applications.

References

1. Samanta S, Mandal A, Thingujam JS. Application of ANN in Identifying Defects in Impacted Composite. *Procedia Materials Science*. 2014;6:926–930. https://doi.org/10.1016/j.mspro.2014.07.162

2. Bar HN, Bhat MR, Murthy CRL. Identification of Failure Modes in GFRP Using PVDF Sensors: ANN Approach. *Composite Structures*. 2004;65(2):231–237. https://doi.org/10.1016/j.compstruct.2003.10.019

3. Dong-Fang Chen, Xia-Ting Feng, Ding-Ping Xu, Quan Jiang, Cheng-Xiang Yang, Pin-Pin Yao. Use of an Improved ANN Model to Predict Collapse Depth of Thin and Extremely Thin Layered Rock Strata during Tunneling. *Tunnelling and Underground Space Technology*. 2016;51:372–386. https://doi.org/10.1016/j.tust.2015.09.010.

4. Cherpakov AV, Akopyan VA, Soloviev AN. Algorithm for Multi-parameter Identification of Defects in Frame Structures. *Technical Acoustics*. 2013;13:1–11. (In Russ.)

5. Rajeswari C, Sathiyabhama B, Devendiran S, Manivannan K. A Gear Fault Identification Using Wavelet Transform, Rough Set Based GA, ANN and C4.5 Algorithm. *Procedia Engineering*. 2014;97:1831–1841. https://doi.org/10.1016/j.proeng.2014.12.337

6. Solovyev AN, Shevtsov MYu. Reconstruction of Defects in Elastic Bodies by Combination of Genetic Algorithm and Finite Element Method. *Vestnik of DSTU.* 2016;16(2):5–12. https://doi.org/10.12737/19686 (In Russ.)

7. Yasser S Mohamed, Hesham M Shehata, Mohamed Abdellatif, Taher H Awad. Steel Crack Depth Estimation Based on 2D Images Using Artificial Neural Networks. *Alexandria Engineering Journal*. 2019;58(4):1167-1174. https://doi.org/10.1016/j.aej.2019.10.001

8. Yanfeng Gong, Hongliang Shao, Jun Luo, Zhixue Li. A Deep Transfer Learning Model for Inclusion Defect Detection of Aeronautics Composite Materials. *Composite Structures*. 2020;252:112681. https://doi.org/10.1016/j.compstruct.2020.112681

9. Adisorn Sirikham, Yifan Zhao, Haochen Liu, Yigeng Xu, Stewart Williams, Jörn Mehnen. Three-Dimensional Subsurface Defect Shape Reconstruction and Visualisation by Pulsed Thermography. *Infrared Physics & Technology*. 2020;104:103151. https://doi.org/10.1016/j.infrared.2019.103151

10. Luiz Felipe Simões Hoffmann, Francisco Carlos Parquet Bizarria, José Walter Parquet Bizarria. Detection of Liner Surface Defects in Solid Rocket Motors Using Multilayer Perceptron Neural Networks. *Polymer Testing*. 2020;88:106559. https://doi.org/10.1016/j.polymertesting.2020.10655

11. Vladimir Puzyrev. Deep Learning Electromagnetic Inversion with Convolutional Neural Networks. *Geophysical Journal International*. 2019;218(2):817–832. https://doi.org/10.1093/gji/ggz204

12. Soloviev AN, Sobol BV, Vasiliev PV. Ultrasonic and Magnetic Flow Inspection Methods of Identification of Cracks in the Pipe Coupled with Artificial Neural Networks. *In book: Parinov I, Chang SH, Jani M. (eds). Advanced Materials. Springer Proceedings in Physics.* Cham: Springer; 2017. P. 381–395. https://doi.org/10.1007/978-3-319-56062-5_32

13. Soloviev A, Sobol B, Vasiliev P, Senichev A. Generative Artificial Neural Network Model for Visualization of Internal Defects of Structural Elements. In book: Parinov I, Chang SH, Long B. (eds). *Advanced Materials. Springer Proceedings in Materials.* Cham: Springer; 2020. P. 587–595. https://doi.org/10.1007/978-3-030-45120-2_48

14. Sobol BV, Soloviev AN, Rashidova EV, Vasiliev PV. Identification of Crack-like Defect and Investigation of Stress Concentration in Coated Bar. *PNRPU Mechanics Bulletin*. 2019;(4):165–174. https://doi.org/10.15593/perm.mech/2019.4.16

15. Fang X, Luo X, Jiong Tang. Structural Damage Detection Using Neural Network with Learning Rate Improvement. *Computers and Structures*. 2005;83(25–26):2150–2160. https://doi.org/10.1016/j.compstruc.2005.02.029

16. Soloviev A, Sobol B, Vasiliev P. Identification of Defects in Pavement Images Using Deep Convolutional Neural Networks. In book: Parinov I, Chang SH, Kim YH. (eds). *Advanced Materials. Springer Proceedings in Physics*. Cham: Springer; 2019. P. 615–626. https://doi.org/10.1007/978-3-030-19894-7_46

17. Kane Yee. Numerical Solution of Initial Boundary Value Problems Involving Maxwell's Equations in Isotropic Media. *IEEE Transactions on Antennas and Propagation*. 1966;14(3):302–307. https://doi.org/10.1109/TAP.1966.1138693

18. LeCun Y, Boser B, Denker JS, Henderson D, Howard RE, Hubbard W, et al. Backpropagation Applied to Handwritten Zip Code Recognition. *Neural Computation*. 1989;1(4):541–551. https://doi.org/10.1162/neco.1989.1.4.541

19. Goodfellow I, Bengio Y, Courville A. *Deep Learning*. Cambridge, MA: MIT Press; 2016. 777 p.

20. Krizhevsky A, Sutskever I, Hinton GE. ImageNet Classification with Deep Convolutional Neural Networks. *Communications of the ACM*. 2017;60(6):1097–1105. http://dx.doi.org/10.1145/3065386

21. Kaiming He, Xiangyu Zhang, Shaoqing Ren, Jian Sun. Deep Residual Learning for Image Recognition. In: *Proc. IEEE Conference on Computer Vision and Pattern Recognition (CVPR)*. New York City, UA: IEEE; 2016. P. 770–778 https://doi.org/10.1109/CVPR.2016.90

22. De Angelo M, Spagnuolo M, D'Annibale F, Pfaff A, Hosche K, Misra A, et al. The Macroscopic Behavior of Pantographic Sheets Depends Mainly on Their Microstructure: Experimental Evidence and Qualitative Analysis of Damage in Metallic Specimens. *Continuum Mechanics and Thermodynamics*. 2019;31:1181–1203. https://doi.org/10.1007/s00161-019-00757-3

23. Nagatani Y, Okumura S, Wu S, Matsuda T. Two-dimensional Ultrasound Imaging Technique Based on Neural Network Using Acoustic Simulation. *arXiv preprint*. arXiv:2004.08775. 2020. https://doi.org/10.48550/arXiv.2004.08775

24. Solov'ev AN, Sobol' BV, Vasil'ev PV. Ultrasonic Location of Inner Crack Defects in a Compound Elastic Cylinder Using an Artificial Neural-Network Apparatus. *Russian Journal of Nondestructive Testing*. 2016;52(3):119–124. https://doi.org/10.1134/S1061830916030098

25. Soloviev AN, Sobol BV, Vasiliev PV, Senichev AV, Novikova AI. Identification of Defects in a Coating Wedge Based on Ultrasonic Non-destructive Testing Methods and Convolutional Neural Networks. *PNRPU Mechanics Bulletin*. 2023;(1):111–124. https://doi.org/10.15593/perm.mech/2023.1.11

Received 30.10.2023
Revised 24.11.2023
Accepted 05.12.2023

About the Authors:

Pavel V. Vasiliev, Senior Lecturer of the Information Technologies Department, Don State Technical University (1, Gagarin sq., Rostov-on-Don, 344003, RF), SPIN-code: 4914-7944, Scopus ID, ORCID, lyftzeigen@mail.ru

Arkadiy N. Soloviev, Dr.Sci. (Phys.-Math.), Professor, Crimean Engineering and Pedagogical University named after Fevzi Yakubov (8, Uchebnyy Ln, Simferopol, 295015, RF), SPIN-code: 8087-8998, ResearcherID, ScopusID, ORCID, solovievarc@gmail.com

Boris V. Sobol, Dr.Sci. (Eng.), Professor, Head of the Information Technologies Department, Don State Technical University (1, Gagarin sq., Rostov-on-Don, 344003, RF), SPIN-code: 5610-9300, Scopus ID, ORCID, b.sobol@mail.ru

Alexandr A. Lyapin, Dr.Sci. (Phys.-Math.), Professor, Head of the Information Systems in Civil Engineering Department, Don State Technical University (1, Gagarin sq., Rostov-on-Don, 344003, RF), SPIN-code: 9961-8883, ScopusID, ORCID, lyapin.rnd@yandex.ru

Claimed contributorship:
PV Vasiliev: basic concept formulation, research objectives and tasks.
AN Soloviev: setting the task, drawing conclusions.
BV Sobol: setting the task, finalizing the text.
AA Lyapin: processing and analysis of the results.

Conflict of interest statement: the authors do not have any conflict of interest.

All authors have read and approved the final manuscript.

Поступила в редакцию 30.10.2023
Поступила после рецензирования 24.11.2023
Принята к публикации 05.12.2023

Об авторах:

Павел Владимирович Васильев, старший преподаватель кафедры информационных технологий Донского государственного технического университета (РФ, 344003, г. Ростов-на-Дону, пл. Гагарина, 1), SPIN-код: 4914-7944, ScopusID, ORCID, lyftzeigen@mail.ru

Аркадий Николаевич Соловьев, доктор физико-математических наук, профессор Крымского инженерно-педагогический университета имени Февзи Якубова (РФ, 295015, г. Симферополь, пер. Учебный, д. 8), SPIN-код: 8087-8998, ResearcherID, ScopusID, ORCID, solovievarc@gmail.com

Борис Владимирович Соболь, доктор технических наук, профессор, заведующий кафедрой информационных технологий Донского государственного технического университета (РФ, 344003, г. Ростов-на-Дону, пл. Гагарина, 1), SPIN-код: 5610-9300, Scopus ID, ORCID, b.sobol@mail.ru

Александр Александрович Ляпин, доктор физико-математических наук, профессор, заведующий кафедрой информационных систем в строительстве Донского государственного технического университета (РФ, 344003, г. Ростов-на-Дону, пл. Гагарина, 1), SPIN-код: 9961-8883, ScopusID, ORCID, lyapin.rnd@yandex.ru

Заявленный вклад соавторов:

П.В. Васильев — формирование основной концепции, цели и задачи исследования.

А.Н. Соловьев — постановка задачи, формирование выводов.

Б.В. Соболь — постановка задачи, доработка текста.

А.А. Ляпин — обработка и анализ результатов.

Конфликт интересов: авторы заявляют об отсутствии конфликта интересов.

Все авторы прочитали и одобрили окончательный вариант рукописи.